Check for updates

15214095, ja, Downloaded from https://onlinelibrary.wiley.com/doi/10.1002/adma.202207454 by Seoul National University, Wiley Online Library on [28/11/2022]. See the Terms and Conditions (https://onlinelibrary.wiley.com/terms-and-conditions) on Wiley Online Library for rules of use; OA articles are governed by the applicable Creative Commons License

Accepted Article

Advances in Solution-processed OLEDs and their Prospects for Use in Displays

Joo Yoon Woo[1,†], Min-Ho Park[2,†], Su-Hun Jeong[3,†], Young-Hoon Kim[4,†], Byungjae Kim[3], Tae-Woo Lee[5,] and Tae-Hee Han[1,*]*

[1]J. Y. Woo, Prof. T.-H. Han

Division of Materials Science and Engineering, Hanyang University, 222 Wangsimni-ro, Seongdong-gu, Seoul, 04763, Republic of Korea.

E-mail: taeheehan@hanyang.ac.kr

[2]Prof. M.-H. Park

Department of Organic Materials and Fiber Engineering, Soongsil University, 369 Sangdo-Ro, Dongjak-Gu, Seoul 06978, Republic of Korea.

[3]Dr. S.-H. Jeong, Dr. B. Kim

Future Technology Research Center, LG Chem, Ltd.

30, Magokjunang 10-ro, Gangseo-gu, Seoul, 07794, Republic of Korea.

[4]Prof. Y.-H. Kim

Department of Energy Engineering, Hanyang University, 222 Wangsimni-ro, Seongdong-gu, Seoul, 04763, Republic of Korea.

[5]Prof. T.-W. Lee

This article has been accepted for publication and undergone full peer review but has not been through the copyediting, typesetting, pagination and proofreading process, which may lead to differences between this version and the Version of Record. Please cite this article as doi: 10.1002/adma.202207454.

This article is protected by copyright. All rights reserved.

Department of Materials Science and Engineering, School of Chemical and Biological Engineering, Institute of Engineering Research, Research Institute of Advanced Materials, Soft Foundry, Seoul National University, 1 Gwanak-ro, Gwanak-gu, Seoul 08826, Republic of Korea.

E-mail: twlees@snu.ac.kr

Keywords: organic light-emitting diodes, solution process, printing, large-area displays

This review outlines problems and progress in development of solution-processed organic light-emitting diodes (SOLEDs) in industry and academia. Solution processing has several advantages such as low consumption of materials, low-cost processing, and large-area manufacturing. However, use of a solution process entails complications, such the needs for solvent resistivity and solution-processable materials, and yields SOLEDs that have limited luminous efficiency, severe roll-off characteristics, and short lifetime compared to OLEDs fabricated using thermal evaporation. These demerits impede production of practical SOLED displays. This review outlines the industrial demands for commercial SOLEDs and the current status of SOLED development in industries and academia, and presents research guidelines for development of SOLEDs that have high efficiency, long lifetime, good processability to achieve commercialization.

This article is protected by copyright. All rights reserved.

Accepted Article

15214095, ja, Downloaded from https://onlinelibrary.wiley.com/doi/10.1002/adma.202207454 by Seoul National University, Wiley Online Library on [28/11/2022]. See the Terms and Conditions (https://onlinelibrary.wiley.com/terms-and-conditions) on Wiley Online Library for rules of use; OA articles are governed by the applicable Creative Commons License

Accepted Article

1. Introduction

Organic light-emitting diodes (OLEDs) are widely used in displays, from small to medium ones for information technology devices, to large televisions (TVs) and large-area displays.[1–10] Compared to liquid crystal displays (LCDs), OLEDs have higher color purity, wider color gamut, wider viewing angle, and higher contrast ratio.[1,2,6] They have fast response, and are therefore also suitable for use in gaming monitors. Additionally, OLEDs do not need any backlight unit, so they enable various lightweight form factors, including foldable, rollable, and transparent displays.[6]

Most OLED panels are mass-produced using ultra-high vacuum (< 10^{-7} Torr) thermal evaporation processes, and have multilayer device architecture composed of many functional layers including charge transport and blocking layers for each type of charge carrier.[11,12] The thermal evaporation technology and its successive multi-layer forming processes entail high fabrication cost for mass production of OLED display panels. Therefore, a solution process to fabricate organic/polymeric emitting and transporting materials is in great demand for low-cost, large-area production of OLED panels by using printing technologies.[12–17]

Solution-processed OLEDs (SOLEDs) can be produced using specially-designed light-emitting polymers (LEPs), which generally bear charge-transporting and light-emitting moieties in their polymer chain. LEPs have good solution processability and multifunctionality, but they yield polymer LEDs (PLEDs) that have limited device efficiency, which has impeded their commercial use.[18,19]

As an alternative, conjugated small organic molecular emitters that enable nearly 100% internal luminescent quantum yield (QY) including phosphorescence and thermally-activated delayed fluorescence (TADF) organic emitters have been considered for commercial use in SOLEDs due to its high efficiency, and thereby reduce the huge efficiency gap in between SOLEDs and evaporated OLEDs (EOLEDs).[12,15,20]

This article is protected by copyright. All rights reserved.

15214095, ja, Downloaded from https://onlinelibrary.wiley.com/doi/10.1002/adma.202207454 by Seoul National University, Wiley Online Library on [28/11/2022]. See the Terms and Conditions (https://onlinelibrary.wiley.com/terms-and-conditions) on Wiley Online Library for rules of use; OA articles are governed by the applicable Creative Commons License

Accepted Article

Small to medium-sized OLED panels are fabricated using the side-by-side thermal evaporation process. They are composed of individually-driven red, green, and blue (RGB) pixels (**Figure 1**a). The process uses fine metal masks (FMMs) to separate pixels, but this approach has limited applicability for production of large-area panels, so large OLED panels for TVs are composed of one-colored, white or blue, OLED pixels and RGB color filters (Figure 1b,c).[10,21,22] In contrast, solution-processed small-to medium-sized SOLEDs are composed of individually-driven RGB pixels, which do not need an FMM to isolate each RGB pixel (Figure 1d).[23–28]

SOLEDs have several advantages over EOLEDs, including simple device structure, availability of top-emission structure, low material consumption, and compatibility with large area-manufacturing using 10.5G (2,940 mm × 3,370 mm) mother glasses.[29] SOLEDs can be produced using inkjet printing (IJP), which uses only the necessary amount of materials to pattern pixels (i.e., drop on demand) (**Figure 2**a). Therefore, the total manufacturing cost of SOLEDs is expected to be ~75% that of the currently mass-produced white EOLED from LG Display Co. (South Korea).[30]

Currently mass-produced EOLEDs for large panels use tandem structures, in which sub-cells are vertically stacked to achieve white emission and high luminance. For tandem structures, > 30 organic layers are required.[10,28,31] In white tandem EOLED panels, red-, green-, or blue-emitting sub-cells are stacked, and their emissions combine to yield white light (Figure 2b, left).[1,10,31] However, tandem OLEDs are difficult to fabricate top-emission structures, so a bottom-emission structure is used. In bottom-emission devices, the emitted light passes through underlying thin film transistors, but this pathway decreases aperture ratio and luminance (Figure 1b).

In contrast, SOLEDs can use simple structures, like RGB EOLEDs and therefore can easily be fabricated in top-emission structures (Figure 2b, right).[24,25,27,32–35] The top-emission structures amplify light intensity and increase luminous efficiency by using the strong resonance-cavity effect

This article is protected by copyright. All rights reserved.

15214095, ja, Downloaded from https://onlinelibrary.wiley.com/doi/10.1002/adma.202207454 by Seoul National University, Wiley Online Library on [28/11/2022]. See the Terms and Conditions (https://onlinelibrary.wiley.com/terms-and-conditions) on Wiley Online Library for rules of use; OA articles are governed by the applicable Creative Commons License

Accepted Article

between two electrodes. Also, top-emission devices emit light in the opposite direction from thin film transistors, so the aperture ratio can also be increased (Figure 1d).[35]

However, the solution-processing method to fabricate SOLEDs has difficulties in fabricating well-defined multilayer-stacked device structure.[5,36–38] EOLEDs use solid-state starting materials, so evaluation of their processability must consider only their thermodynamic properties, including sublimation temperature and decomposition temperature. However, SOLEDs use liquid solutions as starting materials, so other physical properties, including viscosity, vapor pressure, and surface tension, must also be considered.[24–26,32,39,40] These properties are important to guarantee inkjet applicability and film flatness after vacuum drying (Figure 2c). Also, the underlying layer in the SOLED must have resistance to the solution that is used to process the upper layer; this resistance is described as solution orthogonality. Orthogonal solutions enable fabrication of well-defined stacking structures without any dissolution, intermixing, or penetration (Figure 2d).[41,42] Therefore, for mass-production of SOLEDs, the complicated physics of solute-solvent systems must be well understood.

This review outlines the industrial demands and current technical status of SOLEDs in industry and academia, and review research and developments in the viewpoint of solution-processable materials, SOLED devices, and IJP processes of SOLED production.

2. Industrial needs and technical status

The key factors to evaluate OLEDs are luminous efficiency and lifetime. The efficiencies of OLED include external quantum efficiency *EQE*, current efficiency *CE*, and power efficiency *PE*. *EQE* [%] is defined as the percentage of photons emitted into the upper hemisphere compared to the number of charges injected into the OLED. *CE* [cd A^{-1}] is the luminance [cd m^{-2}] along the direction normal to the emitting surface divided by current density [A m^{-2}]. *PE* [lm W^{-1}] is the luminous power emitted to the upper hemisphere divided by the electrical power consumed [W]. The display

This article is protected by copyright. All rights reserved.

15214095, ja, Downloaded from https://onlinelibrary.wiley.com/doi/10.1002/adma.202207454 by Seoul National University, Wiley Online Library on [28/11/2022]. See the Terms and Conditions (https://onlinelibrary.wiley.com/terms-and-conditions) on Wiley Online Library for rules of use; OA articles are governed by the applicable Creative Commons License

Accepted Article

industry widely uses *CE*, because it considers the sensitivity of the human eye.[10,43] These efficiencies are closely related to the power consumption of display panels.

Environmental concerns are boosting the need for increased efficiency of electronic devices. Use of phosphorescent emitters has increased the internal quantum efficiency *IQE* of red-emitting and green-emitting OLEDs up to ~100% by.[44,45] However, blue phosphorescent emitters used in blue phosphorescence OLEDs (PhOLEDs) have a short lifetime, so they are not suitable for use in mass-produced panels.[46] Therefore, panel makers still use fluorescent blue emitters for blue subpixels, despite their limited efficiency. Recently, TADF and hyperfluorescence which combines fluorescence and TADF emitters have shown feasibility for use in mass-produced panels.[21,47]

The lifetime LT_{XX} of an OLED is defined as the median time required to decrease the luminance from 100 to XX percent of the initial luminance.[48] For example, LT_{95} means the median time taken for lifetime to decay to 95% of initial luminance.[2] To measure the lifetime, a constant current for the initial luminance is applied to devices, and the luminance is monitored over time. Different aging rates of red, green, and blue pixels can cause the image-sticking problem in displays, which is also called burn-in.[49] A realistic LT_{95} at a certain luminance requirement of OLEDs for industrial applications has been reported to be > 5,000 h.[21] This luminance is determined depending on the OLED panels' purposes. The panels for outdoor use require relatively higher luminance than those for indoor use.

Currently, only one panel maker, JOLED Inc. (Japan), is mass-producing its OLED panels by using solution IJP.[50] Other OLED panel makers including Samsung Display Co., Ltd.,[28,51] and BOE Technology Group Co., Ltd.,[33] have demonstrated inkjet-printed SOLED display panel prototypes (**Figure 3**).

Recent EOLEDs and SOLEDs reported by various material suppliers have a range of efficiencies (**Table 1**).[27,35,52,53] Regardless of supplier, the blue SOLEDs are less efficient than red- or

This article is protected by copyright. All rights reserved.

15214095, ja, Downloaded from https://onlinelibrary.wiley.com/doi/10.1002/adma.202207454 by Seoul National University, Wiley Online Library on [28/11/2022]. See the Terms and Conditions (https://onlinelibrary.wiley.com/terms-and-conditions) on Wiley Online Library for rules of use; OA articles are governed by the applicable Creative Commons License

Accepted Article

green-emitting SOLEDs. SOLEDs fabricated by the three major SOLED material suppliers (Sumitomo Chemical (Japan), Mitsubishi Chemical (Japan), and Merck KGaA (Germany)) show *CE*s that varying depending on the color index (Table 1).[27,35,53] Bottom-emission SOLED devices have *CE*s (at 1,000 cd m^{-2}) ~20 cd A^{-1} in red emission, ~80 cd A^{-1} in green emission, but < 10 cd A^{-1} in blue emission. Furthermore, red- and green-emitting devices have > 10 times longer lifetimes than blue-emitting devices. The low lifetime of blue SOLEDs is the ongoing challenge to the image-sticking problem of OLED display panels.[21,54] Also, SOLEDs still require an evaporated organic layer according to the reports from SOLED materials suppliers.[27,55] The reason for this need may be the limitation in device efficiency and lifetime, and the lack of solvent resistance of underlying layer. The use of thermal evaporation makes waste of materials inevitable, and the process requires an additional process to flip the substrate before it can be loaded into the evaporator. Full solution-processing avoids these problems, and is therefore ideal in the respect of manufacturing cost.

However, the efficiency and lifetime of SOLEDs are far lower than those of EOLEDs. Recently, the material supplier of TADF emitter, Kyulux (Japan), reported *CE*s 50 cd A^{-1} in red EOLED (at CIE-x,y (0.70, 0.29)), 224 cd A^{-1} in green EOLED (at CIE-x,y (0.17, 0.78)), and 20.25 cd A^{-1} in blue EOLED (at CIE-x,y (0.11, 0.09)) (Table 1). The lifetimes (LT_{95} at 1,000 cd m^{-2}) were 20,000 h in red, 59,000 h in green, and 450 h in blue EOLEDs. In green and blue emission, SOLEDs have less than half the *CE* of EOLEDs. Two major reasons for this inferior efficiency are the difficulty in using the multi-layer structure, and the limited material selection due to the need for solution processability.[37]

State-of-the-art maximum *CE*, *EQE* and operational lifetime (**Figure 4**) of SOLEDs fabricated in academic laboratories differ according to whether the emitters use fluorescence, phosphorescence, TADF, or hyperfluorescence (**Table 2**). Green-emitting SOLEDs fabricated using phosphorescent and TADF emitters have achieved maximum *CE* = ~100 cd A^{-1},[12,20,56] but both red- and blue-emitting devices have only achieved maximum *CE* ~10 cd A^{-1} considering CIE coordinates of

This article is protected by copyright. All rights reserved.

15214095, ja, Downloaded from https://onlinelibrary.wiley.com/doi/10.1002/adma.202207454 by Seoul National University, Wiley Online Library on [28/11/2022]. See the Terms and Conditions (https://onlinelibrary.wiley.com/terms-and-conditions) on Wiley Online Library for rules of use; OA articles are governed by the applicable Creative Commons License

Accepted Article

primary colors defined by the National Television System Committee. These are inferior compared to the luminous efficiencies (at 1,000 cd m^{-2}) reported by the material suppliers, because SOLEDs fabricated in academia have relatively severe efficiency roll-off.[57,58]

Furthermore, half-lifetimes LT_{50} are much lower in SOLEDs fabricated in academia than in those fabricated in industry. (LT_{50} at initial luminance of 1,000 cd m^{-2} can be rescaled from the values evaluated at another initial luminance by using the lifetime scaling rule $L_0^n \times LT_{50} = constant$, where L_0 is an initial luminance, and n = 1.7 is an acceleration factor.[54,59]) Most reported lifetimes of SOLEDs in the literature have been LT_{50} of a few tens of hours at L_0 = 1,000 cd m^{-2}, although some reported LT_{50} of a few hundred hours (Figure 4 and Table 2). The lifetimes of SOLEDs fabricated in academia are rarely reported, and the reported values are far lower than industrial requirements for display use (Table 1, 2; Figure 4).

Conventional OLEDs are composed of a hole-injection layer (HIL), a hole-transport layer (HTL), an emitting layer (EML), an electron-transport layer (ETL), and an electron-injection layer (EIL), with all layers sandwiched between an anode and a cathode.[34] Charge-carrier balance and energy-level alignment have strong effects on the luminous efficiency and lifetime of OLEDs,.[60,61] The energy-level alignment is described by the highest occupied molecular orbital (HOMO), the lowest occupied molecular orbital (LUMO), and the work function (*WF*). To enable Ohmic contact at the charge-injection interfaces, the HOMO energy level or *WF* (ionization potential) of the HIL and LUMO or *WF* (ionization potential) of the EIL must match the *WF* of the respective metallic electrodes.[62–68] Also, to reduce the operating voltage and power consumption of OLEDs, the HIL and EIL must have high electrical conductivity or charge-carrier mobility.[17,69] The HTL and ETL can affect control of the charge balance and exciton confinement in the EML. The EML must have high photoluminescence quantum yield (PLQY) with low full width at half maximum (FWHM) of its photoluminescence (PL)

This article is protected by copyright. All rights reserved.

15214095, ja, Downloaded from https://onlinelibrary.wiley.com/doi/10.1002/adma.202207454 by Seoul National University, Wiley Online Library on [28/11/2022]. See the Terms and Conditions (https://onlinelibrary.wiley.com/terms-and-conditions) on Wiley Online Library for rules of use; OA articles are governed by the applicable Creative Commons License

Accepted Article

and electroluminescence (EL). The growing need for high color purity in the display industry has driven development of EMLs that have narrow FWHM (< 20 nm).[21,43,70]

SOLEDs are fabricated using liquid-state starting materials, so their physical properties, including solution orthogonality,[38,71] viscosity,[72–74] boiling point,[53,75–77] and glass transition temperature T_g[12,78–81] must be carefully controlled. Solution orthogonality is usually determined using the Hansen solubility parameter (HSP).[26] The viscosity and boiling point of solutions strongly influence on IJP jettability and the ability to make flat films.[53] The printability of a solution is generally described using Z-constant space, which is closely related to viscosity.[40] The film flatness can be controlled by the dynamic flow, which is related to viscosity and boiling point in solutions during the vacuum-drying process after the IJP.[53] The dried films must be annealed at a certain temperature, which is optimized by considering the T_g of solid contents, to make amorphous and thermally-stable films.[12] In the case of small molecules used for EMLs, T_g should be increased sufficiently to reduce the tendency to recrystallize in the thin films, and to improve the operating stability of the devices against Joule heating during OLED operation.[82]

3. Solution-processable Materials

3.1. Solution-processable Materials for Common Layers in SOLEDs

Research on EOLEDs has yielded outstanding achievements in mass production of highly-efficient thin, light weight, vivid-color displays for smartphones, tablets, laptops, and large-area displays.[83–86] Furthermore, the multilayered structure for commercialization of EOLEDs has been adopted because the additional common layers in OLEDs can improve the characteristics of charge injection and transport into the EML, and the charge blocking and exciton blocking at the interface, and thereby effectively improve charge balance, device efficiency and device lifetime.

This article is protected by copyright. All rights reserved.

15214095, ja, Downloaded from https://onlinelibrary.wiley.com/doi/10.1002/adma.202207454 by Seoul National University, Wiley Online Library on [28/11/2022]. See the Terms and Conditions (https://onlinelibrary.wiley.com/terms-and-conditions) on Wiley Online Library for rules of use; OA articles are governed by the applicable Creative Commons License

Accepted Article

In contrast, fabrication of multilayers in SOLEDs must consider damage to pre-deposited underlying layers,[38] including chemical damage due to low solvent resistivity,[87,88] and physical rinsing damage during subsequent solution processing;[26] these have been suggested as critical challenges to fabrication of multilayered SOLEDs.[89] This section reviews promising solution-processable inorganic and organic materials for common layers in SOLEDs to overcome these problems.

3.1.1. Solution-processable Inorganic Materials

Inorganic materials can have useful characteristics such as excellent solution processability, chemical stability, solvent resistance, and air stability, so they have been evaluated as substitutes for conventional organic semiconducting materials that have been used for common layers.[90–99] In particular, the insolubility of inorganic materials in common organic solvents can avoid the intermixing problem at interfaces of multilayers stacked for SOLEDs.[100] Metal oxides (MOs), copper thiocyanate (CuSCN)[101], copper phthalocyanine (CuPc)[102], zinc sulfide (ZnS) quantum dots (QDs)[103], and alkali-metal and alkaline-earth-metal compounds[104] have been investigated to fabricate efficient SOLEDs that use inorganic materials as common layers.

MOs are attractive candidates to replace conventional organic common layers, because MOs can have high carrier mobility, high visible-light transmittance, good charge-blocking capability, and high chemical stability in air.[94–97] Depending on the electronic properties, semiconducting MOs can be generally classified as n-type or p-type, which are simply defined by the number of valence electrons in the d orbitals of the transition metals.[105] Moreover, the occupied states in d orbitals of the metal can form a minimum value of the conduction band (CB), and the occupied states in 2p orbitals of oxygen can form a maximum value of the valence band (VB).[105] When the oxides are completely stoichiometric, they can behave as insulators, but such defect-free MOs cannot exist due

This article is protected by copyright. All rights reserved.

15214095, ja, Downloaded from https://onlinelibrary.wiley.com/doi/10.1002/adma.202207454 by Seoul National University, Wiley Online Library on [28/11/2022]. See the Terms and Conditions (https://onlinelibrary.wiley.com/terms-and-conditions) on Wiley Online Library for rules of use; OA articles are governed by the applicable Creative Commons License

Accepted Article

to thermodynamic constraints, so defects are inevitable, and they influence the electronic properties of MOs. MOs that have totally-empty d orbitals naturally have oxygen-vacancy defects, which form defect states within the band gap. The presence of oxygen-vacancy defects causes non-stoichiometric compositions and the presence of metal cations in MOs, which result in a high density of occupied defect states close to the CB minimum.[106] As a result, MoO_3, TiO_2, WO_3, ZrO_2, and V_2O_5 have n-type semiconducting property. In contrast, when d orbitals of MOs are completely occupied, or the MO films have metal-vacancy defects, the Fermi level is positioned near the VB maximum. Therefore, NiO and Cu_2O can behave as p-type semiconductors.[107]

Depending on the *WF* of MOs, the n-type and p-type MOs can be applied as HILs and EILs in SOLEDs. The energy barrier to charge injection exists at the interface between the electrodes and the charge-transporting organic semiconductors, so the energy-level alignment between the *WF* of the electrodes and the HOMO or the LUMO energy levels of the semiconductors should be carefully considered when selecting MOs.[105] High-*WF* MOs such as MoO_3 (6.82 ± 0.05 eV),[108] V_2O_5 (6.8 ± 0.1 eV),[23,109] and WO_3 (6.8 ± 0.4 eV)[110] have a deep VB similar to the HOMO energy level of organic HTL, so they can facilitate efficient hole injection by reducing the hole injection energy barrier.[110]

Solution-processed MoO_3 and WO_3 HILs have been used instead of conventional poly(3,4-ethylene dioxythiophene):poly (styrene sulfonate) (PEDOT:PSS) HIL material.[110,111] The MoO_3 and WO_3 were prepared using 1:120 ethanol-diluted molybdenum(V) ethoxide ($Mo(OEt)_5$)[111] and 1:80 ethanol-diluted tungsten(VI) ethoxide ($W(OEt)_6$)[110] precursor solutions. To convert the precursors to MoO_3 and WO_3, $Mo(OEt)_5$ can be annealed at 150 °C for 10 min under ambient condition, whereas $W(OEt)_6$ must be annealed under inert atmosphere at room temperature, because the tungsten in $W(OEt)_6$ has a valence of +6. As a result, the efficient hole-injection ability of solution-processed MoO_3 and WO_3 HILs decreased the turn-on voltages (V_{TO}) (~4.5 V for MoO_3 and WoO_3, 5.0 V for PEDOT:PSS) and increased the *CE*s (to ~12.0 cd A^{-1} in solution-processed MoO_3 and ~14.0 cd A^{-1} in

This article is protected by copyright. All rights reserved.

15214095, ja, Downloaded from https://onlinelibrary.wiley.com/doi/10.1002/adma.202207454 by Seoul National University, Wiley Online Library on [28/11/2022]. See the Terms and Conditions (https://onlinelibrary.wiley.com/terms-and-conditions) on Wiley Online Library for rules of use; OA articles are governed by the applicable Creative Commons License

Accepted Article

solution-processed WO_3) in SOLEDs with device structures of ITO/solution-processed HILs/ 4,4',4-tris(carbazole-9-yl)triphenylamine (TCTA):bis[2-(4,6-difluorophenyl)pyridinato-N,C2] (picolinato)iridium (Firpic)/ 2,2',2''-(1,3,5-Benzinetriyl)-tris(1-phenyl-1-H-benzimidazole) (TPBi)/LiF/Al. These characteristics are more comparable to those of EOLEDs (V_{TO} ~4.5 V and *CE* ~12.0 cd A^{-1} for MoO_3, V_{TO} ~4.5 V and *CE* ~14.0 cd A^{-1} for WoO_3), than to those of SOLEDs that use a PEDOT:PSS HIL (~8.5 cd A^{-1}).

For solution-processed EIL application of low-*WF* MO materials, the energy level alignment between the *WF* of cathode and LUMO energy level of ETL should be considered.[105] Use of low-*WF* MOs such as TiO_2 (5.4 ± 0.2 eV)[105] and ZnO (5.3 eV)[112] facilitates efficient electron injection by reducing the electron-injection barrier at the interface between the cathode and the ETL.

ZnO nanoparticles (NPs), which can be synthesized by a sol-gel method that uses using Zn acetate and tetramethylammonium hydroxide, have been evaluated for use as a heterojunction interface to enable Auger-assisted energy up-conversion.[113] In the EML this effect is achieved by energy transfer to an Auger electron in ZnO NPs by non-radiative recombination between a hole in the HOMO of LEPs (5.1 eV for hole-dominant poly[2-methoxy-5-(2'-ethylhexyloxy)-1,phenylene vinylene] (MEH-PPV), 5.3 eV for ambipolar poly[(9,9-dioctylfluorenyl-2,7-diyl)-co-(4,4'-(N-(4-s-butylphenyl)diphenylamine) (TFB), 5.8 eV for electron-dominant polyfluorene (PFO)) and an electron in CB of ZnO NP layer (4.2 eV). The strong quantum confinement of low-dimensional nano-sized ZnO by the large overlap of electron and exciton wave functions promotes efficient Auger-like energy transfer. Therefore, 2- to 3-nm ZnO NPs induce efficient energy up-conversion, which yields a low V_{TO} (1.3 V (MEH-PPV), 3.2 V (TFB), 4.5 V (PFO) to emit 0.1 cd m^{-2}) in SOLEDs that consist of ITO/PEDOT:PSS/LEPs (80 nm)/ZnO NPs (40 nm)/Al.[113]

However, use of MOs as HIL or EIL has the disadvantage that they always need a high-temperature annealing process to give them moderate properties as HIL or EIL, then need an

This article is protected by copyright. All rights reserved.

15214095, ja, Downloaded from https://onlinelibrary.wiley.com/doi/10.1002/adma.202207454 by Seoul National University, Wiley Online Library on [28/11/2022]. See the Terms and Conditions (https://onlinelibrary.wiley.com/terms-and-conditions) on Wiley Online Library for rules of use; OA articles are governed by the applicable Creative Commons License

Accepted Article

additional process to deposit a charge-transporting layer that has low solvent resistance and sufficient total thickness of devices.[114] Consequently, metal thiocyanates such as CuSCN and AgSCN have been evaluated as alternative inorganic materials for use as common layers.[115] CuSCN is a p-type semiconductor; it is a promising inorganic material as both HTL and unified HIL/HTL.[101,116] CuSCN has high transmittance across the visible spectrum, and is commercially available at a low cost. For use in SOLEDs, CuSCN has the advantages that it dissolves in diethyl sulfide, which is orthogonal to common organic solvents such as chlorobenzene, and can be solution-processed in air without subsequent thermal annealing.[116] Moreover, CuSCN has a VB maximum of 5.5 eV that facilitates efficient hole injection to the HOMO level of HTL, and a shallow CB minimum of 1.8 eV that provides effective electron blocking at the interface. Therefore, the energy levels of CuSCN contribute to increase device efficiency by improving charge balance within the SOLEDs that have the structure ITO/ CuSCN or PEDOT:PSS/ 2,6-Bis(3-(9H-carbazol-9-yl)phenyl)pyridine (26DCzPPy):TCTA:5% $Ir(ppy)_2(acac)$/ bis-4,6-(3,5-di-3-pyridylphenyl)-2-methylpyrimidine (B3PYMPM)/Ca/Al. As a result, CuSCN SOLEDs achieved higher maximum *CE* = 51 cd A^{-1} and lower V_{TO} = 2.7 V at 1 cd m^{-2} than those of conventional PEDOT:PSS SOLEDs (38 cd A^{-1}, 6.2 V).[101]

Metal phthalocyanines (Pc) such as CuPc and ZnPc have been considered as HTL materials due to their high hole mobility (μ_h = ~8 × 10^{-3} cm^2 V^{-1} s^{-1} (CuPc),[117] ~1.9 × 10^{-3} cm^2 V^{-1} s^{-1} (ZnPc)[118]) and high thermal and chemical stabilities.[119–121] The introduction of a metal Pc layer can improve hole injection for good charge balance and prevent chemical degradation in the devices. However, metal Pc layers have poor solubility in common organic solvents, and therefore have usually been deposited using a thermal evaporation process, which is not compatible with SOLED fabrication.[119,122] To overcome the poor solubility of CuPc, a copper phthalocyanine-3,4′,4″,4‴-tetra-sulfonated acid tetra sodium salt (TS-CuPc), which has high solubility in polar solvents, has been evaluated as the HIL in OLEDs.[123,124] Moreover, TS-CuPc can be used with other water-soluble hole-

This article is protected by copyright. All rights reserved.

15214095, ja, Downloaded from https://onlinelibrary.wiley.com/doi/10.1002/adma.202207454 by Seoul National University, Wiley Online Library on [28/11/2022]. See the Terms and Conditions (https://onlinelibrary.wiley.com/terms-and-conditions) on Wiley Online Library for rules of use; OA articles are governed by the applicable Creative Commons License

Accepted Article

dominant materials such as MoO_3 and WO_3; this application can be beneficial to orthogonal solvent processing with common organic solvents. MOs such as MoO_3 and WO_3 can be dissolved in polar solvents, so MoO_3-doped TS-CuPc can act as HIL/HTL material in OLEDs.[124] MoO_3-doped TS-CuPc solution can be prepared from MoO_3 and TS-CuPc solutions in deionized water by blending them in various volume ratios (10 to 90%). Electron donation from MoO_3 to TS-CuPc generates a charge-transfer complex that induces the large vacuum level shift reducing a hole injection barrier.[125,126] The MoO_3:TS-CuPc layer modifies the *WF* of the indium tin oxide (ITO) electrode to improve the hole injection (*WF* = 4.7 eV (ITO), 5.29 eV (MoO_3), 5.31 eV (TS-CuPc), 5.28 eV (MoO_3:TS-CuPc)),[127] so as the concentration of MoO_3 dopant is increased, the driving voltages of OLEDs decrease (from 4.17 V (10% MoO_3:TS-CuPc) to 3.74 V (90% MoO_3:TS-CuPc)) to emit 1,000 cd m^{-2}). Pristine TS-CuPc OLEDs have high driving voltage (10.40 V to emit 1,000 cd m^{-2}), which is attributed to the crystallization behavior of pristine TS-CuPc, so this result indicated that the added MoO_3 effectively suppresses TS-CuPc crystallization and improves the operational stability of OLEDs.

The hole-injection property of TS-CuPc can be further increased by use of 2,3,5,6-tetrafluoro-7,7,8,8-tetracyanoquinodim ethane (F_4-TCNQ) as a p-type dopant, due to its strong electron affinity.[102] Moreover, F_4-TCNQ-doped TS-CuPc aqueous solution has a neutral pH value (pH: 6.9) which causes less electrode corrosion compared to acidic PEDOT:PSS (pH: 2.0), and therefore can improve the stability of devices. The root mean squared surface roughness of TS-CuPc was reduced from 3.16 nm to 2.34 nm by introduction of F_4-TCNQ, because it can suppress crystallization of TS-CuPc, in the same way as MoO_3 introduction does. The suppressed crystallization of TS-CuPc is also beneficial in reducing the driving voltage of OLEDs. As a result, OLEDs that use F_4-TCNQ:TS-CuPc had longer LT_{50} = 170 h than conventional OLEDs that use PEDOT:PSS (LT_{50} = 62 h). The higher *WF* of F_4-TCNQ:TS-CuPc (5.27 eV) than the *WF* of pristine TS-CuPc (4.68 eV) improved the hole injection to the HOMO energy level of the hole-transporting TCTA layer (5.7 eV). Therefore, F_4-TCNQ:TS-CuPc

This article is protected by copyright. All rights reserved.

15214095, ja, Downloaded from https://onlinelibrary.wiley.com/doi/10.1002/adma.202207454 by Seoul National University, Wiley Online Library on [28/11/2022]. See the Terms and Conditions (https://onlinelibrary.wiley.com/terms-and-conditions) on Wiley Online Library for rules of use; OA articles are governed by the applicable Creative Commons License

Accepted Article

SOLEDs achieved higher device *CE* = 46.0 cd A^{-1} and *EQE* = 22.1%, than the 32.0 cd A^{-1} and 13.9% of pristine TS-CuPc SOLEDs.

To deposit EIL onto underlying organic layers by solution processing, use of orthogonal solvents can protect the layers and prevent interfacial intermixing between them.[128,129] Low-*WF* p-type MOs such as ZnO (5.3 eV)[112] and TiO_2 (5.4 ± 0.2 eV)[105] have been evaluated as solution-processable inorganic EIL materials, due to superior stability, optical transparency, and high electrical conductivity.[105,112] However, the electron-injection energy barrier, which influences the charge balance in devices, is not effectively reduced by the introduction of MO EILs.[130] Therefore, metal sulfide QDs with core-shell structure have been considered as solution-processable EIL materials because of their high solubility in polar solvent, high optical transmittance, and adequate electron mobility (μ_e = ~1.29 cm^2 V^{-1} s^{-1} (mercury sulfide, β-HgS QD),[131] ~0.01 cm^2 V^{-1} s^{-1} (lead sulfide, PbS QD),[132] 2.9 × 10^{-4} cm^2 V^{-1} s^{-1} (ZnCdS core/ZnS shell QD),[133] 1.1 × 10^{-6} cm^2 V^{-1} s^{-1} (CdSe core/ZnSe shell/ZnS shell QD)[134]).[135,136] ZnS QD have been evaluated as a polar solvent-soluble EIL material with efficient electron-injection capability.[103] The concentration of ZnS QDs determines the wettability with other common organic layers. Solutions that have low concentrations of ZnS QDs have a small water contact angle and yield smooth surfaces, which enable good adhesion between cathode and organic layers, and thereby improve electron-injection efficiency. Moreover, the ZnS QD EIL has a moderate *WF* = 3.90 eV, which forms stepwise energy barriers between the Al cathode (*WF* = 4.30 eV) and the LUMO of TPBi ETL (*WF* = 2.70 eV); this arrangement facilitates efficient electron injection, which reduces V_{TO} (8.4 V with ZnS QD EIL, 11.9 V without it, at 1 cd m^{-2}) and improves charge balance in OLED. As a result, SOLEDs that use ZnS QD achieved a maximum *CE* of 12.5 cd A^{-1}, which is a 27.6% improvement compared to SOLEDs without ZnS QD EIL (9.8 cd A^{-1}).

Insulating inorganic alkali metal compounds such as LiF and CsF have been used in EOLEDs as EILs that work by formation of an interfacial dipole, and chemical reaction with metals.[137–139] In

This article is protected by copyright. All rights reserved.

15214095, ja, Downloaded from https://onlinelibrary.wiley.com/doi/10.1002/adma.202207454 by Seoul National University, Wiley Online Library on [28/11/2022]. See the Terms and Conditions (https://onlinelibrary.wiley.com/terms-and-conditions) on Wiley Online Library for rules of use; OA articles are governed by the applicable Creative Commons License

Accepted Article

particular, the device efficiencies of OLEDs that are relatively hole-dominant are determined by the electron injection. Therefore, the efficient electron-injecting characteristic of alkali-metal compounds can be beneficial in SOLEDs when the compounds are ideally deposited by using solution process. Alkali-metal and alkaline-earth-metal compounds such as hydroxides and carbonates can be dissolved in orthogonal alcohol solvents such as ethanol, methanol, and ethanol, and can therefore effectively avoid chemical and physical damage to the underlying layers and interfacial intermixing between them.[104] When the metal compounds are used with a high-*WF* (4.54 eV) Ag electrode in SOLEDs, the electron-injection efficiencies are demonstrated by a decrease in V_{TO} (Ag = 4.25 V, LiOH/Ag = 3.00 V, NaOH/Ag = 2.75 V, KOH/Ag = 2.50 V, K_2CO_3/Ag = 2.25 V). The increased device efficiencies may be a result of formation of a interfacial dipole layer in response to the image-charge effect, which contributes to modification of the *WF* of an EIL/metal cathode.[140] The interfacial dipole layer enables a large shift in the vacuum level at the electrode contact, and this shift lowers charge-injection barriers by decreasing the *WF* of the metal. In particular, when a metal-compound EIL is formed on an organic layer that has a high dielectric constant, strong image charges develop, so a large dipole forms and induces a large shift in surface *WF*.[140] As a consequence, among the alkali-metal and alkaline-earth-metal compounds, NaOH/Ag showed the highest *CE* of 3.76 cd A^{-1} because formation of a large interfacial dipole resulted in the largest decrease in the *WF* of Ag (to 3.86 eV).[140]

Solution-processable inorganic materials have been investigated to utilize their beneficial characteristics including high chemical stability, high tolerance of ambient conditions, high optical transmittance, high charge-carrier mobility, and good solubility in polar solvents. These materials facilitate non-toxic and ecologically-benign solution processing and use of the orthogonal solvent approach for multilayer stacking in SOLEDs. Moreover, the properties of inorganic materials can be effectively modified by blending with solution-processable organic materials.[102,141] Such blending

This article is protected by copyright. All rights reserved.

15214095, ja, Downloaded from https://onlinelibrary.wiley.com/doi/10.1002/adma.202207454 by Seoul National University, Wiley Online Library on [28/11/2022]. See the Terms and Conditions (https://onlinelibrary.wiley.com/terms-and-conditions) on Wiley Online Library for rules of use; OA articles are governed by the applicable Creative Commons License

Accepted Article

can be a versatile strategy to fabricate all-solution-processed OLEDs that have organic EMLs, n-type or p-type inorganic MOs, and metal compounds as charge-injection layers.

3.1.2. Polymeric Materials for Common layers in SOLEDs

Polymer materials can have good solution processability, controllable charge-carrier mobility or electrical conductivity, and can be easily engineered by modification or addition of functional moieties, and are therefore widely used as EMLs, common layers, or interlayers in SOLEDs.[142] According to their energy levels and carrier mobility, some polymers are selectively used as HIL/HTL or EIL/ETL. This section introduces research on various polymeric materials that have been used as common layers for SOLEDs.

PEDOT:PSS is widely used as a polymeric HIL, due to high visible transparency (>80%), high hole conductivity (>1,000 S cm^{-1}) and easily-tunable electrical, optical and structural properties.[143–145] PEDOT has a π–π conjugated backbone that provides a path for electrical current, and PSS stabilizes PEDOT and helps disperse it in water.

Despite the many advantages of PEDOT:PSS, it can limit the device efficiency and lifetime of SOLEDs because its *WF* (~5.0 to 5.2 eV) is lower than the HOMO level of general organic EMLs (5.8 to 6.5 eV), so it has relatively low hole injection efficiency to the EML.[11,15] Furthermore, PEDOT:PSS is acidic (pH: 1 to 4) which can easily etch the underlying ITO anode and allow diffusion of indium and tin species into the overlying layers; these diffused metallic species induce severe exciton quenching and limit the device efficiencies.[63] Therefore, many researchers have tried to increase the *WF* and reduce the diffusion of metallic species caused by PEDOT:PSS.[11,15] These problems of PEDOT:PSS can be ameliorated by incorporating additives or dopants to the PEDOT:PSS for modification of its electrical and chemical properties. [11,15,63,146–150]

This article is protected by copyright. All rights reserved.

15214095, ja, Downloaded from https://onlinelibrary.wiley.com/doi/10.1002/adma.202207454 by Seoul National University, Wiley Online Library on [28/11/2022]. See the Terms and Conditions (https://onlinelibrary.wiley.com/terms-and-conditions) on Wiley Online Library for rules of use; OA articles are governed by the applicable Creative Commons License

Accepted Article

Uses of polymeric composite layers composed of perfluorinated ionomer (PFI) and PEDOT:PSS are effective to increase the surface WF of HIL, prevent surface exciton quenching, and achieve high device efficiency and lifetime in SOLEDs.[11,12,60,61,63,67,146–148,151–155] When blended with PEDOT:PSS, PFI tends to accumulate on top of the PEDOT:PSS layer by self-organization during the spin coating on the substrate, because surface energy is lower in PFI (~20 mN m^{-1}) than PEDOT:PSS (~38 mN m^{-1}).[11,63,146–148] As a result, the concentration of PFI gradually increases from the bottom to the surface in PEDOT:PSS:PFI composite thin film;[63,146–148] the self-organization of polymer chains develops a gradually-increasing *WF* in HIL (called GraHIL). The gradient in composition of PFI in the GraHIL effectively increases hole injection into the EML, because PFI has a high ionization potential, so the PFI-enriched surface layer increases the surface ionization potential of the HIL from 5.20 eV to 5.95 eV.[11,63,146–148] Furthermore, the PFI-enriched insulating surface layer effectively separates the excitons generated in the EML from the PEDOT:PSS layer, which can reduce severe exciton quenching at the HIL/EML interfaces.[11] These synergistic effects of the HIL modification achieves high luminous efficiencies in SOLEDs that use various solution-processed EMLs (*EQE* = 35.5% and *CE* = 97.5 cd A^{-1} in SOLEDs that use orange-red phosphorescent bis(2-phenylbenzothiozolato-N,C2')iridium (acetylacetonate) ($Bt_2Ir(acac)$) emitter; *EQE* = 29% and *CE* = 101.5 cd A^{-1} in SOLEDs that use green phosphorescent emitter, tris[2-phenylpyridinato-C2,N]iridium(III) ($Ir(ppy)_3$); *EQE* = 20.9% and *CE* = 38.7 cd A^{-1} in SOLEDs that use blue phosphorescent emitter FIrpic; *EQE* = 28.5% and *CE* = 74.2 cd A^{-1} in SOLEDs that use white-emitting EML composed of blue-emitting FIrpic and orange-red-emitting $Bt_2Ir(acac)$[12]; *EQE* = 24% and *CE* = 73 cd A^{-1} in SOLED that use green TADF 1,2,3,5-Tetrakis(carbazol-9-yl)-4,6-dicyanobenzene, 2,4,5,6-Tetrakis(9H-carbazol-9-yl) isophthalonitrile (4CzIPN) emitter[15]) (Table 2). Incorporation of some other materials, such as poly(4-styrene sulfonic acid) (PSSA)[149] and polymeric (polysilic acid) nanodots[150] in PEDOT:PSS has also yielded high device efficiencies in SOLEDs (*EQE* = 26.6%, *CE* = 86.2 cd A^{-1} and *PE* = 33.9 lm W^{-1} in SOLEDs that use PEDOT:PSS:PSSA;[149] and *PE* = 35.8 lm W^{-1} in SOLEDs that use PEDOT:PSS:polymeric (polysilic acid)

This article is protected by copyright. All rights reserved.

15214095, ja, Downloaded from https://onlinelibrary.wiley.com/doi/10.1002/adma.202207454 by Seoul National University, Wiley Online Library on [28/11/2022]. See the Terms and Conditions (https://onlinelibrary.wiley.com/terms-and-conditions) on Wiley Online Library for rules of use; OA articles are governed by the applicable Creative Commons License

Accepted Article

nanodots[150]) because PSSA dopants increase the *WF* of PEDOT:PSS from 5.04 eV to 5.63 eV and prevent exciton quenching at the interface, [149] and because polymeric (polysilic acid) nanodot dopants improve charge balance in the devices.[150]

Interfacial layers formed on top of PEDOT:PSS HIL can more facilitate hole injection and prevent exciton quenching at the PEDOT:PSS/EML interface in SOLEDs. A thin self-assembled layer composed of fluorinated polyimide,[156] trimethoxy-(3,3,3-trifluoropropyl) silane [157] or tungsten oxide (WO_x),[114] with hole-transporting polymeric materials such as poly(9-vinylcarbazole) (PVK),[158] TFB[159] or a mixture of PVK and TFB[160] have been used on top of PEDOT:PSS HIL; these interfacial layers increase the *WF* and hole injection to the overlying EML, reduce exciton quenching at the interface, and thus contribute to high device efficiencies in SOLEDs (*EQE* = 25.1% and *CE* = 53.6 cd A^{-1} in SOLEDs that used a PEDOT:PSS/PVK interlayer (which are higher than *EQE* = 18.3% and *CE* = 39.3 cd A^{-1} in SOLEDs that used a PEDOT:PSS without PVK interlayer);[158] *EQE* = 18.86% and *CE* = 55.6 cd A^{-1} in SOLEDs that used a PEDOT:PSS/TFB:PVK interlayer[160]).

The additives have also been applied to other polymeric HILs. Addition of poly(perfluoroethylene-perfluoro-ethersulfonic acid) (PFFSA) to a conducting polymer, polythienothiophene (PTT), increased its *WF*, [161] and concomitantly increased hole-injection efficiency to 75%, compared to the 50% obtained using the conventional PEDOT:PSS.

Intermixing between interlayers (i.e., re-dissolving of underlying HIL during the spin coating of overlying HTL or EML) can degrade hole injection and charge balance in SOLEDs.[162,163] Crosslinked HIL/HTLs can resist certain solvents and allow for sequential solution processes of overlying interlayers that are important to improve the device efficiency and lifetime. A crosslinked HIL forms uniform film morphology and enables efficient injection of holes into the overlying EML.[162,163] Crosslinking can occur between side-groups such as oxetane,[164] organosilanol,[159] nitrene[165] and vinylbenzyl ether [166] in the hole injecting/transporting organic chains, and can be

This article is protected by copyright. All rights reserved.

15214095, ja, Downloaded from https://onlinelibrary.wiley.com/doi/10.1002/adma.202207454 by Seoul National University, Wiley Online Library on [28/11/2022]. See the Terms and Conditions (https://onlinelibrary.wiley.com/terms-and-conditions) on Wiley Online Library for rules of use; OA articles are governed by the applicable Creative Commons License

induced by addition of crosslinking agents, for example, phosphomolybdic acid *n*-hydrate to PVK materials.[167] Thermal crosslinking and photo crosslinking compounds have been used. For instance, (9,9'-bis(4-vinylbenzyl)-9H,9'H-3,3'-bicarbazole) (VyPyMCz) hole-transporting material (HTM) shows a temperature-dependent degree of crosslinking at temperature $T < 230$ °C, but is fully crosslinked at $T > 260$ °C.[163] Thermal crosslinking of a HTL occurs at a temperature that depends on the crosslinkable agents or side chains used, or their combination. TCTA derivatives with two crosslinkable vinylbenzyl ether groups are crosslinked at $T > 150$ °C,[166] phosphomolybdic acid *n*-hydrate with PVK materials are crosslinked at $T \geq 110$ °C,[167] and two vinyl-derived crosslinkable hole transporting materials V-TPAVTPD and V-TPAVCBP are crosslinked at $T \geq 120$ °C.[148]

Photo-crosslinking can be a simple method to develop chemically stable SOLEDs that use a crosslinked HIL/HTL.[165] Photo-crosslinking is induced by addition of photo-initiators and exposure to light at a specific wavelength. For instance, sterically hindered bis(fluorophenyl azide)s (sFPAs), bis(4-azido-2,3,5-trifluoro-6-isopropylbenzoate), shows > 90% crosslinking efficiency upon exposure to light with $\lambda = 254$ nm and intensity of 300 mJ cm^{-2}.

Polymers that have functional groups that form a surface dipole have also been used as the electron-injecting/transporting interlayer in SOLEDs. Reported electron-injecting polymers include conjugated amino-/ammonium-functionalized polyfluorene polymer,[168] conjugated phosphonate-functionalized polyfluorene polymer,[169] imine-containing non-conjugated polymer[170] and polyelectrolyte;[171] all are soluble in polar solvents such as water and alcohol, so they can be formed on top of the EML without intermixing with it. Due to ionic redistribution, these polymeric materials and polyelectrolytes form an interfacial dipole at the interface, induce vacuum-level shift, and reduce the energy barrier for electron injection into the EML.[168,171] Therefore, electron-injection efficiency from cathode to EML greatly increases even without the use of low-WF cathode metals such as Ca and Ba, which are highly reactive in the air,[172,173] or insertion of thin LiF[174] and CsF.[175]

This article is protected by copyright. All rights reserved.

Accepted Article

15214095, ja, Downloaded from https://onlinelibrary.wiley.com/doi/10.1002/adma.202207454 by Seoul National University, Wiley Online Library on [28/11/2022]. See the Terms and Conditions (https://onlinelibrary.wiley.com/terms-and-conditions) on Wiley Online Library for rules of use; OA articles are governed by the applicable Creative Commons License

Accepted Article

The polymeric materials for electron injection also showed high electron-injection efficiency from various metals (e.g., Au, In, Al, Ag, Cu, Sn) to EML[176,177], and achieved comparable or even higher efficiencies than those that used reactive cathode metals (*CE* = 18.5 cd A^{-1} in SOLEDs that used (9,9-bis(30-(N,N-dimethylamino)propyl)-2,7-fluorene)-alt-2,7-(9,9-dioctylfluorene) (PFN), which is similar with that in SOLEDs that have a Ba cathode (*CE* = 16.6 cd A^{-1});[177] *CE* = 15 cd A^{-1} for SOLEDs that use poly(9,9-bis(6'-diethoxylphosphorylhexyl)fluorine), (phosphonate-functionalized polyfluorene), which is higher than that in SOLEDs that use Ba/Al (*CE* = 12.5 cd A^{-1}) or Ca/Al (*CE* = 7.8 cd A^{-1})[169]).

This subsection has reviewed several research strategies to develop optimal polymeric interlayers to improve the efficiency and operating lifetime in SOLEDs. Many researchers have tried to find optimal HIL and EIL interlayers and to dope the conventional polymeric materials to improve injection of holes and electrons into the EML. Diverse efforts by many researchers have achieved great improvements in both efficiency and operating lifetime of SOLEDs, but SOLEDs that use polymeric interlayers still suffer from intermixing between layers during solution processing of multiple layers; some researchers have tried to solve this problem by crosslinking the interlayer. Further improvement requires development of interlayers that simultaneously meet several requirements: 1) increase in *WF* of HIL to facilitate hole injection into the EML; 2) induction of vacuum-level shift by forming interfacial dipole on top of EML and improvement of the electron injection into the EML; 3) prevention of exciton quenching at the HIL/EML or EML/EIL interlayer; 4) prevention of intermixing between layers in SOLEDs.

3.2. Solution-processable Materials for Emitting Layer

Generations of OLEDs have been named according to the type of organic emitter and the light-emission mechanism: fluorescence, phosphorescence, or TADF (**Figure 5**a). The electrons and holes that are injected from electrodes into EMLs have spins and form excitons that attract each

This article is protected by copyright. All rights reserved.

15214095, ja, Downloaded from https://onlinelibrary.wiley.com/doi/10.1002/adma.202207454 by Seoul National University, Wiley Online Library on [28/11/2022]. See the Terms and Conditions (https://onlinelibrary.wiley.com/terms-and-conditions) on Wiley Online Library for rules of use; OA articles are governed by the applicable Creative Commons License

Accepted Article

other by Coulombic interaction. The emission mechanism of each emitter type is generally explained by spin statistics of quantum mechanics.[178,179] According to the combination of spin states of electron and hole pairs, excitons can assume four excited states: a singlet states with one antiparallel spins, and three triplet states with parallel spins (Figure 5a).[180]

The first-generation fluorescent OLEDs with pure organic emitters can use only 25% of the total excitons generated in the singlet states for radiative recombination; the 75% of excitons that are generated in triplet states are wasted because the radiative emission decay time of the relaxation from the triplet state (order of 10 s) is longer than the non-radiative decay time.[178,181] Therefore, in fluorescent OLEDs the emission from the triplet state (i.e., phosphorescence) is quenched in pure organic emitters, and maximum *IQE* is theoretically limited to 25%.

Second-generation PhOLEDs exploited introduction of heavy metal ions such as Ir, Pt, Au, Os, and Re into organic emitters. The ions induce strong spin-orbit coupling (SOC) by a heavy-atom effect that enables fast inter-system crossing (ISC), which is a spin-forbidden transition from triplet to singlet ground states.[180,182,183] Therefore, PhOLEDs can theoretically achieve 100% *IQE*.

Third-generation TADF OLEDs exploit both singlet and triplet excitons. Due to the chemical topography of donor and acceptor, TADF emitters have a small energy gap between triplet energy levels (T_1) and singlet energy levels (S_1), so they allow thermal up-conversion from triplet to singlet states.[184] Therefore, the *IQE* of TADF OLEDs also can reach 100% without use of heavy-metal complexes.

The next sections review organic host and emitter materials in solution-processed EMLs and their development for SOLEDs.

3.2.1. Small-Molecule Organic Host Materials for SOLEDs

This article is protected by copyright. All rights reserved.

15214095, ja, Downloaded from https://onlinelibrary.wiley.com/doi/10.1002/adma.202207454 by Seoul National University, Wiley Online Library on [28/11/2022]. See the Terms and Conditions (https://onlinelibrary.wiley.com/terms-and-conditions) on Wiley Online Library for rules of use; OA articles are governed by the applicable Creative Commons License

Accepted Article

EMLs in multilayered OLEDs are generally positioned between the HTL and the ETL to effectively receive charges through a stair-like energy-band structure.[11,63] When charge-transporting layers are solution-coated onto solution-processed EMLs, the EMLs should have a high resistivity to common organic solvents such as toluene, chlorobenzene, chloroform, tetrahydrofuran and so on. Moreover, host materials in solution-processed EMLs of OLEDs are very important components that influence on charge balance within EML thereby determines device efficiencies and lifetime.

Small-molecule host materials can be classified into various categories but share a common improvement direction. Small-molecule host materials for PhOLEDs have been developed to meet several essential requirements: 1) high S_1 and T_1 energy levels that block reverse energy transfer from dopant to host material, and thus achieve efficient exciton confinement in the light-emitting dopants,[185] 2) high charge-carrier-transporting properties of host materials for balanced charge transport and efficient recombination in EMLs,[186–188] and 3) high thermal and morphological stability of host materials to enable versatile solution processability and operational stability.[185,189,190]

High T_1 (> 2.7 eV) and wide band gap are particularly required for blue-emitting PhOLEDs, for example, that use FIrpic (T_1 = ~2.7 eV)[191] and blue-emitting TADF OLEDs that use 1,2-bis(carbazol-9-yl)-4,5-dicyanobenzene (2CzPN, T_1 = ~2.5 eV).[192,193] To permit solution-processing of PhOLEDs, host materials should also have a high T_g, because small-molecule organic films that have low T_g crystallize easily in the thin film.[194,195] Small-molecule organic materials with phenylamine groups, such as N,N′-di(3-methylphenyl)-N,N′-diphenyl-(1,10-biphenyl)-4,4-diamine (TPD) and N,N′-di(1-naphthyl)-N,N′-diphenyl-(1,10-biphenyl)-4,40-diamine (NPB) that have high μ_h = ~10^{-3} $cm^2 V^{-1} s^{-1}$ are commonly used as HTM,[121,196] but are not suitable for solution processing because they have thermal and morphological instabilities with low T_g (65 °C for TPD; 96 °C for NPB).[78,197]

This article is protected by copyright. All rights reserved.

15214095, ja, Downloaded from https://onlinelibrary.wiley.com/doi/10.1002/adma.202207454 by Seoul National University, Wiley Online Library on [28/11/2022]. See the Terms and Conditions (https://onlinelibrary.wiley.com/terms-and-conditions) on Wiley Online Library for rules of use; OA articles are governed by the applicable Creative Commons License

Accepted Article

To improve thermal stability of TPD, it has been modified using spiro-linked structures such as 2,2′,7,7′-tetrakis(N,N-diphenylamino)-9,9-spirobifluorene (spiro-TAD) with increased T_g,[198] TCTA,[199] and 1,1-bis[(di-4-tolylamino)phenyl] cyclohexane (TAPC) are also widely used hole transporting hosts (HTHs) for PhOLEDs.[200] TCTA has a good μ_h (~10^{-4} cm^2 V^{-1} s^{-1}) and T_g ~151 °C that is high enough to give thermal and morphological stability for solution processing.[201] However, TAPC has low T_g ~82 °C, and therefore has limited compatibility with solution processing despite having high T_1 ~2.98 eV and good μ_h ~10^{-2} cm^2 V^{-1} s^{-1}.[202]

Carbazole derivative is a promising host material for phosphorescent dopants because of its high T_1 level and hole-transporting properties. N,N'-dicarbazolyl-4-4'-biphenyl (CBP) has high μ_h and μ_e, and therefore has been widely used as a host material for PhOLEDs. However, CBP has T_1 ~2.6 eV which is a slightly lower than that of a bluish phosphorescent, FIrpic (T_1 = ~2.7 eV),[191] and a slightly higher than that of TADF emitter, 2CzPN (T_1 = ~2.5 eV),[203] so energy can be transferred in reverse from triplet-harvesting blue emitters to CBP, so it is not useful in blue PhOLEDs. To increase T_1 of carbazole-derived host material, 1,3-bis(N-carbazolyl)benzene (mCP), which has high T_1 ~2.9 eV was developed, but its T_g ~60 °C is too low to ensure morphological stability of its thin film.[204] Therefore, mCP has also been modified using a bulky side group to improve thermal and morphological stability without crystallization during film formation and device operation. The result, 3,5-bis(9-carbazolyl) tetraphenylsilane (SimCP) has significantly increased T_g > 100 °C.[205] Bipolar transporting characteristics of host materials have advantages for balanced charge transport and for formation of a broad recombination zone in EMLs. Therefore, carbazole-derived bipolar host such as 2,6-bis(3-(24arbazole-9-yl)phenyl)pyridine (26DczPPy) with high T_1 ~2.76 eV can also be considered by incorporating an electron-withdrawing pyridine moiety.[206]

Phosphine oxide derivatives have electron-transporting characteristics, and also have high T_1 because the insertion of phosphine oxide disrupts π-conjugation of molecules.[207] A phosphine oxide

This article is protected by copyright. All rights reserved.

15214095, ja, Downloaded from https://onlinelibrary.wiley.com/doi/10.1002/adma.202207454 by Seoul National University, Wiley Online Library on [28/11/2022]. See the Terms and Conditions (https://onlinelibrary.wiley.com/terms-and-conditions) on Wiley Online Library for rules of use; OA articles are governed by the applicable Creative Commons License

Accepted Article

derivative (SPPO1) that uses spiro-fluorene is an electron-transporting phosphorescent host material that has high T_1 (~2.9 eV).[208] Incorporating a phenylcarbazole moiety yields a phosphine-oxide host material (PPO21) that has high T_1 ~3.02 eV and bipolar charge transport (~10^{-6} cm^2 V^{-1} s^{-1}).[207] A 2,7-bis(diphenylphosphoryl)-9,9-spirobi(fluorene) (SPPO13) has been used to fabricate multi-layered blue SOLEDs due to its solubility in alcohol and high T_1 ~2.73 eV, and 2,7-bis(diphenylphosphoryl)-9-phenyl-9H-carbazole (PPO27) has been developed as an alcohol-soluble bipolar transporting host material by introducing electron-donating carbazole.[209,210]

Insertion of an Si atom into a molecule disconnects π-conjugation between phenyl units, so host materials with phenylsilane moiety can provide a wide band gap and high T_1.[12,211] Several kinds of phenylsilane-derived host materials have been developed, including diphenyldi(o-tolyl)silane (UGH1), p-bis(triphenylsilyl)-benzene (UGH2), and m-bis-triphenylsilyl)benzene (UGH3); they all have wide band gap > 4.4 eV and very high T_1 > 3.5 eV.[211] The wide band gap and high T_1 are requirements for small-molecule host materials that can provide efficient energy transfer for blue OLEDs, but these phenylsilane-derived host materials have 26 ≤ T_g ≤ 40 °C, which is too low to form a stable solution-processed thin film. They also have a very deep HOMO energy level ~7.2 eV, which can degrade hole injection into the EML.[211]

4,4′-bis(triphenylsilanyl)-(1,1′,4′,1′)-terphenyl (BST) was developed to improve thermal stability, and it has T_g ~113 °C.[212] However, direct linking of phenyl decreased T_1 to 2.6 eV, which is not suitable for blue phosphorescent or TADF SOLEDs. Furthermore, host materials that have a phenylsilane moiety have poor electron-transporting properties, which increase operation voltage (V_{OP}) and decrease the luminous efficiency of OLEDs. To overcome this problem, electron-transporting hosts (ETHs) with tetrahedral structured silicon compounds have been designed by introducing pyridine moieties; examples include, diphenylbis(3-(pyridine-2-yl)phenyl)silane (2PTPS), diphenylbis(3-(pyridine-3-yl)phenyl)silane (3PTPS) and diphenylbis(3-(pyridine-4-yl)phenyl)silane

This article is protected by copyright. All rights reserved.

15214095, ja, Downloaded from https://onlinelibrary.wiley.com/doi/10.1002/adma.202207454 by Seoul National University, Wiley Online Library on [28/11/2022]. See the Terms and Conditions (https://onlinelibrary.wiley.com/terms-and-conditions) on Wiley Online Library for rules of use; OA articles are governed by the applicable Creative Commons License

Accepted Article

(4PTPS).[12] These tetrahedral silicone compounds have high morphological stability. Moreover, their tetrahedral structure has good solubility and high T_g > 175 °C, which is suitable for use in SOLEDs. In addition, these materials are composed of a central Si atom with a 3d orbital, and a phenyl or pyridyl phenyl group that has short conjugation length, so they have 3d-π interaction between the central Si and the phenyl or pyridyl phenyl, without disconnection of conjugation at the Si atom, and as a consequence have a wider band gap (4.06 to 4.28 eV) and higher T_1 (2.82 to 2.90 eV) than blue phosphorescent or TADF dopants such as FIrpic (T_1 ~2.7 eV) and 2CzPN (T_1 = ~2.5 eV).[191,203] The pyridyl-substituted hosts have better electron-transporting ability than conventional phenylsilane-derived host materials such as UGH1, UGH2, and UGH3.[12]

Practical applications of large-scale SOLEDs require the use of low-toxicity solvents. Academic researchers have generally used toxic chlorinated solvents such as chloroform, chlorobenzene, and dichlorobenzene, but they are not suitable for use in practical mass production, because they are harmful to the environment and to human health. Use of non-halogenated solvents such as cyclohexanone can overcome these problems.[213] The introduction of a solubilizing group such as ethylene oxide (-EO_2) in phosphorescent Ir(III) complex dopant can help to increase its solubility in cyclohexanone, and thereby enable non-toxic solution processability. As a result, a solution-processed PhOLED that used TCTA:TPBi as a mixed host dissolved in cyclohexanone achieved *CE* = 85.22 cd A^{-1} and *EQE* = 23.60%, which are comparable to those of a solution-processed PhOLED produced using chlorobenzene (91.98 cd A^{-1}, 24.08%).

Solution-processable small-molecule organic host materials have been developed by using a variety of functional moieties to modify the electronic properties, improve stability against thermal treatment and device operation, and smooth the film morphology.[204,205,207,209,210,212] These strategies facilitated fabrication of SOLEDs that have efficiency comparable to those of EOLEDs. To effectively exploit the solution processability of organic host materials, one approach is to form dimers, trimers,

This article is protected by copyright. All rights reserved.

15214095, ja, Downloaded from https://onlinelibrary.wiley.com/doi/10.1002/adma.202207454 by Seoul National University, Wiley Online Library on [28/11/2022]. See the Terms and Conditions (https://onlinelibrary.wiley.com/terms-and-conditions) on Wiley Online Library for rules of use; OA articles are governed by the applicable Creative Commons License

Accepted Article

and dendrimers to increase the molecular weight of host molecules and thereby to improve the solvent resistivity of solution-processed organic thin-film during successive solution-processing steps to deposit overlying layers in SOLEDs.

3.2.2. Dimer, Trimer, and Dendrimers

The low solvent resistivity and low chemical robustness of organic small molecules have limited the use of sequential solution processing for multilayered SOLEDs. When they are fabricated using an all-solution process, the underlying deposited thin film with the organic small molecules can be chemically redissolved by common organic solvents (e.g., chloroform, chlorobenzene, toluene, tetrahydrofuran). Even if orthogonal solvents (water, alcohol) are used, the organic thin films can be physically damaged, because small organic molecules interact weakly by van der Waals forces, hydrogen bonds, and π – π stacking.[214–216] When the final organic functional layer uses orthogonal solvent processing with water or alcohol, the organic host matrix in EML should be chemically and physically robust. To fulfill this requirement while using small molecular hosts, an efficient strategy to improve solvent resistivity is to increase the molecular weight of organic small-molecule hosts.[38,214,217] A simple and efficient approach using covalent dimerization and trimerization can improve solvent resistance of conventional hosts in an EML.[38]

Covalent dimerization and trimerization increase the molecular weight of conventional organic small-molecule hosts, and thereby improve the resistance of EMLs to subsequent solution processing using hydrophilic alcohol solvents (e.g., methanol, ethanol, 1-propanol, 2-propanol).[38] Resistivity against alcohol-containing solvents gradually improves as the molecular weight of the host increases, and saturates at molecular weight above ~800 g mol^{-1}.[38] When two synthesized organic hosts with high alcohol solvent resistivity are used as an EML, TPBi dissolved in methanol formed a stable ETL on solution-processed EML, and the resulting improved charge balance from

This article is protected by copyright. All rights reserved.

15214095, ja, Downloaded from https://onlinelibrary.wiley.com/doi/10.1002/adma.202207454 by Seoul National University, Wiley Online Library on [28/11/2022]. See the Terms and Conditions (https://onlinelibrary.wiley.com/terms-and-conditions) on Wiley Online Library for rules of use; OA articles are governed by the applicable Creative Commons License

Accepted Article

mixed hosts yielded high device efficiencies (*EQE* = 23%, *PE* = 96 lm W^{-1}) in a green-emitting SOLED that had the structure ITO/PEDOT:PSS/TFB/3,30:60,300-ter(9-phenyl-9 H-carbazole) (TPCz): 3,30,6,60-tetrakis(9-phenyl-9 H-carbazol-3-yl) benzophenone (TCZBP): $Ir(ppy)_3$/TPBi/Liq/Al.

Another reliable approach to increase the solvent resistance is to increase the molecular weight of organic small molecules by using dendrimers that consist of core, branch, surface groups, and other linking moieties, which control the solution processability and charge-transport characteristics.[129,218,219] Moreover, HOMO energy levels can be tuned by generation of dendrons.[220,221]

Use of solution-processable carbazole-derived dendritic hosts can cause gradual increase of HOMO energy level as the number of carbazole dendrons is increased (Figure 5b).[220] By increasing the HOMO energy levels of carbazole-derived dendritic hosts (5.61, 5.32, and 5.11 eV with increasing generations of dendrons), the hole injection barrier was much decreased, but high T_1 = 2.9 eV was maintained regardless of the attachment of carbazole dendrons, so the *PE* of fabricated blue-emitting solution-processed PhOLEDs increased by 86% compared with that of SOLEDs that use a PVK host.

Highly-efficient white SOLEDs have been obtained by using the identical carbazole-derived dendritic host with co-doping of orange-red-emitting and blue-emitting dopants (iridium complex containing 5-trifluoromethyl-2-(9,9-diethylfluoren-2-yl)pyridine ligand ($Ir(Flpy\text{-}CF_3)_3$) and FIrpic).[222] Efficient energy transfer from the dendritic host with high T_1 to dopant, and the miscibility of dopant with the host yielded white SOLEDs with improved 39.6 ≤ *PE* ≤ 80.9 lm W^{-1}.[222]

Carbazole-derived dendritic hosts have desirable characteristics such as high T_1, high HOMO energy level, and good solubility in common solvents, and therefore satisfy the requirement of the host for solution-processed TADF emitters, which utilize triplet excitons in a reverse intersystem crossing (RISC) process. Incorporation of carbazole dendrons in a non-conjugated adamantane core

This article is protected by copyright. All rights reserved.

15214095, ja, Downloaded from https://onlinelibrary.wiley.com/doi/10.1002/adma.202207454 by Seoul National University, Wiley Online Library on [28/11/2022]. See the Terms and Conditions (https://onlinelibrary.wiley.com/terms-and-conditions) on Wiley Online Library for rules of use; OA articles are governed by the applicable Creative Commons License

Accepted Article

increased the hole-injection and hole-transport in dendritic hosts.[223] Moreover, the dendrimer had higher T_1 (2.98 eV) than the blue-emitting TADF (T_1 = 2.58 eV for (4-(4,6-diphenyl-1,3,5-triazin-2-yl)phenyl)-spiro[acridine-9,90-fluorene] (SpiroAC-TRZ)), so the reverse energy transfer from dopant to host was suppressed in TADF SOLEDs; as a result, this dendrimer effectively worked as a solution-processable triplet-harvesting host for emitters.[190] The unique chemical structure of adamantine-core dendrimers facilitates good solubility in common organic solvents because of the *tert*-butyl groups at the periphery of the carbazole dendrons and their three-dimensional geometry, which suppresses intermolecular stacking.[224] Moreover, attaching a large number of carbazole groups to dendrimers helps to improve their thermal stability and increase glass-transition temperature (T_g = 175 (**G1**), 300 (**G2**), and 376 °C (**G3**) with increasing generation of dendrons, Figure 5c); these changes favor high device stability and high-temperature processing.[197,218]

Heavy-metal complexes that contain Ir, Pt, Au, Os, or Re can be used at the core of light-emitting dendrimers, which consist of cores, dendrons, and surface groups (Figure 5d). Appropriate control of each component can optimize the electronic properties, solubility, and intermolecular interactions of the dendrimers.[225] IrppyD is a light-emitting dendrimer that consists of a fac-tris(2-phenylpyr-idine) iridium core, phenylene dendrons, and 2-ethylhexyloxy surface groups. When CBP and TCTA hosts doped with IrppyD were spin-coated to form EMLs, higher device efficiencies of 23 lm W^{-1} and 30 cd A^{-1} were achieved than when TCTA host was used (8 lm W^{-1}, 17 cd A^{-1} with CBP host and 0.14 lm W^{-1}, 0.47 cd A^{-1} without host).[225] This increase occurs because the dendritic structure of TCTA with three dendrons facilitates film formation, and because TCTA (5.9 eV) and IrppyD (5.7 eV) have similar HOMO levels, so holes become evenly distributed across the EML without heavy charge trapping on the dendrimer.

EMLs that use small molecules for conventional OLEDs have used the host-dopant system. However, SOLED fabrication by subsequent solution processing of overlying layer on the solution-

This article is protected by copyright. All rights reserved.

15214095, ja, Downloaded from https://onlinelibrary.wiley.com/doi/10.1002/adma.202207454 by Seoul National University, Wiley Online Library on [28/11/2022]. See the Terms and Conditions (https://onlinelibrary.wiley.com/terms-and-conditions) on Wiley Online Library for rules of use; OA articles are governed by the applicable Creative Commons License

Accepted Article

processed EML causes inevitable partial washing of dopants at the surface, even though hosts have a high solvent resistance. This washing changes the doping-concentration profile in EMLs and degrades both device efficiency and reproducibility.[87] Self-host dendrimers that include host-function branched dendrons and heavy-metal emitter core in one molecule have been developed because they can effectively resist the subsequent solution process and avoid the dopant washing that occurs in small-molecule host-dopant EMLs.[226] Moreover, core emitters of self-host dendrimers are encapsulated by dendrons; this structure increases solvent resistance, and thereby effectively prevents redissolution of core emitter by alcohol solvents.

Self-host dendrimers with Ir-complex core encapsulated by carbazole dendrons have been evaluated as nondoped EMLs (**G0**, **G1**, and **G2** depending on the generation of carbazole dendrons) for multilayered phosphorescent SOLEDs.[87] **G2** includes second-generation carbazole dendrons; its solvent resistance was highly improved during subsequent orthogonal solvent processing using methanol, ethanol, isopropanol, n-butanol, or isobutanol, because the high density of surrounding second-generation carbazole dendrons effectively shields the iridium core. After films were rinsed using isobutanol, **G0** and **G1** films retained 28.4 and 39.5% of their initial thickness, whereas **G2** film retained nearly all of its thickness with no change in morphology.[87] In particular, the self-host dendrimer encapsulated in carbazole dendrons had superior resistance to two and three cycles of isobutanol rinsing (Figure 5e).[129] Due to the high solution processability of **G2** dendrimer, fabricated SOLEDs that used a solution-processed upper SPPO13 ETL achieved higher device efficiencies (*CE* = 68.4 cd A^{-1}, *EQE* = 21.2%) than did SOLEDs that used a vacuum-processed upper SPPO13 ETL (*CE* = 52.2 cd A^{-1}, *EQE* = 15.7%).[87]

Dimerization and trimerization of organic small molecules and dendrimers can increase their solvent resistivity, especially to alcohol solvent, and thereby increase their compatibility with continuous orthogonal solution processing. Dendrimers have a tunable molecular weight and good

This article is protected by copyright. All rights reserved.

15214095, ja, Downloaded from https://onlinelibrary.wiley.com/doi/10.1002/adma.202207454 by Seoul National University, Wiley Online Library on [28/11/2022]. See the Terms and Conditions (https://onlinelibrary.wiley.com/terms-and-conditions) on Wiley Online Library for rules of use; OA articles are governed by the applicable Creative Commons License

Accepted Article

solubility depending on the generation of dendrons and cores; therefore, dimerization and trimerization improved their electronic properties and thermal stability. Use of these high-molecular-weight organic host materials can simplify the process of fabricating SOLEDs. Moreover, use of solution-processable self-host dendrimers that include both host-function and emitter-function groups has been considered for polymeric emitters in SOLEDs.

3.2.3. Polymeric Emitting Layers

Polymeric emitters have been investigated since the first PLED was developed in 1990 by using poly(p-phenylene vinylene) (PPV) as a green-yellow LEP.[18] Then a PPV derivative, poly[2-methoxy-5-(2-ethylhexy-loxy)-1,4-phenylenevinylene] (MEH-PPV), was evaluated for use as an orange-red LEP to demonstrate the flexibility of PLEDs that use polyaniline (PANI) as a solution-processed anode.[227] MEH-PPV dissolved in xylene was spin-coated onto PANI dissolved in meta-cresol to form an EML without chemical dissolution or physical damage to underlying polymeric anode, and thereby demonstrate fabrication of solution-processed multilayered PLED. The resultant PLEDs that used PPV and that used MEH-PPV had *EQE*s of 0.05% and ~ 1%, respectively.[18]

Since PLEDs that use PPV were reported, other types of polymeric emitters have been actively developed. Unipolar polymers with higher $\mu_h$than μ_e were used during early stages in the development of PLEDs.[228,229] Poly[(9,9-di-n-octylfluorenyl-2,7-diyl)-alt-(benzo[2,1,3]thiadiazol-4,8-diyl)] (F8BT) is a poly(9,9-dioctylfluorene) (PFO) copolymer with a high μ_h ~10^{-3} cm^2 V^{-1} s^{-1} at applied electric fields of 0.5 MV cm^{-1}. F8BT has high μ_e, so it is a promising green-emitting LEP that can make good charge balance in PLEDs.[230] However, although F8BT is an electron-dominant LEP, it has a low LUMO energy level (3.5 eV), and therefore has a high electron-injection energy barrier (1.2 eV) in inverted-structured PLEDs. Therefore, in the PLEDs that use F8BT, holes are the main charge carriers, and the unipolar charge transporting property of the PLED can induce charge accumulation at the

This article is protected by copyright. All rights reserved.

15214095, ja, Downloaded from https://onlinelibrary.wiley.com/doi/10.1002/adma.202207454 by Seoul National University, Wiley Online Library on [28/11/2022]. See the Terms and Conditions (https://onlinelibrary.wiley.com/terms-and-conditions) on Wiley Online Library for rules of use; OA articles are governed by the applicable Creative Commons License

Accepted Article

interface, and thereby quench excitons.[230] To reduce exciton accumulation at the interface to improve the charge balance, TPD has been added into the F8BT matrix. TPD has a 0.4 eV shallower HOMO energy level than F8BT and therefore acts as a hole trap.[231] F8BT EML with added TPD has high hole-trap density, which resulted in charge redistribution in the EML. Moreover, F8BT, which is soluble in xylene, can be spin-coated onto inorganic common layers (TiO_2, ZnO) that are soluble in polar solvent,[231,232] and is also highly resistant to damage by subsequent solution-processed PEDOT:PSS and TFB.[232,233]

The electrical and optical properties of solution-processed polymeric EMLs are affected by the film-forming conditions. When Super Yellow (PDY-132, SY), which is a PPV co-polymer modified with large phenyl side groups,[234] as an LEP is deposited by blade coating method with simultaneous thermal treatment at 70 °C, the SY aggregates, and the process forms defect levels, so the hole current in hole-only devices is higher than in normal spin-coated SY film.[235] The PL intensity of SY films decreased as annealing temperature was increased (up to 150 °C) without changing the shape of the PL spectrum.[236,237] SY has an average molecular weight of 184.3 kDa and T_g = 83 °C. Thus, when SY film is annealed at temperature > T_g = 83 °C, the polymer chains can aggregate due to their increased mobility, but the long side chains in spin-coated SY suppress aggregation.[235] Thermogravimetric analysis (TGA) of SY showed that degradation starts with breaking of long alkoxy chains starting at 50 °C, and accelerates at temperatures > 350 °C **(Figure 6**a**)**. The low PL and poor thermal properties degrade *EQE*s from 4.09% to 2.72% as annealing temperatures are increased from 50 °C to 200 °C, although the current density increased in the SY film annealed at 200 °C.

Although LEPs have higher molecular weight and therefore can show higher solvent resistivity than small inorganic molecules, LEPs are not fully protected from damage such as redissolution and physical washing by the subsequent solution process using organic solvents. One common strategy to increase solvent resistivity of polymeric materials is to immobilize polymer

This article is protected by copyright. All rights reserved.

15214095, ja, Downloaded from https://onlinelibrary.wiley.com/doi/10.1002/adma.202207454 by Seoul National University, Wiley Online Library on [28/11/2022]. See the Terms and Conditions (https://onlinelibrary.wiley.com/terms-and-conditions) on Wiley Online Library for rules of use; OA articles are governed by the applicable Creative Commons License

Accepted Article

chains and link them by using crosslinkers such as silanes,[159,238] styrenes,[239] oxetanes,[164] and acrylates.[240] When a bisazide crosslinker was added to SY (Figure 6b),[241] the crosslinking was activated at 140 °C, and the resulting film had higher solvent resistivity after thermal treatment for 8 h than after 1 h (remaining thickness after toluene rinsing = 98% and 87%, respectively). However, thermal treatment inevitably degrades the luminous efficiency of SY.[236] Furthermore, a crosslinker concentration > 5% broadened the PL spectrum and decreased PLQY from 9.2% (1% crosslinker) to 6.8% (10% crosslinker).[236] In fabricated PLEDs with a solution-processed poly[bis (4-phenyl)(2,4,6-trimethylphenyl)amine (PTAA) layer on crosslinked SY EML, the EL spectrum was stabilized (CIE coordinates (0.49, 0.50)) when compared with reference PLED that used SY (CIE coordinates (0.48, 0.51)), and thereby achieved maximum *EQE* = 6.48% and a reduced efficiency roll-off.

The *EQE*s of fluorescent PLEDs that use LEP are theoretically limited to < 5% by considering the light extraction efficiency of device, the charge balance factor, the singlet/triplet quantum ratio, and the luminescence quantum yield.[242] However, *EQE*s > 5% have been obtained in fluorescent PLEDs, possibly as due to improved light-extraction efficiency, and to triplet-triplet annihilation (TTA, also known as triplet fusion) that yields one excited singlet state from two triplet states.[178,243,244] To utilize triplet excitons, which are wasted in fluorescent LEPs by non-radiative decay, two approaches can be applied to generate phosphorescence: (1) doping of metal complex emitter into a polymeric host (i.e., host-dopant system), and (2) attachment of a metal complex to the polymer backbone (i.e., self-host polymers).

In host-dopant systems such as PVK polymeric host doped with Ir-complex emitter, efficient Dexter energy transfer (DET) can be generated between polymeric host and phosphorescent dopants when the triplet exciton lifetime of the host is longer than microseconds.[245] In particular, the phosphorescent dopants must have a high T_1 to limit the reverse energy transfer from polymeric host to phosphorescent dopant, and thereby facilitate efficient triplet exciton confinement in a

This article is protected by copyright. All rights reserved.

15214095, ja, Downloaded from https://onlinelibrary.wiley.com/doi/10.1002/adma.202207454 by Seoul National University, Wiley Online Library on [28/11/2022]. See the Terms and Conditions (https://onlinelibrary.wiley.com/terms-and-conditions) on Wiley Online Library for rules of use; OA articles are governed by the applicable Creative Commons License

Accepted Article

dopant that has a low T_1.[246,247] Therefore, by optimizing the electronic properties of host and dopant materials and improving the charge balance in devices, *EQE* of PLED using PVK with 0.7 wt % tris(2-(4-tolyl)phenylpyridine)iridium ($Ir(mppy)_3$) as an EML was dramatically improved to 18.8%,[248] whereas that of the first PLED that used a single fluorescent PPV was 0.05%.[18] However, the molecularly-doped two-composition system can cause phase separation within EMLs and can decrease both device efficiency and lifetime.[249,250]

Self-host polymers are composed of backbone units and side groups composed of heavy-metal complexes that utilize triplet excitons (Figure 6c). The self-host system can avoid the phase-separation problem by simplifying the composition of EMLs and thus increasing device lifetime. In the self-host polymer that has a phosphorescent Ir-complex unit connected to the backbone of hole-transporting PVK,[251] the high solubility of synthesized self-host polymers is suitable for solution processing using common organic solvents. The green-emitting self-host polymer had a long PL lifetime (1.2 μs) that had PL decay described by a single exponential function, which indicates efficient phosphorescence from triplet states of the Ir-complex unit side group without fluorescence from the singlet state. As a result, an *EQE* = 11.0% was achieved in a green-emitting PLED that used this self-host polymer. The charge balance in PLEDs that use self-host polymers can be controlled by tuning the hole and electron transporting moieties that connect with the backbone of the polymer. An ambipolar self-host polymer that consists of bis(2-phenylpyridine)iridium (acetylacetonate) ($Ir(ppy)_2(acac)$) as a phosphorescent emitter, TPD as a hole-transporting side group, and 2-(4-biphenyl)-5-(4-tert-butylphenyl)-1,3,4-oxadiazole (PBD) as an electron-transporting side group achieved *EQE* = 11.8% in the optimized PLED with the side-group ratio of 18:79:3 [TPD:PBD:$Ir(ppy)_2(acac)$] (Figure 6d),[252] whereas a PLED with a ratio of 55:41:4 [TPD:PBD:$Ir(ppy)_2(acac)$] showed *EQE* = 1.0%. This result indicates that a self-host polymer that has high μ_h requires a high concentration of electron-transporting moiety and a low concentration of hole-transporting moiety to improve the charge balance and device efficiency in polymeric EMLs.

This article is protected by copyright. All rights reserved.

15214095, ja, Downloaded from https://onlinelibrary.wiley.com/doi/10.1002/adma.202207454 by Seoul National University, Wiley Online Library on [28/11/2022]. See the Terms and Conditions (https://onlinelibrary.wiley.com/terms-and-conditions) on Wiley Online Library for rules of use; OA articles are governed by the applicable Creative Commons License

Accepted Article

The phosphorescence obtained using singlet and triplet excitons can theoretically achieve 100% *IQE*, but the use of heavy metals increases the cost of display panels. A promising method to utilize triplet excitons for 100% *IQE* without using an expensive heavy metal complex is to use polymers that include a TADF emitter. Small-molecule TADF emitters have been investigated in small-molecule OLEDs with host-dopant-mixed EMLs,[253] so LEPs that use TADF also have been evaluated. A main-chain-type TADF polymer consists of 1,4-bis(4-(4,4,5,5-tetramethyl-1,3,2-dioxaborolan-2-yl)phenyl) butane as a high-T_1 backbone monomer, N, N'-bis(4-hexylphenyl)-N,N'-bis(4-(4,4,5,5-tetramethyl-1,3,2-dioxaborolan-2-yl)phenyl)benzene-1,4-diamine as a donor, and 2,4-bis(4-bromophenyl)-6-(4-dodecylphenyl)-1,3,5-triazine as acceptor and TADF emitter (Figure 6e).[254] A small energy gap (ΔE_{ST}) between S_1 and T_1 energy levels can be obtained by careful molecular design of TADF emitter that uses donor and acceptor.[255] In this main-chain-type TADF polymer, the TADF emitter units are embedded in the polymer backbone, and the HOMO of donor and LUMO of acceptor are spatially separated by an intermonomer TADF emitter that is composed of a triazine-amine-triazine unit. Therefore, RISC occurs by formation of a charge-transfer (CT) state that has a small ΔE_{ST} = 0.22 eV, which enables thermal up-conversion from T_1 to S_1. Moreover, the intermonomer in the TADF polymer acts as a charge-transporting unit, which can control the charge balance. The resultant PLED that uses the TADF polymer achieved a maximum *EQE* = 10% at a low current density of 0.01 mA cm^{-2}.

A non-conjugated moiety as a linker can be also incorporated in the polymer backbone.[255] 1,1-diphenylcyclohexane (Cp), which has sp^3 bridges, 10-(4-(4,6-diphenyl-1,3,5-triazin-2-yl)phenyl)-9,9-dimethyl-9,10-dihydroacridine (DMAC-TRZ), has been combined with 2,7-dibromo-10-(4-(4,6-diphenyl-1,3,5-triazin-2-yl)phenyl)-9,9-dimethyl-9,10-dihydroacridine (DMTRZ-2br) as a linker and TADF monomer units to synthesize a polymeric TADF emitter, P(DMTRZ-Cp). The Cp linker increases the solubility of polymers and controls the conjugation length while maintaining the TADF characteristics of the monomer unit. The synthesized polymeric TADF emitter of P(DMTRZ-Cp)

This article is protected by copyright. All rights reserved.

15214095, ja, Downloaded from https://onlinelibrary.wiley.com/doi/10.1002/adma.202207454 by Seoul National University, Wiley Online Library on [28/11/2022]. See the Terms and Conditions (https://onlinelibrary.wiley.com/terms-and-conditions) on Wiley Online Library for rules of use; OA articles are governed by the applicable Creative Commons License

Accepted Article

obtains small ΔE_{ST} = 0.023 eV, and has fast prompt PL decay (12.2 ns) and delayed fluorescence decay (1.8 μs), i.e., TADF behavior. The fabricated TADF PLED showed an *EQE* of 15.4%. Another linker unit that has an aliphatic ring structure has been used to synthesize a TADF polymer composed of a TADF-linker-host structure that can facilitate stable triplet states, and that has design freedom.[256] The TADF polymer that has rigid non-conjugated polyimide consists of diamine 4,4'-(9-phenyl-9H-carbazole-3,6-diyl) dianiline (PhCzPN) as a host, (4-(10H-phenothiazin-10-yl)phenyl) (4-(3,6-bis(4-aminophen-yl)-9H-carbazol-9-yl) phenyl) methanone (PTC-N) as a TADF core unit, and 1,2,4,5-cyclohexanetetracarboxylic dianhydride (HPMDA) as a linker that spatially separates TADF from the host units. The HPMDA linker increases the solubility of the synthesized TADF polymers (i.e., PCPTCN-m/n) in common non-halogen organic solvents such as N,N-dimethylformamide (DMF), dimethyl sulfoxide (DMSO), and N-methyl-2-pyrrolidone (NMP). Moreover, the rigid PI backbone of PCPTCN-m/n gives high thermal stability which is confirmed by high decomposition temperature (5% weight loss in the range of 519.5 to 549.0 °C) and high T_g (308.7 to 362.1 °C). Therefore, the resultant TADF PLEDs has a maximum *EQE* = 21.0%, with a low efficiency roll-off.

Various approaches to synthesize TADF polymers have assessed to further improve the device efficiency of TADF PLEDs. One approach is to link a TADF emitter to the side chains of the polymer backbone. In the side-chain-type TADF polymer, a TADF emitter unit is grafted onto the side chain of the polymer backbone;[257] this structure is in contrast to the main-chain-type TADF polymer in which a single polymer has a TADF emitter embedded in the polymer main chain. The side-chain-type TADF polymer can have independent functions in the polymer backbone and the grafted side chain: the polymer backbone provides the charge-transporting channel and host, and the side chain with grafted TADF emitter does not affect the electronic properties of the polymer.[257,258] One TADF copolymer has side groups of insulating styrene as spacer units and 2-(10*H*-phenothiazin-10-yl)-8-vinyldibenzothiophene-*S*,*S*-dioxide as a pendent TADF group (Figure 6f).[259] The non-emissive spacer units separate TADF units and reduce aggregation between them, and thereby suppress TTA in the

This article is protected by copyright. All rights reserved.

15214095, ja, Downloaded from https://onlinelibrary.wiley.com/doi/10.1002/adma.202207454 by Seoul National University, Wiley Online Library on [28/11/2022]. See the Terms and Conditions (https://onlinelibrary.wiley.com/terms-and-conditions) on Wiley Online Library for rules of use; OA articles are governed by the applicable Creative Commons License

Accepted Article

TADF copolymer.[260] Moreover, the optimized 0.63:0.37 elemental ratio between the insulating styrene and TADF units in TADF copolymer obtained small ΔE_{ST} = 0.35 eV, which effectively enables an efficient RISC. As a result, the fabricated PLED achieved *EQE* = 20.1% and *CE* = 61.3 cd A^{-1}.[260]

To further increase the *EQE* of TADF PLEDs, the host functional unit can be additionally grafted onto the side chain of the polymer backbone with a TADF moiety. One such copolymer consists of 9-vinyl-carbazole (VCz) as the host functional unit and 10,10'-((6-(4-((4-vinylbenzyl)oxy)phenyl)-1,3,5-triazine-2,4-diyl)bis(4,1-phenylene)) bis(9,9-dimethyl-9,10-dihydroacridine) (VTD) as the TADF emitter unit.[261] The host functional unit of VCz increases the charge injection and charge transport properties and improves the charge balance in EMLs. Increase in the proportion of VTD in copolymers caused increase in the HOMO energy level, decrease in the LUMO energy level, and a slight decrease in S_1 from 2.83 to 2.72 eV due to the strong intermolecular interaction.[261] Moreover, at a high VTD proportion = 0.3, the copolymer had its smallest ΔE_{ST} = 0.06 eV but a low PLQY = 51.0% due to concentration quenching. The VTD unit also facilitated efficient electron transport, and thereby increased current density and improved the charge balance in TADF PLEDs. Therefore, the improved charge balance and the high PLQY = 70.9% at the optimized ratio of VTD:VCz (10:90) increased the *EQE* of TADF PLEDs to 22.0%.[261]

The high tunability of polymers that can be enabled by modifications of backbones and functional side groups in the polymer chain has demonstrated the potential as solution-processed materials for the EML. The types of polymeric materials for EML applications include single emitters, hosts, and self-host EMLs composed of a backbone as the host unit and side groups as emitters. In particular, TADF-type polymers can efficiently exploit singlet and triplet excitons by using a charge-transporting backbone host and side chains that have a grafted TADF emitter and that do not require expensive heavy-metal complexes. Therefore, use of the side-chain-type TADF polymers can be expected to be one of the most promising approaches to improve the charge balance and to achieve

This article is protected by copyright. All rights reserved.

15214095, ja, Downloaded from https://onlinelibrary.wiley.com/doi/10.1002/adma.202207454 by Seoul National University, Wiley Online Library on [28/11/2022]. See the Terms and Conditions (https://onlinelibrary.wiley.com/terms-and-conditions) on Wiley Online Library for rules of use; OA articles are governed by the applicable Creative Commons License

Accepted Article

high *EQE*s > 20% and high stability without the problem of phase separation between host and dopant molecules. Thus, the polymeric EML is suitable for low-cost fabrication and simple device configurations of SOLEDs.

4. Solution-processed Organic Light-Emitting Devices

4.1. Host-Dopant Combination in EML for SOLEDs

To achieve SOLEDs that have high luminous efficiency, the effect of the combination of host and dopant materials on the light-emitting mechanism should be considered. The holes injected from the anode and the electrons injected from the cathode attract each other by Coulombic interaction to form excitons. After excitons are formed, the subsequent energy transfer from host to dopant is the key mechanism for highly-efficient EL emission in OLEDs. Exciton energy can be transferred by DET and Förster resonance energy transfer (FRET) processes, depending on the type of emission.[262,263] DET occurs between singlet-singlet states or triplet-triplet states of hosts and dopants by an electron-exchange process that depends on the molecular orbital overlaps and the spin states; therefore DET generally happens within < 1 nm.[264] FRET occurs by long-range dipole-dipole interaction with an intermolecular distance range < 10 nm.[265,266] The distance (*r*) between host donor and dopant acceptor determines the energy transfer rate (k_T) as

$$k_T(r) = \frac{1}{\tau_D}\left(\frac{R_0}{r}\right)^6,$$

where τ_D is the donor fluorescence lifetime and R_0 is Förster radius. The efficiency of energy transfer is related to *r* and R_0 as

$$E = \frac{R_0^6}{R_0^6 + r^6}.$$

This article is protected by copyright. All rights reserved.

15214095, ja, Downloaded from https://onlinelibrary.wiley.com/doi/10.1002/adma.202207454 by Seoul National University, Wiley Online Library on [28/11/2022]. See the Terms and Conditions (https://onlinelibrary.wiley.com/terms-and-conditions) on Wiley Online Library for rules of use; OA articles are governed by the applicable Creative Commons License

Accepted Article

The FRET process is responsible for fluorescent emission, and both FRET and DET processes contribute to phosphorescent emission. The light-emission mechanism of OLEDs depending on the type of host and dopant materials' combination in EMLs can be explained by energy transfer from host to dopant, by direct charge trapping into the dopant molecules in EML, or by both phenomena.

4.1.1. Mixed-host Emitting Layers for SOLEDs

Mixed-host EMLs have been exploited by mixing an HTH and an ETH to improve the charge balance and increase the lifetime, and to reduce the V_{OP} and efficiency roll-off of OLEDs.[12,20,61,267] These changes occur because: (1) the hole and electron-injection energy barriers at both blurred interfaces of mixed-host EMLs are reduced, thereby reducing charge accumulation, which can broaden the recombination zone;[268,269] (2) the mixed host exhibits bipolar charge transport characteristics in the EMLs, which improves the charge balance and reduces the charge and exciton accumulation that cause TTA and triplet-polaron annihilation (TPA);[270–272] and (3) the gaps of both the HOMO and LUMO energy levels between the mixed host and dopant are reduced, so charge trapping is decreased and as a result the charge transport is increased.[273]

The mixed-host system has been developed for SOLEDs by using small-molecule organic and polymeric materials because of their simple synthesis and compatibility with solution processes. Although single host materials such as 3,3'-bis(N-carbazolyl)biphenyl (mCBP) show bipolar transport property, their μ_h and μ_e are not generally equivalent (e.g., in mCBP, μ_h~1×10^{-3} cm^2 V^{-1} s^{-1}, μ_e ~0.3×10^{-3} cm^2 V^{-1} s^{-1}), so charge imbalance can develop in EMLs.[187] Furthermore, the single host of mCBP has a high hole injection barrier at the PEDOT:PSS/EML interface, so holes accumulate there, and thereby degrade device efficiency and operational stability. Therefore, by optimizing the mixing ratio of the second HTH such as TCTA with mCBP in EML, V_{TO} of the device was decreased from 5.8 V to 4.6 V at the ratio of 1:1 mCBP:TCTA, and the luminance and *CE* were maximized at the ratio of 2:1

This article is protected by copyright. All rights reserved.

15214095, ja, Downloaded from https://onlinelibrary.wiley.com/doi/10.1002/adma.202207454 by Seoul National University, Wiley Online Library on [28/11/2022]. See the Terms and Conditions (https://onlinelibrary.wiley.com/terms-and-conditions) on Wiley Online Library for rules of use; OA articles are governed by the applicable Creative Commons License

Accepted Article

mCBP:TCTA (23,340 cd m^{-2}, 14.49 cd A^{-1}); these high values were attributed to a reduced hole injection barrier and improved charge balance in the EML. The improved electrical properties in OLEDs that uses this mixed host were demonstrated by their fast turn-on response to an applied voltage pulse in transient EL characterization.[187] Moreover, when the voltage pulse was turned off, the lowest instantaneous overshoot peak, which originates from hole accumulation, was observed at the ratio of 2:1 mCBP:TCTA.[187]

Red-, green-, blue-, and white-emitting SOLEDs have been obtained using mixed-host EMLs composed of conventional HTH, TCTA, and one of the newly-synthesized ETHs (2PTPS, 3PTPS and 4PTPS), which have sufficiently high T_1 levels of 2.82, 2.82, and 2.90 eV, respectively.[12] The e-hosts have higher T_1 levels than that of a blue phosphorescent dopant, FIrpic (T_1 = 2.7 eV),[191] and are therefore suitable to effectively confine triplet excitons in the dopant and to transport exciton energy from host to dopant. Moreover, the ETHs have wider band gaps (4.06, 4.20, and 4.28 eV, respectively) than that of TPBi (3.30 eV) and are therefore suitable for charge transport in blue PhOLEDs. 2PTPS, 3PTPS, and 4PTPS did not form exciplexes with TCTA, whereas conventional TPBi showed exciplex emission in PL spectra of TPBi:TCTA thin film because of the different intermolecular interaction.[274] Therefore, the dominant recombination mechanism of the exciplex-free xPTPS:TCTA (x = 2,3,4) is direct charge carrier trapping to the phosphorescent dopants from the HIL or ETL, which facilitates more balanced charge transport and efficient direct recombination in the EML according to the molecular concentration of phosphorescent dopants (**Figure 7**a), whereas the dominant recombination mechanism of TPBi:TCTA is energy transfer from an exciplex formed by two hosts, to a phosphorescent dopant (Figure 7b). 2PTPS has the highest μ_e (~10^{-4} cm^2 V^{-1} s^{-1}) which is comparable to the μ_h of TCTA (~3 × 10^{-4} cm^2 V^{-1} s^{-1}).[12] The trend of μ_e was proved by transient EL characterization of mixed-host SOLEDs. The EL signal increased slowly in the SOLED that used TPBi:TCTA, but faster in the SOLED that used 2PTPS:TCTA, because it has higher μ_e than TPBi:TCTA. The balanced μ_h and μ_e in a mixed-host system can improve charge balance and broaden

This article is protected by copyright. All rights reserved.

15214095, ja, Downloaded from https://onlinelibrary.wiley.com/doi/10.1002/adma.202207454 by Seoul National University, Wiley Online Library on [28/11/2022]. See the Terms and Conditions (https://onlinelibrary.wiley.com/terms-and-conditions) on Wiley Online Library for rules of use; OA articles are governed by the applicable Creative Commons License

Accepted Article

the recombination zone located far from the interfaces. In particular, intermixing between layers and dopant aggregation during the solution process can cause severe charge imbalance in solution-processed PhOLEDs. It can be rectified by incorporating a small amount of an assistant small organic molecule such as CBP, which can suppress electron transport between dopants (Figure 7c), resulting in reduced efficiency roll-off characteristics in SOLEDs.[20] As a result, the high T_1 and μ_e of 2PTPS yielded the highest device efficiencies of 20.9% *EQE* and 38.7 cd A^{-1} in FIrpic solution-processed PhOLEDs with 2PTPS:TCTA (*EQE* = 19.6%, *CE* = 32.6 cd A^{-1} with 3PTPS:TCTA, *EQE* = 14.3%, *CE* = 28.8 cd A^{-1} with 4PTPS:TCTA, *EQE* = 10.0%, *CE* = 18.6 cd A^{-1} with TPBI:TCTA). The better electrical characteristics of 2PTPS and 3PTPS than 4PTPS also achieved the highest recorded *EQE*s in orange-red PhOLEDs that use $Bt_2Ir(acac)$ (2PTPS:TCTA host: 35.4%, 3PTPS:TCTA host: 35.5%, 4PTPS:TCTA host: 28.0%) and in green-emitting PhOLEDs that used $Ir(ppy)_3$ (2PTPS:TCTA host: 29.0%, 3PTPS:TCTA host: 23.7%) (Figure 7d).

To fulfill the industrial standards for lighting and display applications, the efficiency roll-off at high luminance in SOLEDs must also be reduced. In solution-processed PhOLED that used TCTA:2PTPS:$Ir(ppy)_2(acac)$:CBP EML, the efficiency roll-off was reduced by the improved charge balance that had been obtained by using a mixed-host system with a charge-balance-assistant CBP, and by the low exciton quenching induced by low dopant aggregation (i.e., TTA, TPA) with heteroleptic $Ir(ppy)_2(acac)$ dopant, which reduces intermolecular interaction compared to homoleptic $Ir(ppy)_3$ dopant (Figure 7e).[20] Therefore, strategies to improve the charge balance and reduce exciton quenching due to dopant aggregation in solution-processed PhOLEDs suggest practical ways to achieve large-area solution-processed device applications with reduced efficiency roll-off (Figure 7f).[12]

4.1.2. Exciplex-forming Mixed Host

This article is protected by copyright. All rights reserved.

15214095, ja, Downloaded from https://onlinelibrary.wiley.com/doi/10.1002/adma.202207454 by Seoul National University, Wiley Online Library on [28/11/2022]. See the Terms and Conditions (https://onlinelibrary.wiley.com/terms-and-conditions) on Wiley Online Library for rules of use; OA articles are governed by the applicable Creative Commons License

Accepted Article

An exciplex is generated in an excited CT complex by charge transfer at the excited states between electron donor and accepter. The exciplex is accompanied by a red-shifted and broadened PL emission spectrum, compared to those of respective donor and acceptor molecules, respectively.[275,276] The broad, featureless, and red-shifted PL spectrum of an exciplex can be ascribed to the different structural configurations and undefined vibrational character of the ground state.[274] Exciplexes can be classified into two types: (1) interfacial exciplexes that form at the interface of bilayers between EML and adjacent charge-transporting layers;[277] and (2) bulk exciplexes that can be constructed by mixture of e-host and h-host in EMLs in a mixed-host system.[278]

Opinions about the exciplex have changed. Early studies of exciplex formation regarded it as an undesirable emission route that reduces PL and EL efficiencies because the emission spectrum can originate not from the emitters but from the exciplex.[204] Later, researchers exploited exciplexes to tune the EL color of OLEDs.[279,280] Recent studies regarding exciplex-assisted OLEDs have proved that the energy transfer from exciplex to dopant molecules can help to improve luminous efficiency when the exciton energy levels of host and dopant molecules are designed appropriately.[281,282] Moreover, in OLEDs that exploit exciplexes, energy transfer from exciplex to dopant is dominant, rather than direct charge trapping at dopant molecules.[283] Therefore, the exciplex-forming couple of electron donor and acceptor should have the following conditions: 1) a lower T_1 level than that of each constituent to avoid both undesirable emission spectrum and energy transfer to one of the host constituents; and 2) a higher T_1 level than that of the phosphorescent dopant to enable efficient energy transfer from exciplex to phosphorescent dopant without reverse energy transfer.[284] Moreover, the separated HOMO and LUMO in the exciplex, which are respectively located at electron donor and acceptor molecules, contribute to low exchange energy, thereby producing a small ΔE_{ST} between S_1 and T_1.[285] RISC from T_1 to S_1 occurs in the exciplex host, and the triplet

This article is protected by copyright. All rights reserved.

15214095, ja, Downloaded from https://onlinelibrary.wiley.com/doi/10.1002/adma.202207454 by Seoul National University, Wiley Online Library on [28/11/2022]. See the Terms and Conditions (https://onlinelibrary.wiley.com/terms-and-conditions) on Wiley Online Library for rules of use; OA articles are governed by the applicable Creative Commons License

Accepted Article

excitons can be effectively harvested in conventional fluorescent emitters; therefore, 100% *IQE* can be theoretically achieved in fluorescent OLEDs that use an exciplex host (Figure 7b).[281,286,287]

An interfacial exciplex can be formed by sequentially depositing electron-accepting and electron-donating layers that have distinct gaps of > 0.4 eV between both each HOMO and LUMO energy levels.[276] The interfacial exciplex has advantageous charge injection and charge transport properties, so it reduces efficiency roll-off and operation voltage, and therefore yields OLEDs that have high *PE*. Moreover, in SOLEDs that have the interfacial exciplex-forming structure, the phase separation that can occur a mixed-host system can be eliminated, and a simple device structure can be designed.[288,289]

Exciplex type can affect the operational stability of OLEDs. In a PhOLED that uses an interfacial exciplex-forming (3'-(4,6-diphenyl-1,3,5-triazin-2-yl)-(1,1'-biphenyl)-3-yl)-9-carbazole (CzTrz) and TCTA donor, TPA is reduced by the efficient long-range FRET, so the device achieved approximately two orders of magnitude longer device lifetime and lower efficiency roll-off at a low dopant concentration of 3 wt% than PhOLEDs that use bulk-exciplexes.[290] Therefore, exploitation of the interfacial exciplex can be a simple strategy for fabrication of SOLEDs. In the interfacial exciplex, the distance between the interface and dopant position influences the energy-transfer efficiency. The FRET rate from the interfacial exciplex to phosphorescent dopant such as $Ir(ppy)_3$ increases when the dopant position approaches the interface between CBP as a host and B3PYMPM as an ETL. As a result, the EL spectrum that originates from the exciplex emission can be suppressed by improved exciplex energy transfer, and the efficiency roll-off can also be reduced.[282]

An interfacial exciplex for blue PhOLEDs formed at the interface between TAPC as a HTL and 5',5''''-sulfonyl-di-1,1':3',1''-terphenyl (BTPS) as a host. The exciplex had higher T_1 levels (T_1 = 2.98 eV for TAPC, T_1 = 2.79 eV for BTPS, T_1 = 2.82 eV for TAPC/BTPS exciplex) than that of blue phosphorescent dopant, FIrpic (T_1 = 2.77 eV).[291] The suitable T_1 level configuration of these blue

This article is protected by copyright. All rights reserved.

15214095, ja, Downloaded from https://onlinelibrary.wiley.com/doi/10.1002/adma.202207454 by Seoul National University, Wiley Online Library on [28/11/2022]. See the Terms and Conditions (https://onlinelibrary.wiley.com/terms-and-conditions) on Wiley Online Library for rules of use; OA articles are governed by the applicable Creative Commons License

Accepted Article

PhOLEDs that used interfacial exciplex minimizes triplet exciton quenching at the interface and facilitates efficient DET from the T_1 level of the interfacial exciplex to the T_1 level of FIrpic. Moreover, V_{TO} (2.5 V at 1 cd m^{-2}) and V_{OP} (2.9 V at 100 cd m^{-2}) were decreased by the recombination of the exciplex and a barrier-free charge recombination process (blue PhOLEDs with TCTA layer inserted: V_{TO} = 2.8 V at 1 cd m^{-2}; V_{OP} = 3.3 V at 100 cd m^{-2}). These results indicate that the short distance between the interfacial exciplex and the dopant position in EML favored rapid DET. Efficient energy transfer was confirmed in PhOLEDs that had a high FIrpic concentration of 11 wt% and a short distance between the interface of TAPC/BTPS and FIrpic-doped region.

A *PE* has been greatly increased in yellow-emitting SOLEDs that used 5-trifluoromethyl-2-(9,9-diethylfluoren-2-yl)pyridine ligand (Ir(Flpy-CF_3)$_3$) as a dopant and an exciplex host composed of 4, 4′ , 4″ -tris[3-methylphenyl(phenyl)amino]triphenylamine (*m*-MTDATA) and 1,3,5-tri(m-pyrid-3-yl-phenyl) benzene (TmPyPB).[292] The device configuration facilitates effective charge injection and transport, and forms a negligible injection barrier at the EML interface because of the direct recombination of exciplex at *m*-MTDATA/TmPyPB interface (i.e., a barrier-free process), followed by energy transfer to the yellow dopant. Energy transfer from the interfacial exciplex can eliminate the direct charge trapping at dopants that have shallow energy levels, so V_{OP} can be decreased. The higher T_1 level of interfacial exciplex host (2.49 eV), *m*-MTDATA/TmPyPB, than that of Ir(Flpy-CF_3)$_3$ (2.24 eV) enables effective harvest of triplet excitons, and thereby minimizes the triplet exciton quenching. Moreover, the *EQE* was maintained > 20% at a luminance of 100 cd m^{-2} when the distance between *m*-MTDATA/TmPyPB interface and dopant was increased to 5 nm; this result indicates efficient energy transfer (Figure 7g). These results indicate that the concentration of phosphorescent dopants and the distance for energy transfer are essential considerations in OLEDs that exploit interfacial exciplexes.

This article is protected by copyright. All rights reserved.

15214095, ja, Downloaded from https://onlinelibrary.wiley.com/doi/10.1002/adma.202207454 by Seoul National University, Wiley Online Library on [28/11/2022]. See the Terms and Conditions (https://onlinelibrary.wiley.com/terms-and-conditions) on Wiley Online Library for rules of use; OA articles are governed by the applicable Creative Commons License

Accepted Article

Bulk exciplexes that are formed by a mixture of donor and acceptor provide a promising approach 1) to improve charge balance by the bipolar charge-transporting characteristic of mixed-host EML in SOLEDs, 2) to reduce the efficiency roll-off at high luminance by a broad emission zone that reduces the populations of triplet excitons and polarons at local interfaces, and 3) to utilize efficient singlet and triplet energy transfers to dopants distributed in the EML regardless of the distance between exciplex host and dopant or from the interfaces.[274,284] When HTL and ETL materials compose the exciplex-forming mixed host, charge-injection barriers at both sides of EML interfaces become negligible, so V_{TO} and V_{OP} of OLEDs can be reduced. No overshoot occurred after voltage turn-off in transient EL characterization using a device (ITO/TAPC/TCTA/TCTA:B3PYMPM (1:1):8% $Ir(ppy)_2(acac)$/B3PYMPM/LiF/ Al);[274] this trait can be attributed to the energy-transfer mechanism in OLEDs that exploit exciplexes. Therefore, the dominant emission mechanism of the OLEDs that use bulk exciplexes is not by direct charge trapping at dopants (Figure 7a), but by energy transfer to the dopant from the exciplex-forming mixed host (Figure 7b); this process can be observed by measuring the overshoot of transient EL and the reduced V_{OP}.[274]

The miscibility of electron donor and acceptor, and the morphological property of bulk exciplex-forming mixed host film should be considered as factors that determine the efficiency of SOLEDs that use bulk exciplexes.[293] Solution-processed mixed-host film can form the bulk exciplex and has bipolar charge transport characteristics, but phase separation of an EML such as *m*-MTDATA:TmPyPB can reduce exciton diffusion and decrease energy transfer compared to use of SOLEDs that use interfacial exciplexes, and thereby degrade device efficiency.[292] SOLEDs and EOLEDs that exploit a mixed host that forms bulk exciplexes may show different efficiencies depending on ETH.[293] When OLEDs used *m*-MTDATA:TmPyPB films, the V_{TO} and V_{OP} were much smaller in EOLEDs than in SOLEDs, although the efficiencies of OLEDs that use *m*-MTDATA: 1,3-bis[(p-tert-butyl)phenyl-1,3,4-oxadiazoyl]benzene (OXD-7) were almost identical in both thermal evaporation and solution process.[293] In particular, the hole-transporting property of *m*-

This article is protected by copyright. All rights reserved.

15214095, ja, Downloaded from https://onlinelibrary.wiley.com/doi/10.1002/adma.202207454 by Seoul National University, Wiley Online Library on [28/11/2022]. See the Terms and Conditions (https://onlinelibrary.wiley.com/terms-and-conditions) on Wiley Online Library for rules of use; OA articles are governed by the applicable Creative Commons License

Accepted Article

MTDATA:TmPyPB film was greatly degraded in solution-processed films, whereas that of *m*-MTDATA:OXD-7 film was maintained. The different effects of deposition processes on electrical properties of *m*-MTDATA:TmPyPB film originate from poor film quality caused by severe phase separation, and not from the intrinsic characteristics of the mixed host. Therefore, fabrication of SOLEDs that use this film requires selection of the ideal host material that can guarantee good mutual miscibility of constituting hosts, and thus avoid phase separation.

Use of a bulk-exciplex host in fluorescent OLEDs requires minimization of direct exciton trapping at fluorescent dopants, and of DET from the T_1 level of exciplex to T_1 of fluorescent dopant.[281] Moreover, the spectral overlap between PL emission from the exciplex and absorption spectra by fluorescent dopant facilitates efficient FRET (Figure 7h), which can be identified by extended PL lifetime by delayed fluorescence decay of exciplex host compared to that of a single dopant.[291] To fulfil these requirements, exciton trapping should be minimized by engineering small differences in HOMO and LUMO energy levels between the exciplex-forming hosts and fluorescent dopant, and DET should be minimized by using a suitably low fluorescent dopant concentration in the exciplex host to facilitate efficient long-range energy transfer (FRET) between S_1 levels.[291] To fabricate efficient fluorescent OLEDs that use exciplexes, the FRET should be dominated by direct FRET from S_1 of the exciplex host to S_1 of the fluorescent dopant, and by the RISC process, followed by subsequent FRET to the dopant; the latter process causes delayed fluorescence in the fluorescent dopant (Figure 7b).[294] Therefore, nearly 100% triplet harvesting in the conventional green fluorescent dopant, 10-(2-benzothiazolyl)-1,1,7,7-tetramethyl-2,3,6,7-tetrahydro-1H,5H,11H-benzo[1]pyrano[6,7,8-ij]quinolizin-11-one (C545T), was achieved by using 0.2% doping concentration in a bulk exciplex host composed of TAPC and 3-(4,6-diphenyl-1,3,5-triazin-2-yl)-9-phenyl-9H-carbazole (DPTPCz) (EQE_{max} = 3.9% (DPTPCz:1% C545T), 7.5% (DPTPCz:1% C545T), 14.5% (DPTPCz:0.2% C545T).[281] Other work has determined that the concentration of conventional red fluorescent dopant, 4-(dicyanomethylene)-2-t-butyl-6-(1,1,7,7-tetramethyljulolidyl-9-enyl)-4H-pyran (DCJTB)

This article is protected by copyright. All rights reserved.

15214095, ja, Downloaded from https://onlinelibrary.wiley.com/doi/10.1002/adma.202207454 by Seoul National University, Wiley Online Library on [28/11/2022]. See the Terms and Conditions (https://onlinelibrary.wiley.com/terms-and-conditions) on Wiley Online Library for rules of use; OA articles are governed by the applicable Creative Commons License

affects the energy transfer efficiency.[294] As the DCJTB concentration increased from 1.0 to 1.5% in the exciplex host of TCTA:2,4,6-tris(3-(1H-pyrazol-1-yl)phenyl)-1,3,5-triazine (3P-T2T), maximum *EQE*s of devices were decreased from 21.5% to 10.1% by high charge trapping, dopant aggregation, and increased short-range DET process between triplet states.

To develop high-efficiency SOLEDs that use host-dopant EML, the strategy of using hosts that form interfacial and bulk exciplexes has been investigated because it is regarded as an effective way to decrease efficiency roll-off, V_{TO}, and V_{OP} of devices, and to increase their luminous efficiencies. In particular, the high T_1 level and efficient triplet harvesting by RISC of exciplex hosts can help to achieve 100% *IQE* with either fluorescent or phosphorescent dopants. Despite these possible advantages to achieve high-efficiency SOLEDs, fulfillment of industrial standards requires overcoming the operational instability caused by phase separation of mixed hosts that form bulk exciplexes.

4.2. Delayed Fluorescence for SOLEDs

SOLEDs that exploit TADF were invoked as the 3rd generation in the evolution of OLEDs, following fluorescent OLEDs (1st generation) and phosphorescent OLEDs (2nd generation).[193] Use of TADF has been studied for development of future mass-producible OLED devices, because TADF can achieve 100% *IQE* without using expensive rare-earth heavy metals such as Ir and Pt.[15] In OLEDs, injected charge carriers form singlet excitons and triplet excitons in a ratio of 1:3 according to the spin statistics; singlet excitons emit fluorescence, and triplet excitons generate phosphorescence.[295] In 1st generation OLEDs, conventional organics consisted of light elements such as carbon and nitrogen, and the energy level of singlet states was > 0.5 eV higher than that of triplet excited states, so only pure florescence (by 25% of all possible excitons) was possible. [295] In 2nd generation OLEDs, organics that include heavy metals such as Ir and Pt and singlet excited excitons (25% of total

This article is protected by copyright. All rights reserved.

Accepted Article

15214095, ja, Downloaded from https://onlinelibrary.wiley.com/doi/10.1002/adma.202207454 by Seoul National University, Wiley Online Library on [28/11/2022]. See the Terms and Conditions (https://onlinelibrary.wiley.com/terms-and-conditions) on Wiley Online Library for rules of use; OA articles are governed by the applicable Creative Commons License

Accepted Article

excitation) were converted to triplet excited excitons by ISC, then radiatively decayed to the ground state S_0 (100% of all possible excitons).[296,297] In 3rd generation OLEDs, TADF organics have spatially-separated donor and acceptor moieties and have very small ΔE_{ST}; this small energy difference induces RISC by which electrons in triplet excited states are converted to single excited states and produce delayed fluorescence (100% of all possible excitons).[193] TADF emitters are also attractive due to low material price because they do not require expensive heavy-metal complexes. [193]

Several strategies can be used to harvest TADF in OLEDs: 1) use of TADF dopants to convert the excitons on triplet excited states to singlet excited states of TADF emitters, and then to emit delayed fluorescence from the dopant (Subsection 4.2.1) (**Figure 8**a); 2) use of TADF host sensitizer with normal fluorescent dopant emitters (Subsection 4.2.2) (Figure 8b); and 3) use of both host and TADF sensitizing host with normal fluorescent dopant emitters (Subsection 4.2.3) (Figure 8c).

4.2.1. Thermally-activated Delayed Fluorescence Solution-processed OLEDs

The first TADF SOLEDs used TADF-emitting dopants (Figure 8a).[193] EMLs that incorporated 4CzIPN dopant and bis-4-(N-carbazolyl)phenyl)phenylphosphine oxide (BCPO) host material were printed using a roll-to-roll process. An HTL, N,N'-bis(4-diphenylamino-40-biphenyl)-N,N'-diphenyl(1,10-biphenyl)-4,4'-diamine (TPT1), was fabricated using a dry transfer method; this layer facilitated hole injection into the BCPO:4CzIPN EML, improved charge balance in the devices, and achieved *EQE* of 19.1% in SOLEDs.[298] A different host material, (9-carbazolyl)phenyl)silane (SiCz), has higher T_1 (3 eV) than that of TADF dopant materials (T_1 = 2.39 eV), and therefore induced efficient energy transfer to the dopants and achieved efficient carrier confinement, and achieved high *EQE* of 18.3% in SOLEDs that used 4CzIPN.[299]

This article is protected by copyright. All rights reserved.

15214095, ja, Downloaded from https://onlinelibrary.wiley.com/doi/10.1002/adma.202207454 by Seoul National University, Wiley Online Library on [28/11/2022]. See the Terms and Conditions (https://onlinelibrary.wiley.com/terms-and-conditions) on Wiley Online Library for rules of use; OA articles are governed by the applicable Creative Commons License

Accepted Article

Subsequently, researchers have tried to optimize device structures and find optimal host materials to increase the device efficiency in SOLEDs that use TADF dopant molecules. One major research stream in device engineering is to find host materials that have high T_1 and that efficiently confine excitons in the TADF dopants. Compounds that have been used to demonstrate high-efficiency TADF SOLEDs include 1,3-bis{3-[3-(9-carbazolyl)phenyl]-9-carbazolyl}benzene (CPCB) with high T_1 = 2.79 eV (maximum *EQE* of SOLEDs: 10%),[194] (2'-(9H-carbazol-9-yl)-[1,1'-biphenyl]-2-yl)diphenylphosphine oxide (POBPCz) with high T_1 = 3.01 eV (maximum *EQE* of SOLEDs: 12.9%),[300] 9,10-dihydro-9,9-dimethyl-10-(3-(6-(3-(9,9-dimethylacridin-10(9H)-l)phenyl)pyridin-2-yl)phenyl acridin (DDMACPy) with T_1 = 2.8 eV (maximum *EQE* of SOLEDs: 21.0%) and N-(3-(6-(3-(diphenyl amino)phenyl)-pyridin-2-yl)phenyl)-N-phenylbenzenamine (DTPAPy) with T_1 = 2.7 eV (maximum *EQE* of SOLEDs: 8.7%),[301] 10-(4-(4-(9H-carbazol-9-yl)phenylsulfonyl)phenyl)-9,9-dimethyl-9,10-dihydroacridine (CzAcSF) (maximum *EQE* of SOLEDs: 20.1%),[302] new styrene-derived copolymers (ABP73) composed of diphenyl acridine (DPAc) and 2,12-di-tert-butyl-7-phenyl-5,9-dioxa-13bboranaphtho[3,2,1-de]anthracene (TDBA) (maximum *EQE* of SOLEDs: 22.2%), [195] and BCzTC, a bipolar host molecule composed of two 9-phenyl-9H-3,9'-bicarbazole (PBCz) moieties and two 2,12-di-tertbutyl-7-phenyl-5,9-dioxa-13b-boranaphtho[3,2,1-de]anthracene (PDBNA) moieties with triplet states of 2.92 eV (maximum *EQE* of SOLEDs: 30.1%).[303] Electron transport material, (oxybis(3-(tert-butyl)-6,1-phenylene))bis(diphenylphosphine oxide) (DPOBBPE), has also been used in the EML as a host material and has achieved *EQE* of 25.8% in blue-emitting TADF SOLEDs.[304]

Researchers have also made efforts to optimize electron transport layers to improve charge balance, facilitate electron injection and confine excitons in the EML in TADF SOLEDs. A simple modification of conventional TPBi electron transport materials by introduction of a cyano moiety increased T_g to 139 °C, deepened the LUMO level to 2.79 eV, and increased *CE* to 37.7 cd A^{-1} in SOLEDs compared to those of conventional electron transporting TPBi (T_g = 124 °C, LUMO level = 2.38 eV, *CE* = 26.1 cd A^{-1}).[305]

This article is protected by copyright. All rights reserved.

15214095, ja, Downloaded from https://onlinelibrary.wiley.com/doi/10.1002/adma.202207454 by Seoul National University, Wiley Online Library on [28/11/2022]. See the Terms and Conditions (https://onlinelibrary.wiley.com/terms-and-conditions) on Wiley Online Library for rules of use; OA articles are governed by the applicable Creative Commons License

Accepted Article

Double ETL (dETL) composed of 2,4,6-tris(biphenyl-3-yl)-1,3,5-triazine (T2T) and 2,7-bis(2,20-bipyridine-5-yl)triphenylene (Bpy-TP2) was used in TADF SOLEDs instead of the conventional single ETL. A T2T has a high T_1 (~2.8 eV) and therefore confines excitons inside the EML[306] and a Bpy-TP2 has high electron mobility and therefore increases electron injection to the EML.[307] New electron transport materials, 3,3'',5,5''-tetra(3-pyridyl)-1,10;3',100-terphenyl (B3PyPB) and bis-4,6-(3,5-di-4-pyridylphenyl)-2-methylpyrimidine (B4PyMPM), were also developed because they have high triplet excited state > 2.7 eV and can efficiently confine excitons in the TADF-emitting dopants, and achieved *EQE* = 16% in TADF SOLEDs.[308]

Similar studies have been performed on hole injection/transport layers to prevent exciton quenching and facilitate hole injection at the interface between conventional PEDOT:PSS and TADF EML. A major strategy to achieve such a goal is to insert additional hole transporting interlayers between the PEDOT:PSS and the EML. A mixture of PVK and TFB layer on top of PEDOT:PSS formed a uniform EML, facilitated hole injection, improved charge carrier balance and increased the resistance against other solution process; these various effects of PVK:TFB interlayer achieved *EQE* = 18.19% in SOLEDs.[160]

A buffer HIL in which PEDOT:PSS and PFI self-organized to yield a PFI-enriched top surface has been used in TADF SOLEDs. The PFI-enriched top surface has an increased *WF* = 5.95 eV compared to PEDOT:PSS (WF = 5.20 eV), and therefore improves hole injection to the EML and prevents exciton quenching at the interface.[15] These strategies in TADF SOLEDs achieved *EQE* = 24% in green emission, *EQE* = 13.3% in red emission and *EQE* = 8.1% in blue emission (Figure 8d-f).[15]

Crosslinked HTLs have been used on top of PEDOT:PSS in TADF SOLEDs because crosslinked HTLs endure subsequent solution processes of overlying TADF EMLs. Crosslinked X-TPACz consists of N-(4-(9H-carbazol-3-yl)phenyl)-N-([1,1'-biphenyl]-4-yl)bicyclo[4.2.0]octa-1(6),2,4-trien-3-amine as a thermally-crosslinkable pendant, and bicyclo[4.2.0]octa-1,3,5-trien-3-yl group as a thermally-

This article is protected by copyright. All rights reserved.

15214095, ja, Downloaded from https://onlinelibrary.wiley.com/doi/10.1002/adma.202207454 by Seoul National University, Wiley Online Library on [28/11/2022]. See the Terms and Conditions (https://onlinelibrary.wiley.com/terms-and-conditions) on Wiley Online Library for rules of use; OA articles are governed by the applicable Creative Commons License

Accepted Article

crosslinkable unit. X-TPACz has high μ_h = 2.01 × 10^{-4} cm^2 V^{-1} s^{-1}, which exceeds that of conventional PVK (μ_h = 1.32 × 10^{-5} cm^2 V^{-1} s^{-1}), uniform surface, and resistivity against common organic solvents and thus achieved high *EQE* = 19.18% in TADF SOLEDs.[309]

The resistivity of crosslinked HTLs to solution processing allows formation of multiple HTLs in which the first crosslinked HTL, N,N'-bis(4-(6-((3-ethyloxetan-3-yl)methoxy))-hexylphenyl)-N,N'-diphenyl-4,4'-diamine (OTPD), has high μ_h and facilitates hole injection, whereas the second crosslinked HTL, N,N-bis(4-(6-((3-ethyloxetan-3-yl)methoxy)hexyloxy)phenyl)-3,5-di(9H-carbazol-9-yl)benzenamine (Oxe-DCDPA), has high T_1 states and confines the exciton in the dopants by suppressing triplet energy transfer from dopant to HTL (backward energy transfer).[310] This double multiply-crosslinked HTL improves the charge balance and increases the radiative recombination of excitons in SOLEDs, and thereby achieved high *EQE* = 30.8% in green emission and *EQE* = 27.2% in bluish-green emission.[310]

Interfacial exciplexes have also been used in TADF SOLEDs because formation of exciplexes can yield negligible barriers to both electron injection and hole injection, and therefore can efficiently reduce V_{OP} (Subsection 4.1.1). Device engineering to exploit exciplexes has been performed in TADF SOLEDs. For example, 4,4'-bis(9-carbazolyl)-2,2'-dimethylbiphenyl (CDBP) has been used with 2,4,6-tris[3-(diphenylphosphinyl)phenyl]-1,3,5-triazine (PO-T2T) as an exciplex-forming mixed host to suppress TPA and facilitate charge injection to the TADF emitters; this method achieved *EQE* = 21% in blue emission and 20.8% in white emission from TADF SOLEDs, and also suppressed efficiency roll-off (*EQE* = 20.2% at 100 cd m^{-2} in both blue-emitting and white-emitting TADF SOLEDs).[311] The *EQE* in TADF SOLEDs that use exciplexes was further improved to 31.2% by using poly(9,9-diphenyl-10-(4-vinylbenzyl)-9,10-dihydroacridine) (P(Bn-DPAc)) as a polymer donor and 2-(4'-(tertbutyl)-[1,1'-biphenyl]-4-yl)-4,6-diphenyl-1,3,5-triazine (tPTRZ) as a small-molecule acceptor mixed host.[56]

This article is protected by copyright. All rights reserved.

15214095, ja, Downloaded from https://onlinelibrary.wiley.com/doi/10.1002/adma.202207454 by Seoul National University, Wiley Online Library on [28/11/2022]. See the Terms and Conditions (https://onlinelibrary.wiley.com/terms-and-conditions) on Wiley Online Library for rules of use; OA articles are governed by the applicable Creative Commons License

Accepted Article

4.2.2. Host-sensitized TADF for Solution-processed OLEDs

Although TADF emitting dopants open a new era in both SOLEDs and evaporated OLEDs by achieving 100% *IQE* without using expensive rare-earth heavy elements, they still have serious problems: a very delicate molecular design is needed to obtain small ΔE_{ST} while maintaining high luminescent efficiency; the limited number of configurations of the TADF emitters limits the color purity of their emit light (i.e., increases the FWHM); and a long exciton lifetime (> μs) induces severe efficiency roll-off in a device.[312,313] A new TADF emitting mechanism, called "host sensitized TADF" (hsTADF), was proposed to solve such problems in TADF emitters (Figure 8b).[312,313] Excitons are electrically generated in triplet excited states, then transferred to the singlet excited states by RISC in host materials, not in a TADF dopant; excited excitons are then transferred from singlet excited states in the host to singlet excited states in normal fluorescent emitters, which can theoretically harvest 100% of excitons without phosphorescent dopants or TADF-emitting dopants. In this mechanism, FRET occurs rapidly from TADF-sensitizing host to fluorescent dopants, and thus decreases efficiency roll-off and increases operating stability in SOLEDs. Furthermore, hsTADF can utilize normal fluorescence dopants, which have narrower FWHM than that of TADF emitter, and that can achieve 100% *IQE* in fluorescence with relatively high color purity.[312]

To achieve hsTADF, a fluorescent emitter should have large spectral overlap with host materials so that it can rapidly accept the energy from TADF by the FRET.[312] 2,8-bis(diphenylphosphine oxide)dibenzofuran (DBFPO) has a high T_1 of 3.2 eV, and therefore can convert 75% of excitons from triplet states to singlet states by RISC; the excitons are then transferred to the singlet states of N,N'-bis-dibenzofuran-4-yl-N,N'-bis-(2,5-dimethyl-phenyl)-pyrene-1,6-diamine (BPPyA). SOLEDs that used hsTADF in the configuration (ITO/HATCN/TAPC/DCDPA/DBFPO:DMAC-DMT/TsPO1/TPBi/LiF/Al) showed *EQE* = 22.5% and

This article is protected by copyright. All rights reserved.

15214095, ja, Downloaded from https://onlinelibrary.wiley.com/doi/10.1002/adma.202207454 by Seoul National University, Wiley Online Library on [28/11/2022]. See the Terms and Conditions (https://onlinelibrary.wiley.com/terms-and-conditions) on Wiley Online Library for rules of use; OA articles are governed by the applicable Creative Commons License

Accepted Article

operating stability of 2.8 h, which is four times longer than that of normal TADF SOLEDs that have the configuration (ITO/HATCN/TAPC/3,5-di(9H-carbazol-9-yl)-N,N-diphenylaniline (DCDPA)/MADN:BPPyA/diphenyl-4-triphenylsilylphenyl-phosphine oxide (TSPO1)/LiF/Al).[312] TADF SOLEDs that used DPOBBPE TADF-sensitizing host 2,5,8,11-tetra-tertbutylperylene (TBPe) achieved *EQE* = 25.8% in blue emission.[304]

The exciplex system has also been used in hsTADF SOLEDs.[314] An electron-donating material, TCTA, and an electron-accepting material 2,4,6-tris(3'-(pyridin-3-eyl)biphenyl-3-yl)-1,3,5-triazine (Tm3PyBPZ), form an exciplex in the EML. A TCTA:Tm3PyBPZ mixed host has a small ΔE_{ST} = 27 meV, so RISC can rapidly convert triplet excitons to single excitons.[314] Then theoretically, 100% of excitons can be transferred from the S_1 of the hosts to the S_1 of the normal fluorescence dopants by fast FRET, and achieve decent *EQE*s in SOLEDs (11.9% for C545T dopant, 13% for 5,6,11,12-tetraphenyltetracene (rubrene) dopant).[314]

hsTADF in which TADF-sensitizing hosts are co-deposited with normal fluorescence dopant in EML can prevent efficiency roll-off in TADF SOLEDs by sensitizing RISC in host materials but not in dopant materials, but high concentration of TADF-sensitizing host materials could induce exciton quenching due to their high population in SOLEDs. Beyond hsTADF, additional host matrices can be co-deposited with TADF sensitized hosts and normal fluorescence dopants (i.e., triple components in EML); these triple-materials system is called hyperfluorescence.

4.2.3. Hyperfluorescence for Solution-processed OLEDs

Hyperfluorescence is a proposed phenomenon in which TADF molecules work in the organic host as assistant dopants that facilitate energy transfer from triplet excited states to singlet excited states, then convert the singlet exciton to normal fluorescence dopant (Figure 8c).[315] In the three

This article is protected by copyright. All rights reserved.

15214095, ja, Downloaded from https://onlinelibrary.wiley.com/doi/10.1002/adma.202207454 by Seoul National University, Wiley Online Library on [28/11/2022]. See the Terms and Conditions (https://onlinelibrary.wiley.com/terms-and-conditions) on Wiley Online Library for rules of use; OA articles are governed by the applicable Creative Commons License

components (normal host, TADF sensitizers, fluorescent emitters), the carriers are electrically injected into the host materials then transported to the TADF sensitizer molecules (TADF assistant dopants) due to their smaller bandgap than that of host, then RISC converts triplet excitons to their singlet states due to the small ΔE_{ST} of TADF sensitizers. Then FRET transfers excitons on the singlet excited states in TADF sensitizer molecules to the singlet excited states of fluorescence dopants (Figure 9c). An optimal concentration of TADF sensitizer molecules in host materials can facilitate carrier recombination and prevent concentration quenching and unnecessary DET from TADF sensitizers to triplet excited states in the fluorescent emitter. The first hyperfluorescence OLEDs (maximum *EQE* = 17.2%) used mCBP hosts, 2,4,6-tri(4-(10Hphenoxazin-10H-yl)phenyl)-1,3,5-triazine (tri-PXZ-TRZ) TADF sensitizer molecules and 2,8-ditert-butyl-5,11-bis(4-tert-butylphenyl)-6,12-diphenyltetracene (TBRP) fluorescent dopants, and an EML fabricated by thermal deposition.[315] In SOLEDs that used hyperfluorescence TADF, 4CzIPN with adhered tert-butyl group sensitized RISC and favored energy transfer to the fluorescent emitter, cibalackrot, in the CBP host materials, and yielded *EQE* = 7.7%.[316] In addition to the hyperfluorescence system based on small organic molecules, SOLEDs that use hyperfluorescence TADF polymers have been developed; hyperfluorescent polymers have both a sensitizer group and fluorescent chromophore group and induce both RISC and FRET (*EQE* = 10.3% for red emission, 19.2% for green emission, and 14.6% for blue emission).[317]

Subsection 4.2 introduces several research strategies to harvest TADF in SOLEDs: TADF dopant system (subsection 4.2.1), TADF host sensitizer:normal fluorescence dopant system (subsection 4.2.2), hyperfluorescence system (subsection 4.2.3). Research efforts in SOLEDs that use delayed fluorescence have greatly increased device efficiency and operating lifetime, but LT_{95} of SOLEDs that use delayed fluorescence is still far below the requirement of OLEDs for industrial applications[21]. Therefore, to enable commercialization of SOLED that exploit delayed fluorescence, methods must be found to improve charge balance and radiative recombination of excitons. These

This article is protected by copyright. All rights reserved.

Accepted Article

15214095, ja, Downloaded from https://onlinelibrary.wiley.com/doi/10.1002/adma.202207454 by Seoul National University, Wiley Online Library on [28/11/2022]. See the Terms and Conditions (https://onlinelibrary.wiley.com/terms-and-conditions) on Wiley Online Library for rules of use; OA articles are governed by the applicable Creative Commons License

goals require research to improve methods of materials synthesis to increase the stability of organic molecules.

4.3. Operational Stability of Solution-processed OLEDs

The biggest obstacle to commercialization of SOLEDs is that they are less operationally stable than EOLEDs (Tables 1 and 2). The first challenge to solve is to increase the operational instability of SOLEDs.

One of the main differences between solution-processed and vacuum-evaporated organic film is the film morphology, which can be affected by the choice of organic solvent.[16] Organic thin films produced by a solution process are usually less dense than those fabricated by thermal evaporation, because during the solution process, organic molecules can aggregate, and phases can segregate (**Figure 9**a). The morphological and photophysical characteristics of organic thin films and their OLED devices have been systematically compared according to fabrication methods.[16] SOLEDs showed higher luminance and current density at the same voltage compared to those of EOLEDs that had with same device architecture; the difference is a result of an increased μ_h in solution-processed EML film.[16] Local aggregation of molecules that causes altered film morphology increases μ_h of the organic film by shortening the charge-transport pathways in the film, but solvent residues in thin film provide easy paths for oxygen diffusion into the film.[16] The resulting oxygen impurities in the film act as the electron traps during OLED operation, so altered charge balance within the EML results in accumulation of excess charges at the interface between the EML and the charge-transporting layer; this accumulation decreases operational stability of SOLEDs compared to their vacuum-deposited counterparts (Figure 9b).

This article is protected by copyright. All rights reserved.

Accepted Article

15214095, ja, Downloaded from https://onlinelibrary.wiley.com/doi/10.1002/adma.202207454 by Seoul National University, Wiley Online Library on [28/11/2022]. See the Terms and Conditions (https://onlinelibrary.wiley.com/terms-and-conditions) on Wiley Online Library for rules of use; OA articles are governed by the applicable Creative Commons License

Accepted Article

The different molecular structures of guest molecules within the EML of SOLEDs also affect the initial film morphology due to different intermolecular interactions, which can cause molecular aggregation and phase separation.[59] Therefore, solution-processed EML may develop a strong new emission band in the photoluminescence spectrum, as a result of greater molecular aggregation of guest molecules than in the vacuum-deposited EML (Figure 9 c-e).

The electrical stress applied to the EML during OLED operation also aggravates molecular aggregation of guest molecules, and coexistence of polarons and excitons accelerates guest aggregation due to the polaron-exciton interaction, which greatly shorten device operational lifetime.[59]

The choice of solvent can affect film morphology, because the low solubility of guest materials in organic solvent makes them prone to aggregate by exciton-polaron interaction.[59] Therefore, the molecular structure of guest molecules must also be considered when attempting to engineer the morphological characteristics of films and their stability during OLED operation.

The formula of OLED lifetime used to estimate LT_{50} for OLEDs is $L_0^n \times LT_{50}$= *constant* (Section 2), where acceleration factor *n* differs for each OLED. [318] The formula indicates that high initial luminance of OLEDs accelerates their degradation because of high electrical current density in the device.[319] For practical display and lighting application of OLEDs, high luminance is essentially required (e.g., ~500 cd m^{-2} for general displays, ~1,000 cd m^{-2} for indoor lighting, ~5,000 cd m^{-2} for outdoor displays or lighting), so OLEDs must have good operational stability at high luminance.[320]

Application of high bias to OLEDs to induce high luminance causes severe excessive charge accumulation at the interfaces of each functional layer in the device;[321] this accumulation leads to severe exciton-exciton annihilation (e.g., TTA) and exciton-charge interaction (e.g., TPA). Especially in SOLEDs, the aggregation of molecules in solution-processed organic film increases the population of triplet excitons and the frequency at which they are annihilated.[20] By these processes, such as TTA

This article is protected by copyright. All rights reserved.

15214095, ja, Downloaded from https://onlinelibrary.wiley.com/doi/10.1002/adma.202207454 by Seoul National University, Wiley Online Library on [28/11/2022]. See the Terms and Conditions (https://onlinelibrary.wiley.com/terms-and-conditions) on Wiley Online Library for rules of use; OA articles are governed by the applicable Creative Commons License

Accepted Article

and a TPA, carrier accumulation leads to non-radiative recombination at the interface, and thereby reduces luminous efficiency at high luminance,[20] and can also cause chemical degradation of organic conjugated molecules by undesirable photochemical pathways rather than the radiative channel.[322] Therefore, for both EOLEDs and SOLEDs, controlling charge balance is a main strategy to increase device efficiency and stability, and decrease efficiency roll-off.

SOLED devices usually have a simple device structure because solution processing can cause intermixing or redissolution; both processes can impede deposition of multilayers. Therefore, charge balance within SOLEDs is not easily achieved;[12,20] many strategies to improve it have been tried, such as use of charge-transporting materials that have high charge-carrier mobility,[323] modification of energy levels,[324] and use of a mixed-host system.[318]

The operational stabilities of phosphorescent and TADF SOLEDs have been increased by synthesizing novel hole-transporting phenothiazine and phenoxazine-substituted materials that have a fluorene core; both materials have higher $\mu_h > 5.7 \times 10^{-3}$ cm^2 V s^{-1} than the conventional hole transporting NPB,[325] ($\mu_h = 2.6 \times 10^{-4}$ cm^2 V s^{-1}).[323]To verify the improved device characteristics with high μ_h of HTMs, SOLEDs that incorporate these newly-synthesized HTMs were compared with those with conventionally-used NPB that uses a phosphorescent yellow emitter, Bis(4-phenylthieno[3,2-c]pyridinato-N,C2') (acetylacetonate) iridium(III) (PO-01), (ITO/PEDOT:PSS/HTMs/CBP:PO-01/TPBi/Al) and also a device that uses a TADF green emitter, 4CzIPN (ITO/PEDOT:PSS/HTMs/CBP:4CzIPN/TPBi/Al). In both phosphorescent and TADF SOLEDs, operational lifetime LT_{50} was obviously increased improvements (to 11.7 h from 3.8 h for phosphorescent SOLEDs and to 14.9 h from 4.9 h for TADF SOLEDs at L_0 = 10,000 cd m^{-2}).

Use of a mixed-host in the EML is another way to increase operational stability without using multilayers. The mixed-host system prevents charge carrier accumulation at the interface; this accumulation degrades OLED stability.[12,20,61,318] The mixed-host EML improved electron-hole charge

This article is protected by copyright. All rights reserved.

15214095, ja, Downloaded from https://onlinelibrary.wiley.com/doi/10.1002/adma.202207454 by Seoul National University, Wiley Online Library on [28/11/2022]. See the Terms and Conditions (https://onlinelibrary.wiley.com/terms-and-conditions) on Wiley Online Library for rules of use; OA articles are governed by the applicable Creative Commons License

Accepted Article

carrier balance with thickness-controlled blade coating of functional layers in SOLEDs.[318] Use of the mixed host in SOLED devices simplifies their structure and thereby reduced the number of interfaces that contribute to the degradation of OLEDs.

In one case, a TFB was used as an HTL to improve hole injection by reducing the energy barrier to hole injection between HIL and EML, and to protect the EML from the acidic PEDOT:PSS HIL.[318] Also, hole transporting NPB and electron transporting 2-methyl-9,10-di-2naphthylanthracene (MADN) were adopted in a mixed-host EML that used 3% N, N'-(4,4'-(1E, 1'E)-2,2'-(1,4-phenylene) bis(ethene-2,1-diyl)bis (4,1-phenyl-ene))-bis(2-ethyl-6-methyl-N-phenylaniline) BUBD-1 (in the structure ITO/PEDOT: PSS/TFB/10%NPB: 87%MADN: 3% (BUBD-1)/97%MADN: 3%BUBD-1/Alq_3/LiF/Al); in blue fluorescent SOLEDs, the device showed extended lifetime of 117.7 h at initial luminance of 500 cd m^{-2}.[318]

The charge-transport behavior of materials can also control the location of the recombination zone in EML. The intermixed interface between layers is where exciton-polaron quenching and successive chemical degradation of molecules occur. A shift of the recombination zone away from this interface can contribute to increase in device operational lifetime.[324] 7,7-dimethyl-5-phenyl-2-(9-phenyl-9H-carbazol-3-yl)-5,7-dihydroindeno [2,1-b] Carbazole (PCIC) and 2,4 - diphenyl - 6 - bis(12 - phenylindolo)[2,3 - a] carbazole - 11 - yl) - 1,3,5 - triazine (DIC-TRZ) were used to verify that the charge transporting ability of host molecules and the location of recombination zone affect the operational lifetime. PCIC has a shallow HOMO level (~5.5 eV), which facilitates hole injection to the EML (HOMO: ~6 eV). In contrast, DIC-TRZ has a deep LUMO level (~2.8 eV), which favors electron injection over hole injection. By using two different EML compositions, the location of the recombination zone was controlled to be different locations. To verify the influences on device lifetime, two SOLEDs were fabricated [device I: ITO/PEDOT:PSS/crosslinked HTM/PCIC:$Ir(mppy)_3$ /DIC-TRZ/2-[4-(9,10-dinaphthalen-2-yl-anthracen-2-

This article is protected by copyright. All rights reserved.

15214095, ja, Downloaded from https://onlinelibrary.wiley.com/doi/10.1002/adma.202207454 by Seoul National University, Wiley Online Library on [28/11/2022]. See the Terms and Conditions (https://onlinelibrary.wiley.com/terms-and-conditions) on Wiley Online Library for rules of use; OA articles are governed by the applicable Creative Commons License

Accepted Article

yl)-phenyl]-1-phenyl-1H-benzoimidazole(dNAPPBi):Liq/Liq/Al; device II: ITO/PEDOT:PSS/ crosslinked HTM/DIC-TRZ:Ir(mppy)$_3$ /DIC-TRZ/dNAPPBi:Liq/Liq/Al]. Device I that uses PCIC had longer LT_{50} = 42 h than device II (14 h) because the recombination zone in Device I formed far from the interface between HTL and EML (Figure 9f).[324] To prevent intermixing of layers in SOLEDs, which causes low stability, a solvent additive 1,8-diiodooctane (DIO), was added to amino-functionalized polyfluorene (PFN) to crosslink polyelectrolyte used as an electron-injection layer.[326] After thermal annealing of PFN film at low temperature, DIO residues in the film bind the amino-side groups of PFN, so the crosslinked PFN layer is not dissolved by non-polar solvents. This use of the crosslinked PFN layer increased the LT_{70} to 4 h for the polymer LED (in the structure ITO/PEDOT:PSS/Super yellow/PFN/Ag) compared to 2 h in the device that used non-crosslinked PFN.[326]

High operational temperature induced by Joule heating can also cause degradation of SOLEDs.[327] The lifetime of an OLED is generally one or two orders of magnitude lower at 60 to 70 °C than at room temperature.[328] At 33 V, surface temperature of operating OLEDs (Al/Alq$_3$/TPD/ITO) can be increased to 86 °C,[293] which is higher than T_g = 65 °C of TPD. [198] The high temperature causes severe breakdown because temperature > T_g induces recrystallization of organic materials. This phenomenon emphasizes the importance of operational temperature and T_g of the materials of SOLEDs. Molecular vibrations are inevitable in organic materials that have low T_g, and may cause them to migrate from their initial positions inside the device layers. This movement can affect nearby layers and lead to destruction of the display.[329] Increased electron injection and transport of ETL as well as high T_g of host material can increase the operational stability of SOLED devices. [194] CPCB was adopted as a host material due to high T_1 (2.79 eV) and high T_g = 165 °C, which is higher than T_g of conventionally used CBP (62 °C); this difference implies that the morphological stability will increase when CPCB is used in SOLEDs.[194] TADF SOLEDs with CPCB (structure ITO/PEDOT:PSS/4CzIPN:CPCB/T2T/Bpy-TP2)/LiF/Al) showed improved T_{50} ~184 h at initial luminance of 1,000 cd m^{-2} (Figure 9g).

This article is protected by copyright. All rights reserved.

15214095, ja, Downloaded from https://onlinelibrary.wiley.com/doi/10.1002/adma.202207454 by Seoul National University, Wiley Online Library on [28/11/2022]. See the Terms and Conditions (https://onlinelibrary.wiley.com/terms-and-conditions) on Wiley Online Library for rules of use; OA articles are governed by the applicable Creative Commons License

Accepted Article

Other device components such as the conducting electrodes,[330] substrates,[331] and encapsulation[332] can also effect the operational stability of SOLEDs. The *WF* and electrical conductivity (inversely, sheet resistance) of transparent conducting electrodes effect the charge-carrier injection and concomitant charge-carrier balance inside the LED devices, and thereby determine luminous efficiency and operational stability of devices.[64,67,154,330,333] The surface roughness also has a crucial influence on operational stability because the protruding regions on the electrode cause local path shortening, which can cause leakage current and degrade device efficiencies significantly.[63,64] Also, good surface topography of substrates can contribute to reducing the number of dark spots in OLED devices, and thus increasing device stability.[331] Also, realization of SOLED displays that have lifetime that is sufficient to make commercialization feasible requires development of a device-passivation technique that does not cause pinholes, and that has low-water-vapor-transmission-rate.[332]

5. Inkjet processing

IJP is a process in which inks are ejected by piezoelectricity and the droplets land on the intended pixels. IJP greatly reduces material consumption compared to conventional thermal evaporation. Also, the substrate lies on a plate during IJP, so the method is suitable for large area-manufacturing, especially on mother glasses over 10.5G (2,940 mm × 3,370 mm).[29,71]

The display industry has used IJP to manufacture SOLED panels. For proprietary reasons, most panel makers do not disclose their recent luminous characteristics of SOLED panels. However, we can infer these characteristics from the data of material suppliers (Table 1). Only one panel maker (JOLED Inc., Japan), mass-produces SOLED panels.[50] The size of mass-produced panels is 22, 27, or 32 inch, with 204, 163, and 139 ppi, respectively. LG Display Co., LTD (South Korea) has been reported to test the inkjet printer for 8G mother glasses (2,200 mm × 2,500 mm) mother in pilot

This article is protected by copyright. All rights reserved.

15214095, ja, Downloaded from https://onlinelibrary.wiley.com/doi/10.1002/adma.202207454 by Seoul National University, Wiley Online Library on [28/11/2022]. See the Terms and Conditions (https://onlinelibrary.wiley.com/terms-and-conditions) on Wiley Online Library for rules of use; OA articles are governed by the applicable Creative Commons License

Accepted Article

production.[330] Juhua Co. Ltd. (China) demonstrated a 31-inch rollable FHD OLED TV manufactured by IJP in 2020.[331]

Most solid materials introduced in this review were evaluated using devices that had been prepared using spin-coating, not by IJP. Their processability in IJP must also be evaluated. For a solution process to deposit multilayer stacked structures, it must use IJP, vacuum drying, and baking process (**Figure 10**a). To achieve uniform and flat films, the physical properties of inks, including solution orthogonality[26,38,71], viscosity[40,74,332], boiling point[162,333], and surface tension[53,334,335], must be finely controlled. Here, we review the required physical properties of inks to make uniform and well-defined multilayer stacked structures by using IJP and vacuum drying.

5.1. Solution orthogonality

For IJP, the underlying organic layers must have a resistance to the solvents that are used for the upper layers, i.e., two adjacent layers must have high solution orthogonality.[71] High molecular weight of polymers or crosslinkable molecules can guarantee solution orthogonality, and these approaches, which were introduced in earlier sections, have successfully produced HILs and HTLs. However, small molecules, especially for EMLs and ETLs, have required use of a different strategy to introduce orthogonal solvents.

The HSPs describe solute-solvent and solvent-solvent miscibility, and can be used to identify orthogonal solvents.[336] The HSP domain can be determined by the following equations:

$$(\partial_t)^2 = (\partial_D)^2 + (\partial_P)^2 + (\partial_H)^2, \quad (1)$$

$$(R_a)^2 = 4(\partial_{D1} - \partial_{D2})^2 + (\partial_{P1} - \partial_{P2})^2 + (\partial_{H1} - \partial_{H2})^2, \quad (2)$$

This article is protected by copyright. All rights reserved.

15214095, ja, Downloaded from https://onlinelibrary.wiley.com/doi/10.1002/adma.202207454 by Seoul National University, Wiley Online Library on [28/11/2022]. See the Terms and Conditions (https://onlinelibrary.wiley.com/terms-and-conditions) on Wiley Online Library for rules of use; OA articles are governed by the applicable Creative Commons License

Accepted Article

where ∂_t is the total HSP, ∂_D, ∂_P, and ∂_H are HSPs of atomic (D), dipolar (P), and hydrogen bonding (H) interactions, respectively, and R_a is the geometric distance, within the HSP domain, between two molecules in the mixture. To achieve solution orthogonality, the solutions for two adjacent organic layers must be as far apart as possible in the HSP domain. A single-solvent system cannot easily meet HSP for orthogonality concurrent with solubility for solid contents. Therefore, most inks use a multi-solvent system in which a primary solvent provides good solubility for solutes, and a secondary or third solvent maintains the HSP distance with the solution that was used for the underlying layers.[26]

A solvent-resistance test can be used to test the orthogonality of inks.[38] In the test, the thin film sample is rinsed by the solvents of desirable inks for the overlying layer, then the PL of the sample is measured. By comparing the integrated intensities of the rinsed film and an untreated the film, the thickness remaining after the test can be calculated. This test has revealed that solvent resistance can be improved by increasing the molecular weight of small molecules in EMLs (Figure 10b).[26,38]

The solvent wash-out test can also assess the solution orthogonality of EMLs.[26] This test is performed by spin-coating with solvent-only ink over the EML film on anode/HIL/HTL, then thermally annealing the resulting film. Then tested sample is transferred to a thermal evaporation chamber to finalize the device fabrication process. Devices in which the EML dissolves show lower luminance, compared with EMLs that do not dissolve (Figure 10c).

5.2. Inkjet jettability

This article is protected by copyright. All rights reserved.

15214095, ja, Downloaded from https://onlinelibrary.wiley.com/doi/10.1002/adma.202207454 by Seoul National University, Wiley Online Library on [28/11/2022]. See the Terms and Conditions (https://onlinelibrary.wiley.com/terms-and-conditions) on Wiley Online Library for rules of use; OA articles are governed by the applicable Creative Commons License

Accepted Article

During IJP, each ink droplet must be precisely dropped on the desired pixel. This goal is complicated by the process in which ejected droplets are consolidated (Figure 10d).[332,337] At the break-off point, the ejected droplet first forms a head with an attached tail, which quickly merges with the head at a point that is separated from the nozzle by a 'consolidation gap'. A suitable consolidation gap between each pairs of drops is ~500 μm.[162] However, the ink tail can disconnected from its head, to yield small 'satellite' droplets.[39] They can disturb accurate drop placement, because they can be misdirected by aerodynamic and electrostatic forces. Use of polymer inks, in which polymer chains have a viscoelastic coil-stretch transition, can reduce the formation of satellite droplets.[40]

The rheological properties of solution during IJP can be described using three non-dimensional parameters: the Reynolds (*Re*), Weber (*We*), and Ohnesorge (*Oh*) numbers:[338]

$$Re = \frac{\rho v L}{\sigma}, \tag{3}$$

$$We = \frac{\rho v^2 L}{\sigma}, \tag{4}$$

$$Oh = \frac{v}{\sqrt{\rho \sigma L}} = \frac{\sqrt{We}}{Re}, \tag{5}$$

where ρ is the density of the fluid, v is the velocity, L is the drop diameter, and σ is the dynamic viscosity.

The Z constant is the inverse of *Oh*, and has been widely used to predict whether the ink is printable (Figure 11e).[72–74] Z < 1 means that the ink is too viscous to be ejected from the IJP head, whereas Z > 10 indicates the viscosity is too low, so the tail of the droplet does not recombine with

This article is protected by copyright. All rights reserved.

15214095, ja, Downloaded from https://onlinelibrary.wiley.com/doi/10.1002/adma.202207454 by Seoul National University, Wiley Online Library on [28/11/2022]. See the Terms and Conditions (https://onlinelibrary.wiley.com/terms-and-conditions) on Wiley Online Library for rules of use; OA articles are governed by the applicable Creative Commons License

Accepted Article

the main head, and as a result satellites form. Also, if an ink is composed of only solvents with low boiling points, it is unstable, because it tends to evaporate in transit during the IJP process.[162]

The viscosity can be controlled by using a co-solvent system.[74,333] A solvent mixture with high boiling point and surface tension enables drops of small-molecule EMLs to travel straight down to the pixels.[333]

For high-resolution panels, accuracy for drop-placement and drop size are very important. The minimum pixel pitch is determined by the sum of drop size and two times the drop-placement inaccuracy (Figure 10f). For panels that have 300-ppi resolution, the drop size must be < 4 pL and the drop must be placed with an error < 10 μm.[28] Therefore, IJP of high-resolution SOLED panels requires strictly-controlled ink properties and accurate equipment.

5.3. Film flatness

IJP uses droplets, and the dye is suspended in residual solvent after they land on substrate. These solvents can degrade device characteristics, including device efficiency and lifetime, and can damage the thermal evaporator during vacuum evaporation of overlying layers, so vacuum drying must be applied to remove solvents.[53] Uniform film flatness is very important to avoid uneven electrical current and non-uniform luminance in pixel.[28] While most organic films from thermal evaporation are uniform without any additional treatment, in the case of IJP, film flatness depends on the Marangoni effect caused by the surface-tension gradient within ink drops during vacuum drying (Figure 10g).[53,75–77] The convection flow by the Marangoni effect occurs from areas of low surface tension to areas of high surface tension.[53,334] When surface tension is higher in the outer area than in the inner area, the flow gives the film a concave shape, whereas when surface tension is higher in the inner area in than the outer area, the film becomes convex.

This article is protected by copyright. All rights reserved.

15214095, ja, Downloaded from https://onlinelibrary.wiley.com/doi/10.1002/adma.202207454 by Seoul National University, Wiley Online Library on [28/11/2022]. See the Terms and Conditions (https://onlinelibrary.wiley.com/terms-and-conditions) on Wiley Online Library for rules of use; OA articles are governed by the applicable Creative Commons License

Accepted Article

The viscosity of the ink increases during the drying process, and this change can help to prevent Marangoni flow and yield a flat film.[53] One strategy to control the viscosity during the drying process is to use a multi-solvent system.[335,339,340] When solvents have different vapor pressures, they dry at different speeds, so the overall viscosity changes during vacuum drying. Viscosity can also be changed by adjusting the amounts of aggregate parts in polymer chains (Figure 10h).[27,53] This control of viscosity by both the solvent system and by solid content can yield flat films.

Hydrophilicity and hydrophobicity of substrates can also cause pile-up at the edges of banks that are required to separate pixels.[341,342] Control of these characteristics can minimize this pile-up. Ink droplets assume a low contact angle on a hydrophilic surface, and a high contact angle on hydrophobic surface. The bank material is usually composed of acrylic molecules, so droplets can become pinned at the edge of a bank and pile up over it.[76] Different hydrophilic and hydrophobic treatments on the substrate and bank can alleviate the pile-up phenomenon.[343,344] Use of a hydrophobic top interface on a bank can prevent ink overflow and lower the pinning point to avoid pile-up.[345]

The solvent formulation of inks also affects its wetting capability and the uniformity of films.[333,335] An ink that has high surface tension usually recedes from contact with the bank, and thus dewets it.[346] Therefore, to obtain a flat film, the surface-energy mismatch and the dewetting phenomenon must be avoided. Addition of a surfactant can lower the contact angle of ink droplets on substrates.[77,335] The best range of surface tension for uniform PEDOT:PSS films is 28 to 40 mN m^{-1}, but the optimal surface tension can be different depending on the characteristics of the underlying layer.

For high-resolution (> 200 ppi) panels, viscosity control is most important. The inks for high-require resolution panels require a higher solid concentration of inks than low-resolution panels, to

This article is protected by copyright. All rights reserved.

15214095, ja, Downloaded from https://onlinelibrary.wiley.com/doi/10.1002/adma.202207454 by Seoul National University, Wiley Online Library on [28/11/2022]. See the Terms and Conditions (https://onlinelibrary.wiley.com/terms-and-conditions) on Wiley Online Library for rules of use; OA articles are governed by the applicable Creative Commons License

Accepted Article

achieve the same thickness.[27,53] In this case, as the concentration increases, the viscosity of ink increases, so production of flat films becomes difficult. Therefore, fabrication of high ppi-panels by IJP requires deep understanding of the relationship between ink properties and film flatness.[76,347]

6. Conclusion

This review presented the advantages and disadvantages of the SOLEDs compared to those of the EOLEDs, and has considered the industrial needs for OLED display applications. SOLEDs have several advantages for industrial display applications, such as low consumption of materials, easy processing, and large area-manufacturing with 10.5G (2,940 mm × 3,370 mm) mother glasses.[29] The manufacturing cost of SOLEDs produced by IJP is estimated to be ~25% lower than those of currently-used white EOLEDs produced by LG Display Co..[30] However, SOLEDs still have big challenges that must be solved before they are suitable for industrial uses. The most important considerations are regarding solution processing, such as liquid-state processability of materials,[24–26,32,35,39,40] intermixing of layers or redissolution of underlying layers in OLEDs,[41,42] limited efficiencies and their severe roll-off[20] and operational instability caused by less-densely packed solution-processed organic film and their SOLEDs[16] compared to the thermally-evaporated counterparts. EOLED devices have been developed to have multiple functional layers including charge injection, transporting, and blocking layers for better charge balance, and therefore have high luminous efficiency and high operational stability.[11] However, SOLEDs have several processing limitations that result from solution processing of the layers, so a simplified device architecture is more suitable rather than a multilayered structure.[12]

Therefore, materials that compose the common charge-injection/transporting layers must be developed toward multifunction in simplified OLEDs. Basically, the interfacial common layers must have appropriate energy levels to reduce the charge-injection energy barrier into the EML, and

This article is protected by copyright. All rights reserved.

15214095, ja, Downloaded from https://onlinelibrary.wiley.com/doi/10.1002/adma.202207454 by Seoul National University, Wiley Online Library on [28/11/2022]. See the Terms and Conditions (https://onlinelibrary.wiley.com/terms-and-conditions) on Wiley Online Library for rules of use; OA articles are governed by the applicable Creative Commons License

must have charge-carrier mobilities that balance the numbers of charge carriers and prevent charge accumulation within the device. Furthermore, the injection/transporting layer must be able to block opposite charge carriers and to act as a buffer layer near the EML to prevent exciton dissociation in a simple-structured device.[11,12,60,63,152] Also, common layers such as HILs and HTLs are usually located under the solution-processed EML, so the materials must have solvent resistivity to minimize redissolution and intermixing between them. Fabrication of highly-efficient and operationally stable SOLEDs with simple device structure requires development of methods to crosslink organic transporting materials[148,166,167] or to modify the interface between polymeric materials.[169–171]

The dimerization, trimerization or dendrimerization of host or self-host materials for EML is a promising approach to simultaneously render good solvent resistance, high solubility, and wide and easily tunable physical and optoelectronic properties.[129] Also, development of highly-tunable polymeric materials for self-host EML is a suitable research direction. One approach is to incorporate 100%-emissive triplet-harvesting emitters such as phosphorescent and TADF emitters into carefully-designed polymer chains[252,260,261] to achieve solution processability, film formability, solvent resistance, high luminous efficiency and high device stability.

Practically-usable SOLEDs must have high efficiency, low efficiency roll-off, and long-term operational stability. To achieve these traits, the characteristics of the devise must be understood, and their attributes must be characterized in depth. The emission and energy-transfer mechanisms, and influences of host compositions in the device must be further studied for each phosphorescent, TADF, and hyperfluorescence emitter and host system. Specific subjects include direct charge trapping[12,20] and exciplex-forming mixed host EML structure.[293] Also, characterization tools must be developed and used in studies of the interfaces of SOLEDs fabricated by the solution process. Targets for study include the intermixing zone, inter-diffusion, and partial dissolution.

This article is protected by copyright. All rights reserved.

Accepted Article

15214095, ja, Downloaded from https://onlinelibrary.wiley.com/doi/10.1002/adma.202207454 by Seoul National University, Wiley Online Library on [28/11/2022]. See the Terms and Conditions (https://onlinelibrary.wiley.com/terms-and-conditions) on Wiley Online Library for rules of use; OA articles are governed by the applicable Creative Commons License

Accepted Article

The tandem SOLED structure composed of two-or more stacked EL units is another efficient method to increase operational lifetime and decrease the efficiency roll-off characteristics compared to single-EL structure.[348,349] Development of tandem SOLEDs requires a method to fabricate the charge-generation layer between two EL units. Furthermore, tandem OLEDs include more layers than a single device, so the solvent orthogonality or crosslinking of materials in each layer must be carefully designed.

This review has suggested important development directions of materials, devices and processing techniques to reduce the gap between industrial standards of commercial EOLEDs and SOLEDs, as well as the gap between SOLEDs fabricated in industry and in academia. Academic researchers should work to develop novel materials and characterization tools for in-depth understanding the phenomena that occur only in solution-processed devices. The research directions of materials, devices, and solution-processing technologies for SOLEDs reviewed and suggested in this review will guide for both academia and industry toward practically usable, mass-produced SOLEDs displays.

Acknowledgements

This work was supported by the National Research Foundation (NRF) of Korea grant funded by the Korea government (Ministry of Science, ICT & Future Planning) (NRF-2020R1C1C1008485, NRF-2016R1A3B1908431, NRF-2022R1C1C1008282, NRF-2022R1F1A1071707). This work was supported by LG Display under LGD-Hanyang university Incubation Program (C2021007310). J. Y. Woo, M.-H. Park, S.-H. Jeong, and Y.-H. Kim contributed equally to this work.

This article is protected by copyright. All rights reserved.

15214095, ja, Downloaded from https://onlinelibrary.wiley.com/doi/10.1002/adma.202207454 by Seoul National University, Wiley Online Library on [28/11/2022]. See the Terms and Conditions (https://onlinelibrary.wiley.com/terms-and-conditions) on Wiley Online Library for rules of use; OA articles are governed by the applicable Creative Commons License

Accepted Article

Received: ((will be filled in by the editorial staff))
Revised: ((will be filled in by the editorial staff))
Published online: ((will be filled in by the editorial staff))

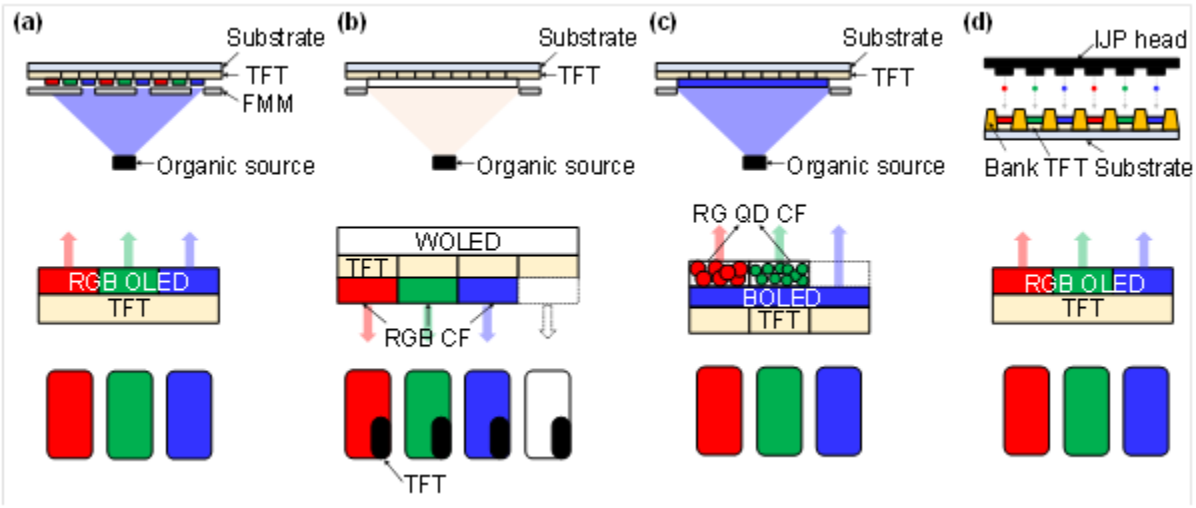

Figure 1. Schematics of structure and light-emission by mass-produced large area panels. (a) Evaporated RGB OLED, (b) Evaporated tandem white-emitting OLED, (c) Evaporated quantum dot tandem blue-emitting OLED, (d) RGB SOLED.

This article is protected by copyright. All rights reserved.

15214095, ja, Downloaded from https://onlinelibrary.wiley.com/doi/10.1002/adma.202207454 by Seoul National University, Wiley Online Library on [28/11/2022]. See the Terms and Conditions (https://onlinelibrary.wiley.com/terms-and-conditions) on Wiley Online Library for rules of use; OA articles are governed by the applicable Creative Commons License

Accepted Article

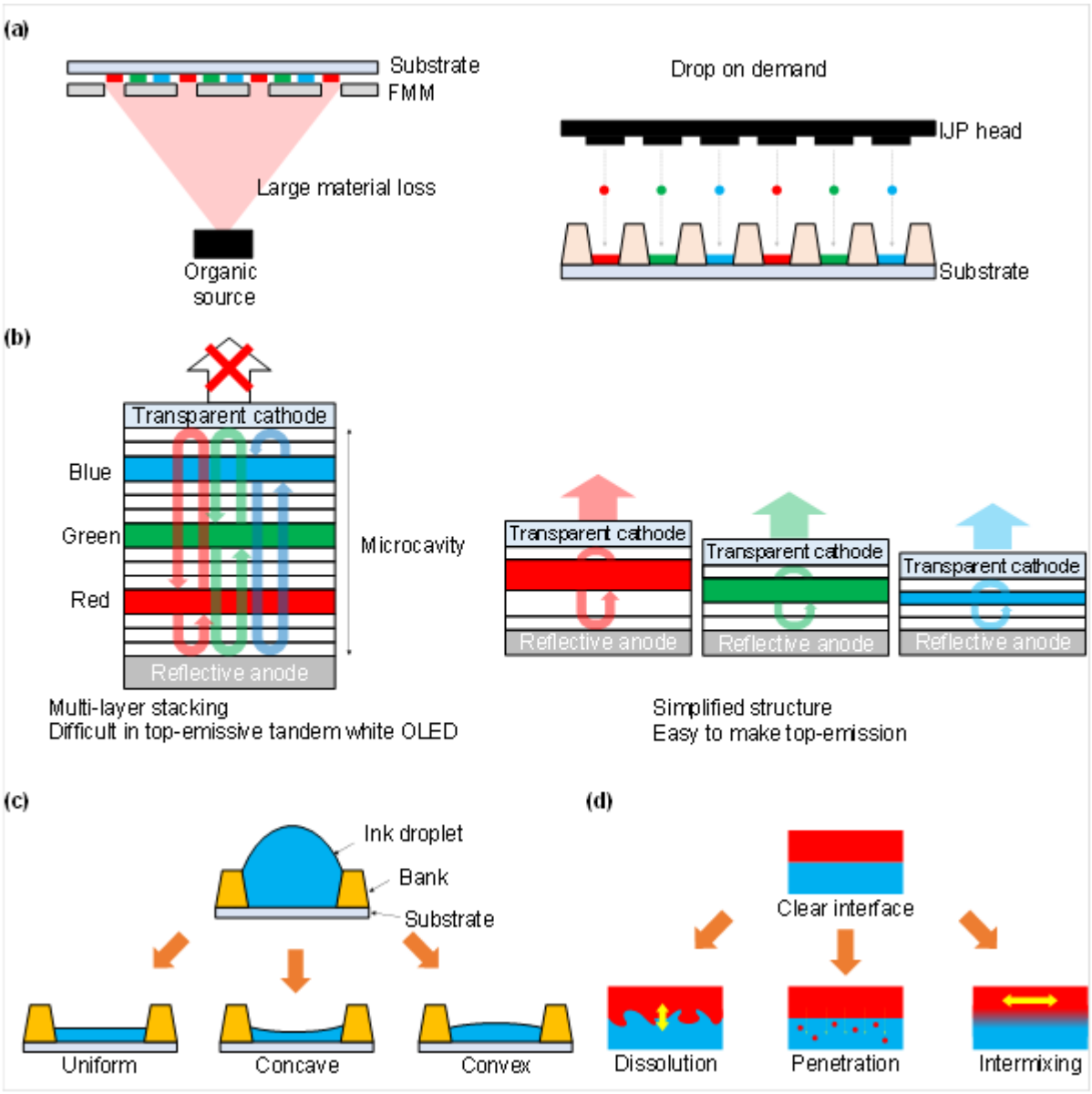

Figure 2. Schematic diagram of advantages and disadvantages of SOLEDs: Advantages of (a) low material consumption and (b) simple and top-emission structure. Disadvantages of difficulty in making well-defined multi-layers in the respect of (c) film shapes after IJP and vacuum drying and (d) various phenomena between adjacent layers during solution processes.

This article is protected by copyright. All rights reserved.

15214095, ja, Downloaded from https://onlinelibrary.wiley.com/doi/10.1002/adma.202207454 by Seoul National University, Wiley Online Library on [28/11/2022]. See the Terms and Conditions (https://onlinelibrary.wiley.com/terms-and-conditions) on Wiley Online Library for rules of use; OA articles are governed by the applicable Creative Commons License

Accepted Article

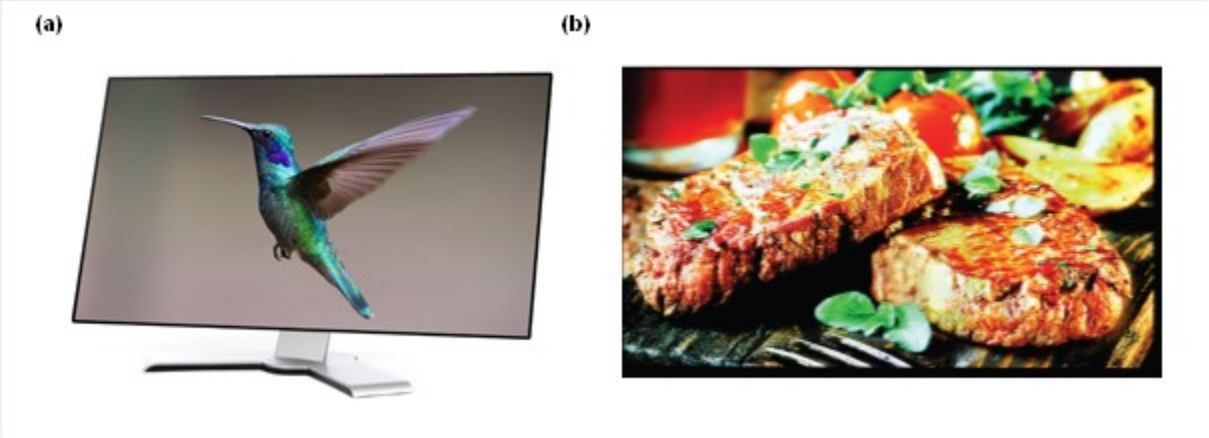

Figure 3. Optical image of (a) commercial inkjet-printed 4K OLED monitor produced by JOLED (j-oled.com), and (b) prototype of 18.2-inch 202-ppi inkjet-printed OLED panel demonstrated by Samsung Display Co., Ltd. Reproduced with permission.[28] Copyright 2020, Wiley.

This article is protected by copyright. All rights reserved.

15214095, ja, Downloaded from https://onlinelibrary.wiley.com/doi/10.1002/adma.202207454 by Seoul National University, Wiley Online Library on [28/11/2022]. See the Terms and Conditions (https://onlinelibrary.wiley.com/terms-and-conditions) on Wiley Online Library for rules of use; OA articles are governed by the applicable Creative Commons License

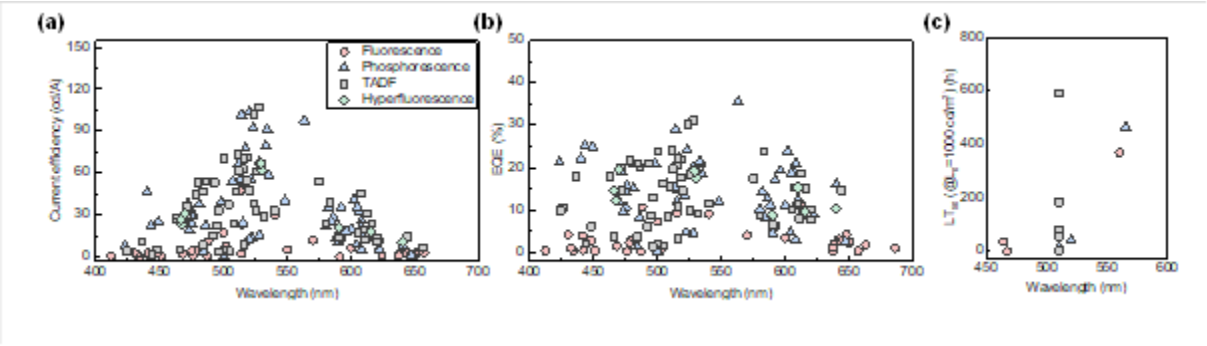

Figure 4. Literature survey of (a) maximum current efficiency, (b) maximum external quantum efficiency and (c) operational lifetime (LT_{50} at 1,000 nit) according to emission wavelength of SOLEDs fabricated in academic laboratories.

This article is protected by copyright. All rights reserved.

Accepted Article

15214095, ja, Downloaded from https://onlinelibrary.wiley.com/doi/10.1002/adma.202207454 by Seoul National University, Wiley Online Library on [28/11/2022]. See the Terms and Conditions (https://onlinelibrary.wiley.com/terms-and-conditions) on Wiley Online Library for rules of use; OA articles are governed by the applicable Creative Commons License

Accepted Article

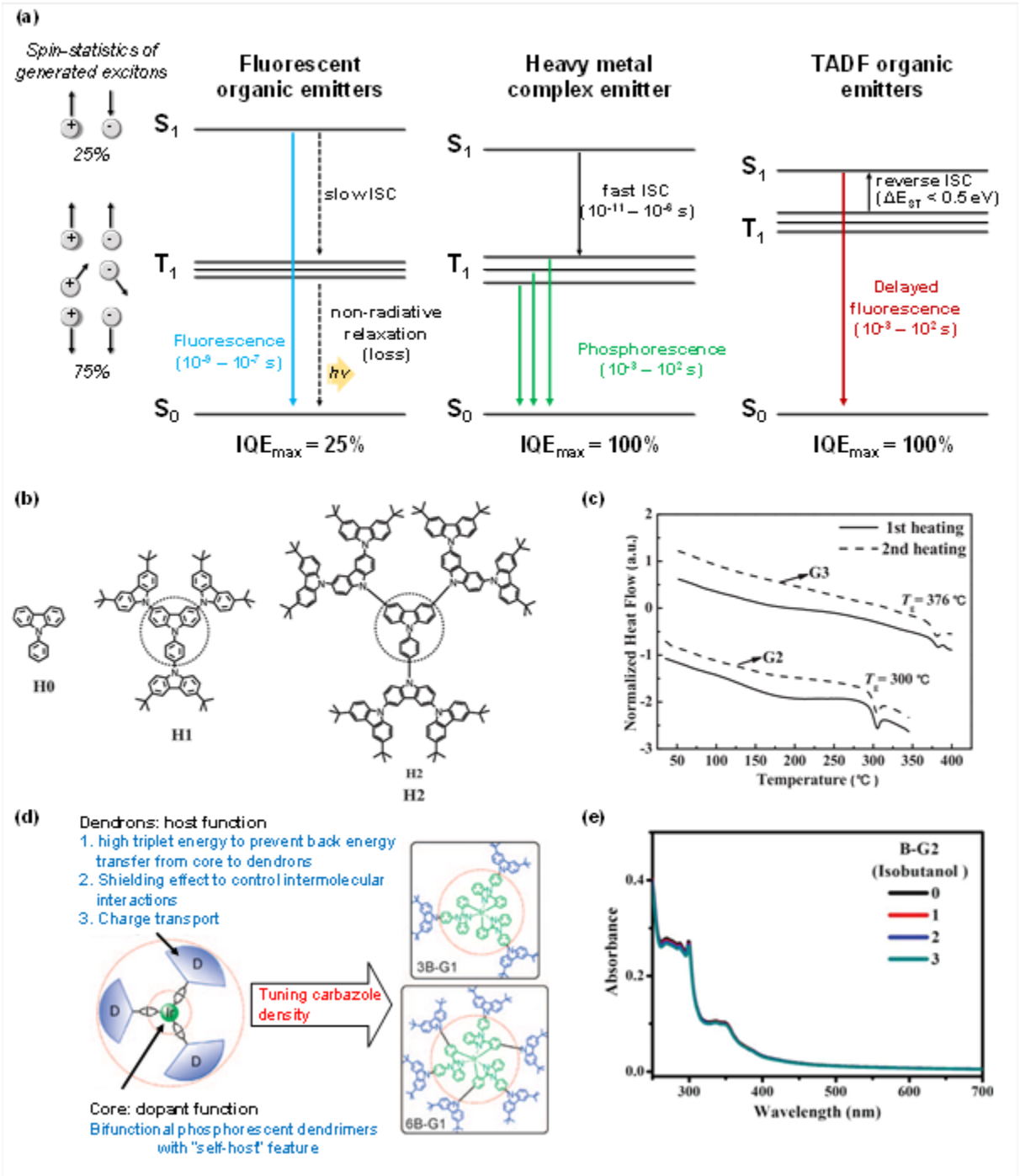

Figure 5. (a) Spin statistics of the generated singlet and triplet excitons, and energy diagram of fluorescent organic emitters, phosphorescent heavy metal complex, and thermally-activated delayed fluorescence (TADF) organic emitters (ISC: intersystem crossing, *IQE*: internal quantum efficiency, S_0: singlet ground state, S_1: singlet excited state, T_1: triplet excited state). (b) Molecular structures of N-phenylcarbazole core (H0) and 1st-generation (H1) and 2nd-generation (H2) carbazole-derived

This article is protected by copyright. All rights reserved.

15214095, ja, Downloaded from https://onlinelibrary.wiley.com/doi/10.1002/adma.202207454 by Seoul National University, Wiley Online Library on [28/11/2022]. See the Terms and Conditions (https://onlinelibrary.wiley.com/terms-and-conditions) on Wiley Online Library for rules of use; OA articles are governed by the applicable Creative Commons License

dendrimers. Reproduced with permission.[220] Copyright 2009, WILEY-VCH. (c) Thermal stability of carbazole dendrimer measured by differential scanning calorimetry (DSC) with a heating rate of 10 °C min^{-1}. Reproduced with permission.[218] Copyright 2013, WILEY-VCH. (d) The features of phosphorescent dendrimers with iridium cores. Reproduced with permission.[226] Copyright 2009, WILEY-VCH. (e) UV-vis absorption spectra measurement for anti-solvent resistance test by isobutanol for 1 to 3 cycles. Reproduced with permission.[129] Copyright 2019, WILEY-VCH.

Accepted Article

This article is protected by copyright. All rights reserved.

15214095, ja, Downloaded from https://onlinelibrary.wiley.com/doi/10.1002/adma.202207454 by Seoul National University, Wiley Online Library on [28/11/2022]. See the Terms and Conditions (https://onlinelibrary.wiley.com/terms-and-conditions) on Wiley Online Library for rules of use; OA articles are governed by the applicable Creative Commons License

Accepted Article

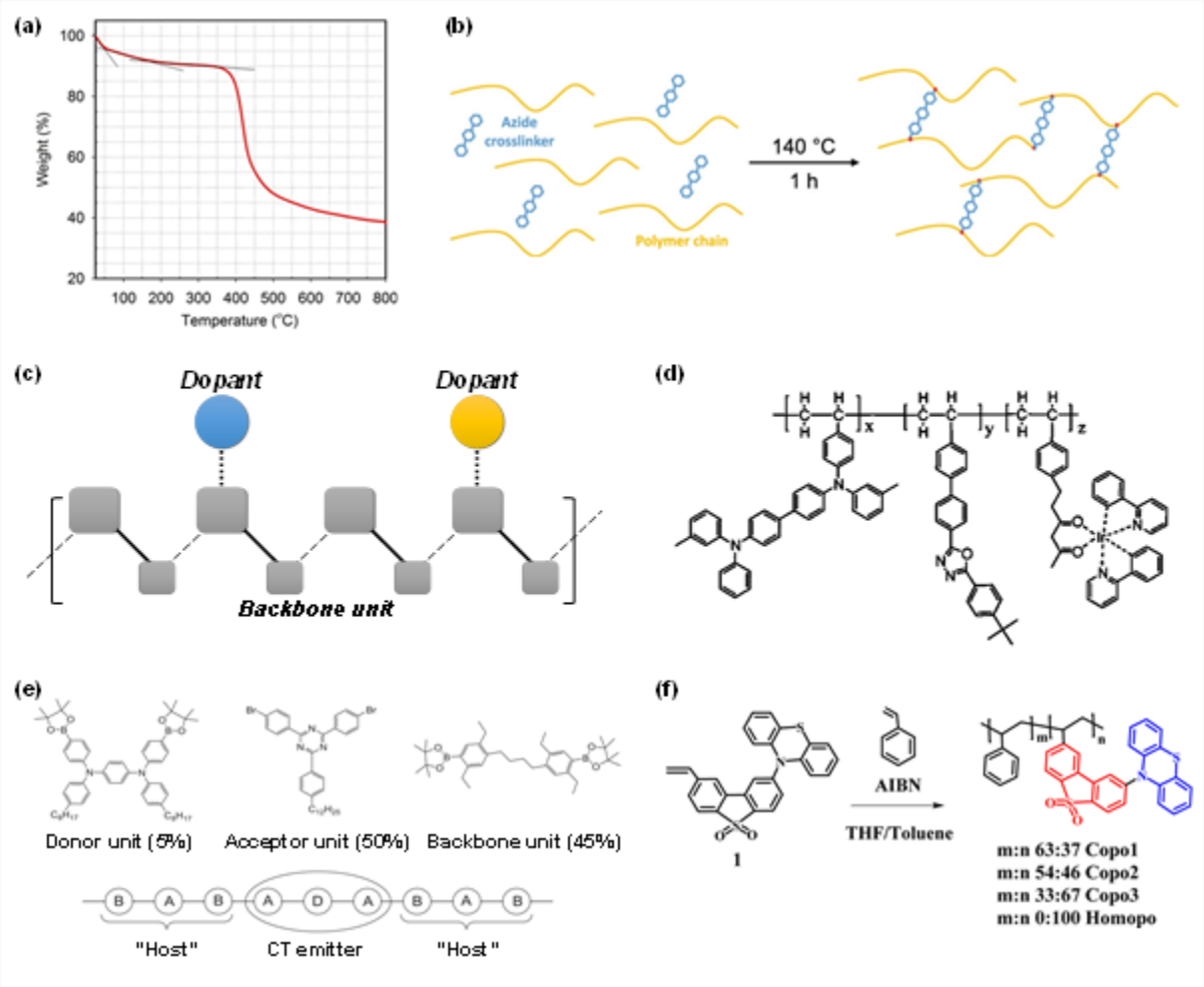

Figure 6. (a) Glass-transition temperature of polymeric light emitter, super yellow (SY, PDY-132) measured by thermogravimetric analysis (TGA). Reproduced with permission.[236] Copyright 2017, Springer Nature. (b) Schematic crosslinking mechanism of SY with azide crosslinker. Reproduced with permission.[241] Copyright 2022, WILEY. (c) Schematic chemical structure of self-host polymers. (d) Molecular structure of ambipolar self-host polymer with a phosphorescent emitter, and hole-transporting and electron-transporting side groups. Reproduced with permission. [252] Copyright 2005, AIP Publishing. (e) Chemical and polymer structures of main-chain-type TADF polymer containing a high-triplet energy level backbone (B) monomer, donor (D) and acceptor (A) units. Reproduced with permission.[254] Copyright 2015, WILEY-VCH. (f) Synthesis route and chemical

This article is protected by copyright. All rights reserved.

15214095, ja, Downloaded from https://onlinelibrary.wiley.com/doi/10.1002/adma.202207454 by Seoul National University, Wiley Online Library on [28/11/2022]. See the Terms and Conditions (https://onlinelibrary.wiley.com/terms-and-conditions) on Wiley Online Library for rules of use; OA articles are governed by the applicable Creative Commons License

structure of the side-chain-type TADF copolymer. Reproduced with permission.[259] Copyright 2016, American Chemical Society.

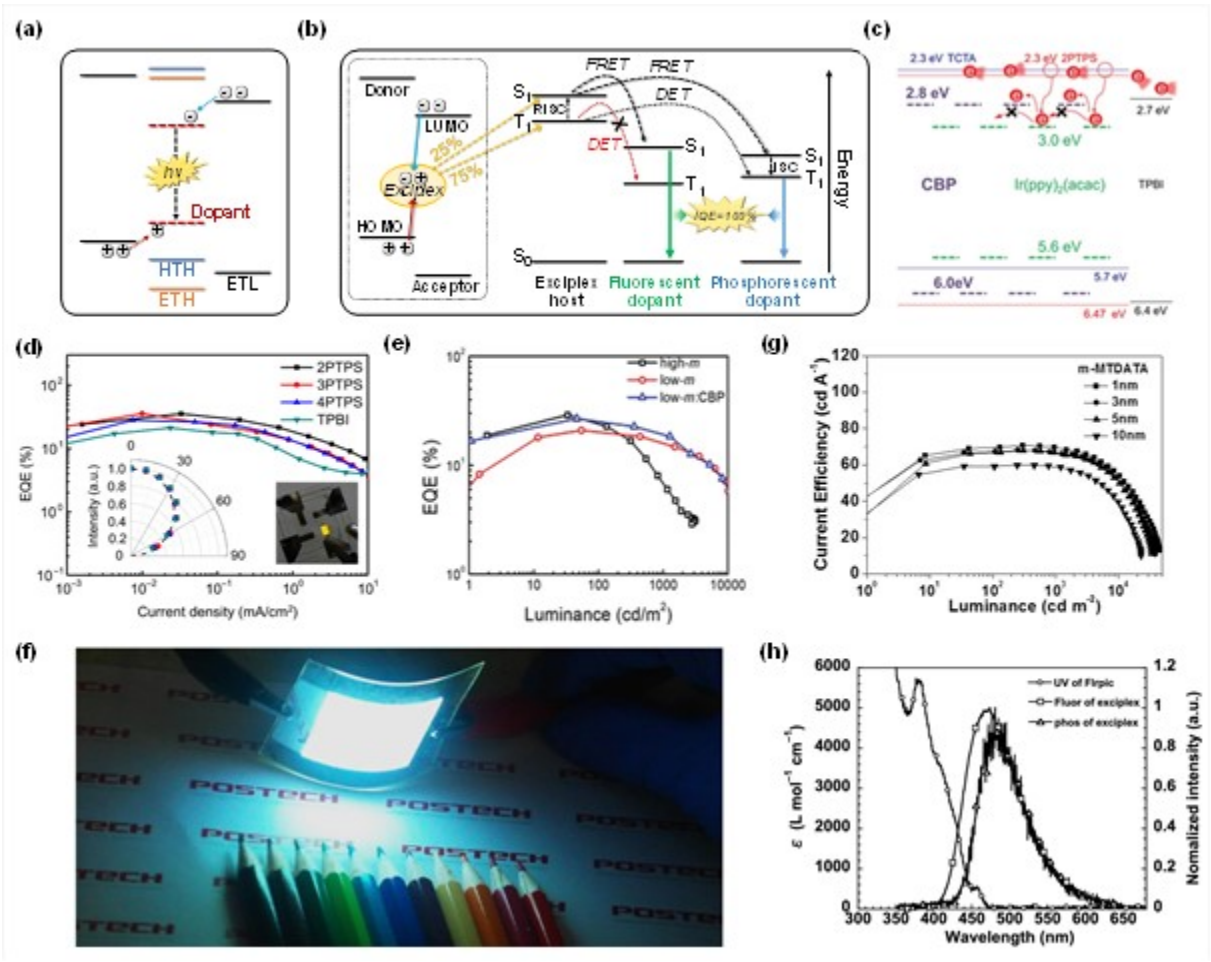

Figure 7. Schematic diagram of two emission mechanisms: (a) direct charge trapping at dopant in mixed host system and (b) energy transfer from exciplex-forming host to fluorescent or phosphorescent dopants by Förster resonance energy transfer (FRET) and Dexter energy transfer (DET). (c) Electron-transport mechanism for improved charge balance in solution processed PhOLEDs with a charge-balance-assistant CBP molecule in mixed host EML. Reproduced with permission.[20] Copyright 2020, WILEY-VCH. (d) External quantum efficiencies of orange-red solution processed PhOLEDs (inset: angular EL intensity profile (left) and photograph of the operating device). Reproduced with permission.[12] Copyright 2016 American Association for the Advancement of

This article is protected by copyright. All rights reserved.

Accepted Article

15214095, ja, Downloaded from https://onlinelibrary.wiley.com/doi/10.1002/adma.202207454 by Seoul National University, Wiley Online Library on [28/11/2022]. See the Terms and Conditions (https://onlinelibrary.wiley.com/terms-and-conditions) on Wiley Online Library for rules of use; OA articles are governed by the applicable Creative Commons License

Science. (e) Efficiency roll-off characteristics of solution processed PhOLEDs with TCTA:2PTPS:Ir(ppy)$_3$ and TCTA:2PTPS:Ir(ppy)$_2$(acac):CBP EMLs. Reproduced with permission.[20] Copyright 2020, WILEY-VCH. (f) Demonstration of large-area flexible white solution processed PhOLED lighting device. Reproduced with permission.[12] Copyright 2016, American Association for the Advancement of Science. (g) Current efficiency-luminance characteristics depending on the distance between interfacial exciplex and dopant. Reproduced with permission.[292] Copyright 2015 Springer Nature. (h) PL spectra of exciplex-forming TAPC and 5',5''''-sulfonyl-di-1,1':3',1''-terphenyl (BTPS) hosts and UV-vis absorption spectrum of Firpic dopant. Reproduced with permission.[291] Copyright 2014, WILEY-VCH.

This article is protected by copyright. All rights reserved.

Accepted Article

15214095, ja, Downloaded from https://onlinelibrary.wiley.com/doi/10.1002/adma.202207454 by Seoul National University, Wiley Online Library on [28/11/2022]. See the Terms and Conditions (https://onlinelibrary.wiley.com/terms-and-conditions) on Wiley Online Library for rules of use; OA articles are governed by the applicable Creative Commons License

Accepted Article

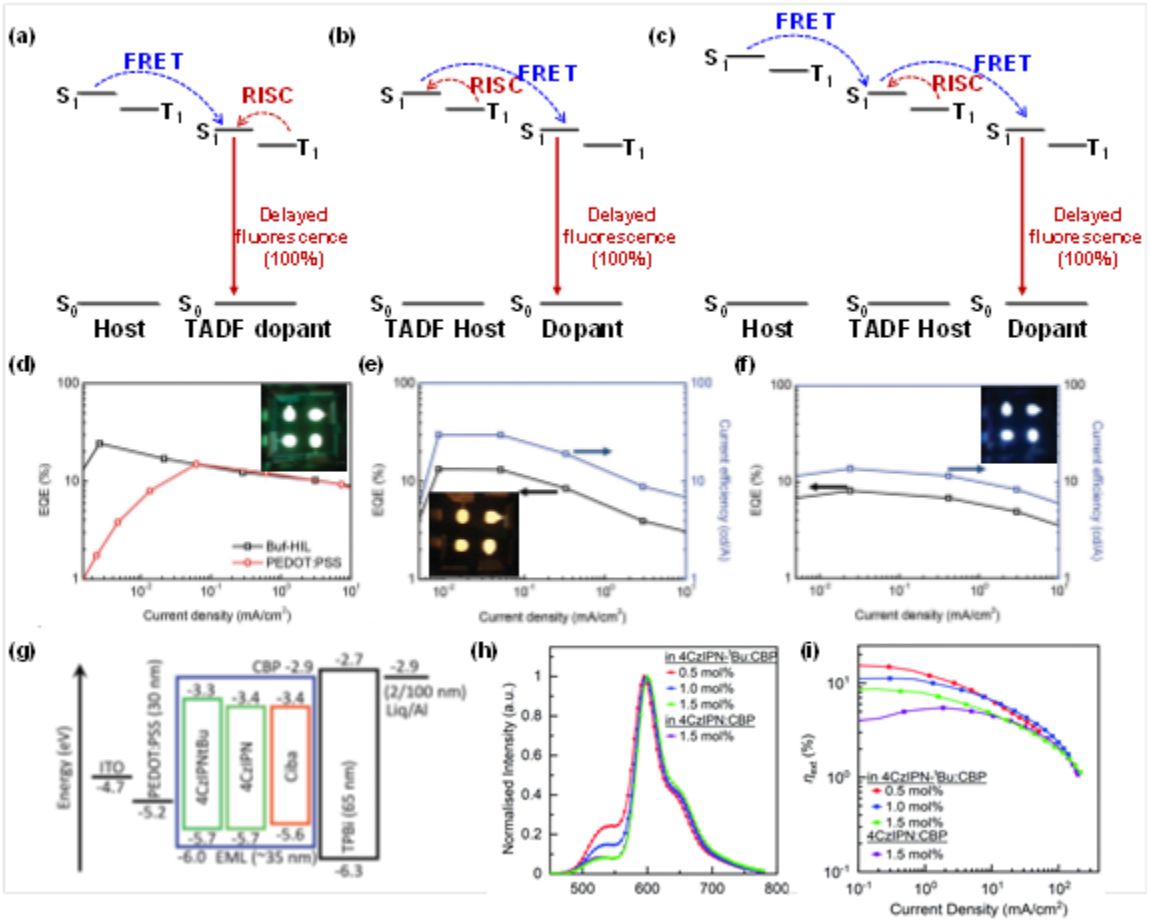

Figure 8. Delayed fluorescence mechanisms based on (a) delayed fluorescence dopant system, (b) host sensitizer system and (c) hyperfluorescence system. Device efficiencies of TADF-SOLEDs that use delayed fluorescence dopants emitting (d) green, (e) red and (f) blue. Reproduced with permission.[15] Copyright 2016, WILEY-VCH. (g) Energy level diagram, (h) electroluminescence spectrum and (i) external quantum efficiencies of TADF-SOLEDs based on hyperfluorescence system. Reproduced with permission.[316] Copyright 2022, The Royal Society of Chemistry.

This article is protected by copyright. All rights reserved.

15214095, ja, Downloaded from https://onlinelibrary.wiley.com/doi/10.1002/adma.202207454 by Seoul National University, Wiley Online Library on [28/11/2022]. See the Terms and Conditions (https://onlinelibrary.wiley.com/terms-and-conditions) on Wiley Online Library for rules of use; OA articles are governed by the applicable Creative Commons License

Accepted Article

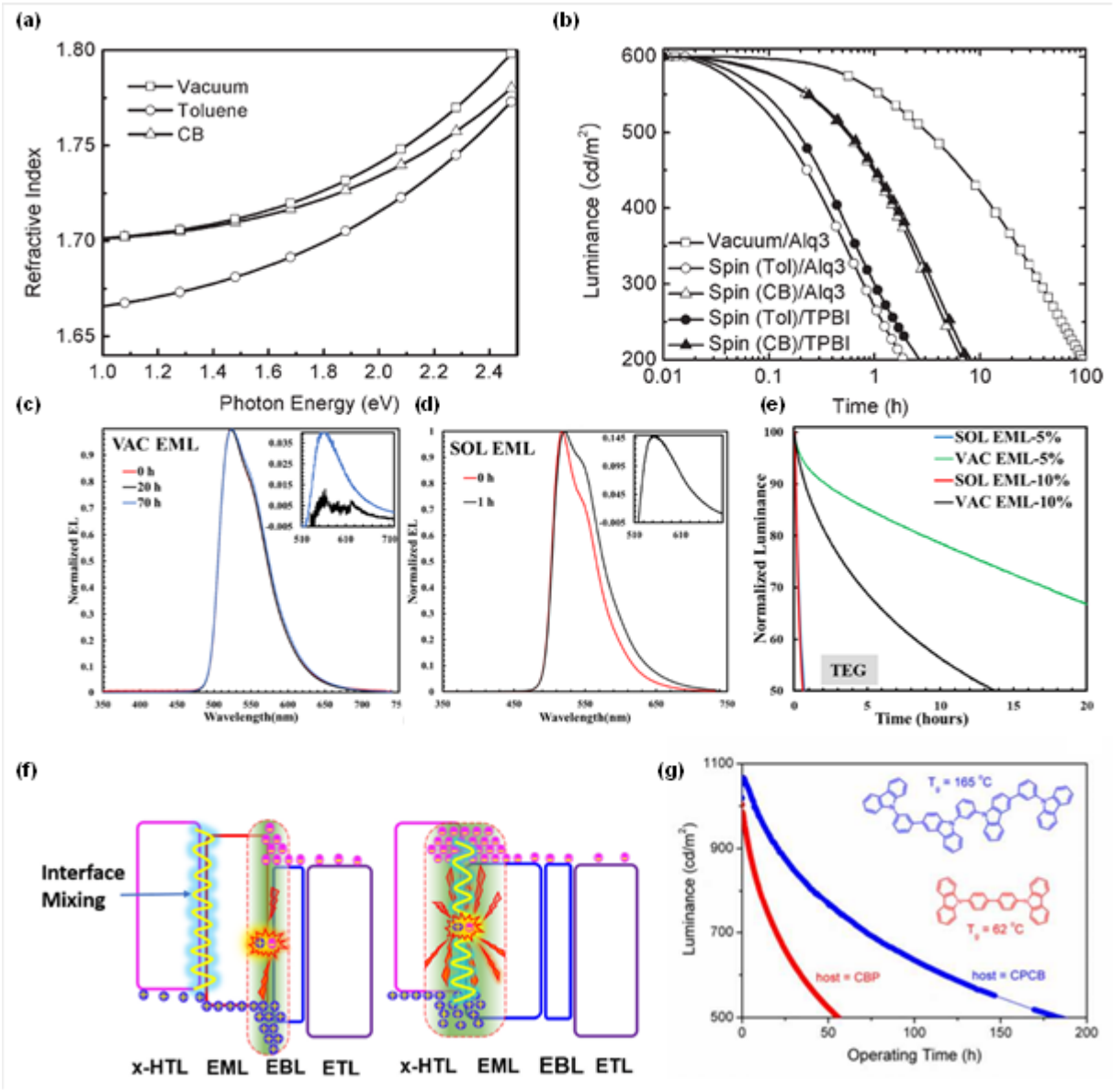

Figure 9. (a) Refractive index of solution-processed and vacuum-deposited TBADN films, (b) luminance versus time characteristics of solution-processed and vacuum-deposited OLEDs. Reproduced with permission.[16] Copyright 2009, WILEY-VCH. Normalized EL spectra of TED guest device with (c) vacuum-deposited EML, (d) solution-processed EML and (e) luminance versus time characteristics of vacuum-deposited and solution-processed film with different TEG wt%. Reproduced with permission.[59] Copyright 2022, American Chemical Society. (f) Scheme of Exciton-polaron quenching according to the location of recombination zone. Reproduced with permission.[324] Copyright 2022, Elsevier (g) luminance versus time characteristics between device

This article is protected by copyright. All rights reserved.

15214095, ja, Downloaded from https://onlinelibrary.wiley.com/doi/10.1002/adma.202207454 by Seoul National University, Wiley Online Library on [28/11/2022]. See the Terms and Conditions (https://onlinelibrary.wiley.com/terms-and-conditions) on Wiley Online Library for rules of use; OA articles are governed by the applicable Creative Commons License

that has low-T_g material host (CBP), and device that has high-T_g material host (CPCB). Reproduced with permission.[194] Copyright 2015, Royal Society of Chemistry.

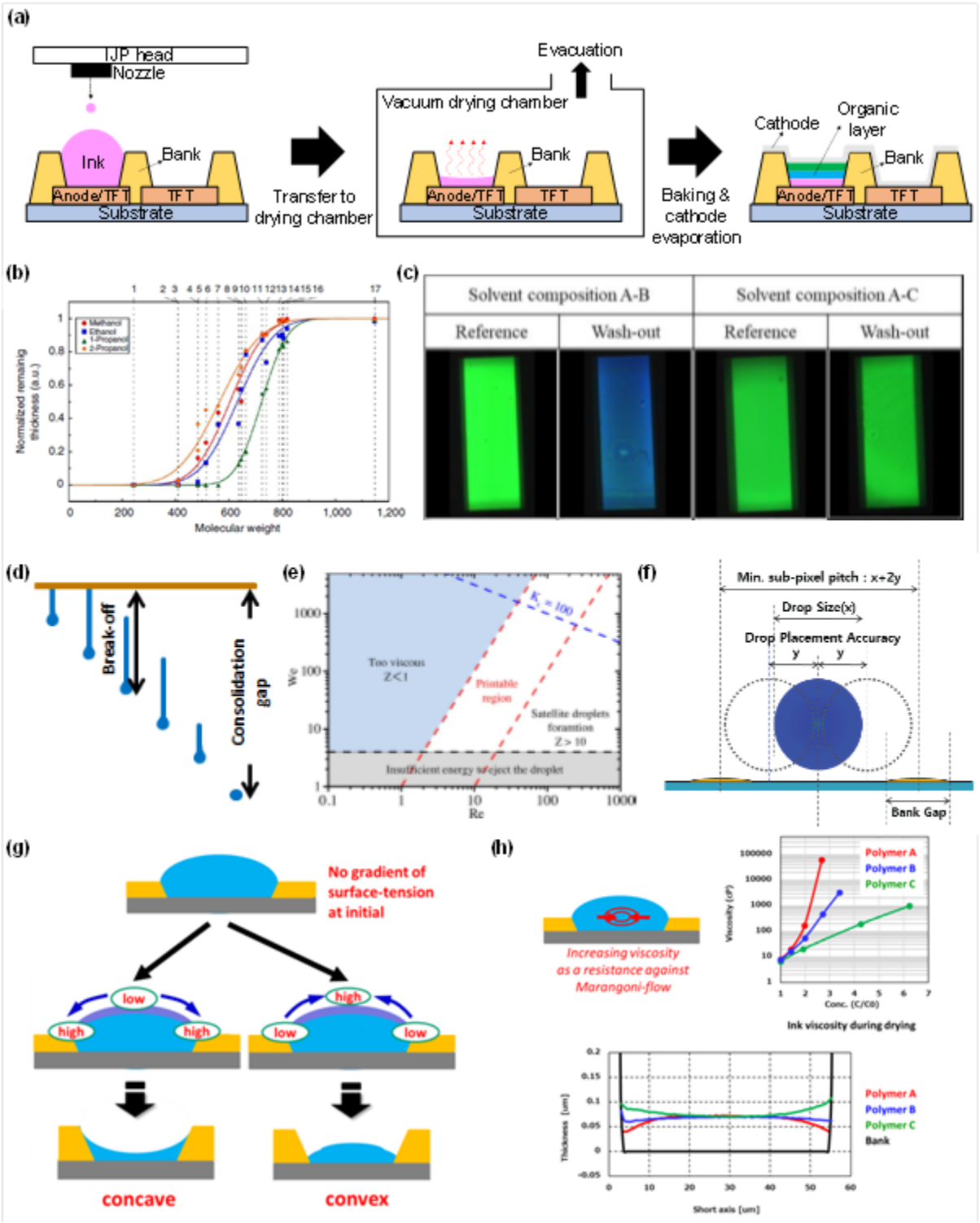

This article is protected by copyright. All rights reserved.

Accepted Article

15214095, ja, Downloaded from https://onlinelibrary.wiley.com/doi/10.1002/adma.202207454 by Seoul National University, Wiley Online Library on [28/11/2022]. See the Terms and Conditions (https://onlinelibrary.wiley.com/terms-and-conditions) on Wiley Online Library for rules of use; OA articles are governed by the applicable Creative Commons License

Figure 10. Physical properties of materials required for solution-processes: (a) Schematic fabrication processes of SOLEDs. (b) Solvent resistance[38] and (c) wash-out test for solution orthogonality[26]. (d) Schematics of droplet ejected from inkjet head.[332] (e) Printable region of inks described by Z constant.[40] (f) Required ink-drop-placement accuracy depending on pixel pitch.[28] Film shape depending on (g) Marangoni flow[53] and (h) ink viscosity[53]. (b) Reproduced with permission.[38] Copyright McMillan Publishers Limited, 2014. (c) Reproduced with permission.[26] Copyright 2021, WILEY. (d) Reproduced with permission. [332] Copyright 2018, WILEY. (e) Reproduced with permission.[40] 2018 Elsevier B.V. (f) Reproduced with permission.[194] Copyright 2020, WILEY. (g, h) Reproduced with permission.[53] Copyright 2021, WILEY.

This article is protected by copyright. All rights reserved.

Accepted Article

15214095, ja, Downloaded from https://onlinelibrary.wiley.com/doi/10.1002/adma.202207454 by Seoul National University, Wiley Online Library on [28/11/2022]. See the Terms and Conditions (https://onlinelibrary.wiley.com/terms-and-conditions) on Wiley Online Library for rules of use; OA articles are governed by the applicable Creative Commons License

Table 1. Recent luminous characteristics of EOLEDs and SOLEDs from various material suppliers

Material supplier	OLED type	Emission type	Red			Green			Blue			Ref.
			CE[a] [cd A^{-1}] (at 1,000 cd m^{-2})	CIE-x,y	*LT*$_{95}$[b] [h] (at 1,000 cd m^{-2})	*CE* [cd A^{-1}] (at 1,000 cd m^{-2})	CIE-x,y	*LT*$_{95}$ [h] (at 1,000 cd m^{-2})	*CE* [cd A^{-1}] (at 1,000 cd m^{-2})	CIE-x,y	*LT*$_{95}$ [h] (at 1,000 cd m^{-2})	
Kyulux (Japan)	EOLED	BE[c]	50	0.70, 0.29	20,000	224	0.17, 0.78	59,000	20.25	0.11, 0.09	450	[52]
Sumitomo Chemical (Japan)	SOLED	BE (SC[e])	18.0	0.68, 0.32	11,000	76.1	0.32, 0.63	26,000	6.4	0.13, 0.10	1,050	[53]
		TE[d] (SC)	43.6	0.68, 0.32	38,000	102.8	0.24, 0.72	10,000	5.8	0.13, 0.06	390	
Mitsubishi Chemical (Japan)	SOLED	BE (SC)	24	0.67, 0.33	4,000	82	0.31, 0.64	11,000	7.4	0.13, 0.12	300	[27]
Merck KGaA (Germany)	SOLED	BE (IJP)	17.1	0.69, 0.31	4,700	86.7	0.33, 0.64	6,800	9.5	0.14, 0.13	600	[35]
		TE (IJP)	22.1	0.70, 0.30	8,300	108.7	0.28, 0.70	6,000	3.5	0.14, 0.06	200	

[a] *CE* measured at 1,000 cd m^{-2}; [b] *LT*$_{95}$ measured at 1,000 cd m^{-2}; [c] Bottom emission; [d] Top emission; [e] spin-coating

This article is protected by copyright. All rights reserved.

Accepted Article

15214095, ja, Downloaded from https://onlinelibrary.wiley.com/doi/10.1002/adma.202207454 by Seoul National University, Wiley Online Library on [28/11/2022]. See the Terms and Conditions (https://onlinelibrary.wiley.com/terms-and-conditions) on Wiley Online Library for rules of use; OA articles are governed by the applicable Creative Commons License

Table 2. State-of-the-art SOLEDs fabricated in academic laboratories

Year	Emitter type	Emission type	Device structure	Maximum $CE^{a)}$ [cd A^{-1}]	Maximum *PE* [lm W^{-1}]	Maximum *EQE* [%]	Peak wavelength [nm]	CIE-x,y	$LT_{50}^{b)}$ [h] (at 1,000 cd m^{-2})	Ref.
2019	Fluorescence	BE[c)] (SC[d)])	ITO / PEDOT:PSS / CBP : 2DPATrxSO_2 / TPBI / LiF / Al	11	4.5	10.6	~488	(0.16,0.34)	-	[350]
2018	Fluorescence	BE (SC)	ITO / PEDOT:PSS / TFB / F8BT / poly(DDA)TFSI / Al	30.1	32.4	9	~540	-	-	[351]
2021	Fluorescence	BE (SC)	ITO/ PEDOT:PSS/ TCTA:H-DPPN/ TPBI/ LiF/ Al	11.8	8.3	4	570	(0.50,0.48)	-	[352]
2020	Fluorescence	BE (SC)	ITO/ PEDOT:PSS/ mCP: Pt2a/ DPEPO/TmPyPB/ Liq/ Al	14.3	4.1	8.7	614	(0.56,0.43)	-	[353]
2020	Fluorescence	BE (SC)	ITO/ PEDOT:PSS / BTZ2 / TPBI / LiF /Al	-	-	4.15	648	(0.65,0.36)	-	[354]
2022	Phosphorescence	BE (SC)	ITO / PEDOT:PSS / TSPO1 : mer-Ir$(CF_3pbp)_3$ / TSPO1 / TPBI / LiF / Al	7.7	4.1	21.2	423	(0.161,0.054)	-	[355]
2016	Phosphorescence	BE (SC)	ITO / GraHIL / TCTA : 2PTPS : Ir$(ppy)_3$ / TPBI / LiF / Al	101.5		29	~514	-	-	[12]
2020	Phosphorescence	BE (SC)	ITO / m-PEDOT:PSS / TCTA : TPBi : Ir3 / TPBI / LiF / Al	91.98	48.16	24.08	523	(0.335,0.612)	-	[213]
2016	Phosphorescence	BE (SC)	ITO / GraHIL / TCTA : 3PTPS : $Bt_2Ir(acac)$ / TPBI / LiF / Al	97.5		35.5	563	-	-	[12]
2017	Phosphorescence	BE (SC)	ITO / GraHIL / TCTA : TPBI : Ir(Th-$PQ)_2$ / TPBI / LiF / Al	26	-	21	~612	(0.64,0.34)	-	[356]
2015	Phosphorescence	BE (SC)	ITO / PEDOT:PSS / P-R-3 / TPBI / LiF / Al	8.31	2.95	16.07	640	(0.68,0.31)	-	[58]
2021	TADF	BE (SC)	ITO / PEDOT:PSS / PVK / mCP : BO-tCzPhICz / TPBI / LiF / Al	10.5	7.36	17.8	436	(0.15,0.077)	-	[57]

This article is protected by copyright. All rights reserved.

Accepted Article

15214095, ja, Downloaded from https://onlinelibrary.wiley.com/doi/10.1002/adma.202207454 by Seoul National University, Wiley Online Library on [28/11/2022]. See the Terms and Conditions (https://onlinelibrary.wiley.com/terms-and-conditions) on Wiley Online Library for rules of use; OA articles are governed by the applicable Creative Commons License

Accepted Article

Year	Emitter type	Emission type	Device structure	Maximum *CE*[a] [cd A^{-1}]	Maximum *PE* [lm W^{-1}]	Maximum *EQE* [%]	Peak wavelength [nm]	CIE-x,y	LT_{50}[b] [h] (at 1,000 cd m^{-2})	Ref.
2021	TADF	BE (SC)	ITO / PEDOT:PSS / PVK / DMeCzIPN: mCP / DPEPO / TmPyPB / LiF / Al	44.3	23.7	21.6	478	(0.16,0.30)	-	[357]
2016	TADF	BE (SC)	ITO / Buf-HIL / CBP : 4CzIPN / TPBI / LiF / Al	73	58	24	~511	-	-	[15]
2022	TADF	BE (SC)	ITO / PEDOT:PSS / PVK/ P(Bn-DPAc) : tPTRZ : t4CzIPN / TPBI / LiF / Al	107.3	84.3	31.2	~528	(0.33,0.60)	-	[358]
2022	TADF	BE (SC)	ITO/ PEDOT:PSS/ 2SPAC-DBP-2tBuCz : TCTA : 26DCzPPy / B4PyPPM / LiF / Al	38.6	48.8	23.7	583	(0.54,0.45)	-	[359]
2020	TADF	BE[b] (SC[d])	ITO / PEDOT:PSS / TCTA : oDTBPZ-DPXZ / TmPyPB / LiF / Al	31.0	27.1	18.5	612	(0.60,0.40)	-	[360]
2018	hyperfluorescence	BE (SC)	ITO / MoO_3 / Poly-TPD / PVK / DPOBBPE : 5CzCN : TBPe / TSPO1 / TPBI / LiF / Al	31.1	16.3	19.5	470	(0.15,0.23)	-	[361]
2021	hyperfluorescence	BE (SC)	ITO / PEDOT:PSS / GP-10 : TBPAD / TSPO1 / TmPyPB / LiF / Al	66.5	-	19.2	529	(0.34,0.59)	-	[317]
2021	hyperfluorescence	BE (SC)	ITO / PEDOT:PSS / RP-05 : NTTPA / TSPO1 / TmPyPB / LiF / Al	20.7	-	8.8	~590	(0.50,0.48)	-	[317]
2022	hyperfluorescence	BE (SC)	ITO / PEDOT:PSS / CBP : 4CzIPN-^{t}BU : Cibalackrot / TPBI / Liq / Al	-	-	15.3	~610	-	-	[316]
2021	hyperfluorescence	BE (SC)	ITO / PEDOT:PSS / RP-15 : NTTPA / TSPO1 / TmPyPB / LiF / Al	10.6	-	10.3	640	(0.60,0.38)	-	[317]
2017	Fluorescence	BE (BC[e])	ITO / PEDOT:PSS / TFB / NPB : MADN : BUBD-1 / MADN : BUBD-1 / Alq_3 / LiF / Al	5.68	1.75	2.57	464	-	36	[318]
2015	TADF	BE (SC)	ITO / PEDOT:PSS / CPCB : 4CzIPN / T2T / Bpy-TP2 / LiF / Al	-	-	9.9	510	-	184	[194]
2022	TADF	BE	ITO / PEDOT:PSS / DDPPFPh / CBP :	71.6	53.2	25	~510	(0.29,0.58)	590	[323]

This article is protected by copyright. All rights reserved.

15214095, ja, Downloaded from https://onlinelibrary.wiley.com/doi/10.1002/adma.202207454 by Seoul National University, Wiley Online Library on [28/11/2022]. See the Terms and Conditions (https://onlinelibrary.wiley.com/terms-and-conditions) on Wiley Online Library for rules of use; OA articles are governed by the applicable Creative Commons License

Accepted Article

Year	Emitter type	Emission type	Device structure	Maximum *CE*[a] [cd A^{-1}]	Maximum *PE* [lm W^{-1}]	Maximum *EQE* [%]	Peak wavelength [nm]	CIE-x,y	LT_{50}[b] [h] (at 1,000 cd m^{-2})	Ref.
		(SC)	4CzIPN / TPBI / LiF / Al							
2017	Fluorescence	BE (BC)	ITO / PEDOT:PSS / TFB / NPB : MADN : BUBD-1 : Rubrene / Alq3 / LiF / Al	10.87	2.44	3.35	~560	(0.41,0.48)	369.3	[318]
2022	Phosphorescence	BE (SC)	ITO / PEDOT:PSS / DDPPFPh / CBP : PO-01 / TPBI / LiF / Al	50.6	45.4	19.6	565	(0.51,0.48)	465	[323]
2017	phosphorescence	BE (BC)	ITO / PEDOT:PSS / TFB : EPH409 : Ir $(mppy)_3$ / LiF / Al	14.14	6.4	3.98	520	-	95.4	[318]
2017	phosphorescence	BE (BC)	ITO / PEDOT:PSS / TFB /TFB : EPH409 : Ir$(mppy)_3$: PER54 / CsF / Al	10.93	5.28	7.15	610	-	48.6	[318]

[a] *CE* measured at its maximum, [b] T_{50} measured at 1,000 cd m^{-2}; [c] Bottom emission; [d] Spin-coating; [e] Blade-coating

This article is protected by copyright. All rights reserved.

15214095, ja, Downloaded from https://onlinelibrary.wiley.com/doi/10.1002/adma.202207454 by Seoul National University, Wiley Online Library on [28/11/2022]. See the Terms and Conditions (https://onlinelibrary.wiley.com/terms-and-conditions) on Wiley Online Library for rules of use; OA articles are governed by the applicable Creative Commons License

Accepted Article

References

[1] D. Park, Y. Kim, Y. Park, *SID Symp. Dig. Tech. Pap.* **2019**, *50*, 1138.

[2] S. Sudheendran Swayamprabha, D. K. Dubey, Shahnawaz, R. A. K. Yadav, M. R. Nagar, A. Sharma, F. Tung, J. Jou, *Adv. Sci.* **2021**, *8*, 2002254.

[3] S. Shahnawaz, S. Sudheendran Swayamprabha, M. R. Nagar, R. A. K. Yadav, S. Gull, D. K. Dubey, J.-H. Jou, *J. Mater. Chem. C* **2019**, *7*, 7144.

[4] T. Tsujimura, *OLED Display Fundamentals and Applications*, John Wiley & Sons, Inc., Hoboken, New Jersey, **2017**.

[5] S. Wang, H. Zhang, B. Zhang, Z. Xie, W.-Y. Wong, *Mater. Sci. Eng. R Reports* **2020**, *140*, 100547.

[6] H. W. Chen, J. H. Lee, B. Y. Lin, S. Chen, S. T. Wu, *Light Sci. Appl.* **2018**, *7*, 17168.

[7] D. K. Dubey, S. Sahoo, C.-W. Wang, J.-H. Jou, *Org. Electron.* **2019**, *69*, 232.

[8] S. J. Zou, Y. Shen, F. M. Xie, J. De Chen, Y. Q. Li, J. X. Tang, *Mater. Chem. Front.* **2020**, *4*, 788.

[9] E. Hsiang, Z. Yang, Q. Yang, Y. Lan, S. Wu, *J. Soc. Inf. Disp.* **2021**, *29*, 446.

[10] Y. Yin, M. U. Ali, W. Xie, H. Yang, H. Meng, *Mater. Chem. Front.* **2019**, *3*, 970.

[11] T.-H. Han, M.-R. Choi, S.-H. Woo, S.-Y. Min, C.-L. Lee, T.-W. Lee, T.-H. Han, M.-R. Choi, S.-H. Woo, S.-Y. Min, T.-W. Lee, C.-L. Lee, *Adv. Mater.* **2012**, *24*, 1487.

[12] T. H. Han, M. R. Choi, C. W. Jeon, Y. H. Kim, S. K. Kwon, T. W. Lee, *Sci. Adv.* **2016**, *2*, e1601428.

[13] *Nat. Photonics* **2009**, *3*, 441.

This article is protected by copyright. All rights reserved.

15214095, ja, Downloaded from https://onlinelibrary.wiley.com/doi/10.1002/adma.202207454 by Seoul National University, Wiley Online Library on [28/11/2022]. See the Terms and Conditions (https://onlinelibrary.wiley.com/terms-and-conditions) on Wiley Online Library for rules of use; OA articles are governed by the applicable Creative Commons License

[14] L. Duan, L. Hou, T. W. Lee, J. Qiao, D. Zhang, G. Dong, L. Wang, Y. Qiu, *J. Mater. Chem.* **2010**, *20*, 6392.

[15] Y.-H. Kim, C. Wolf, H. Cho, S.-H. Jeong, T.-W. Lee, *Adv. Mater.* **2016**, *28*, 734.

[16] T.-W. Lee, T. Noh, H.-W. Shin, O. Kwon, J.-J. Park, B.-K. Choi, M.-S. Kim, D. W. Shin, Y.-R. Kim, *Adv. Funct. Mater.* **2009**, *19*, 1625.

[17] T.-W. Lee, Y. Chung, O. Kwon, J.-J. Park, *Adv. Funct. Mater.* **2007**, *17*, 390.

[18] J. H. Burroughes, D. D. C. Bradley, A. R. Brown, R. N. Marks, K. Mackay, R. H. Friend, P. L. Burns, A. B. Holmes, *Nature* **1990**, *347*, 539.

[19] M. C. Gather, A. Köhnen, A. Falcou, H. Becker, K. Meerholz, *Adv. Funct. Mater.* **2007**, *17*, 191.

[20] Y. Kim, T. Han, C. Lee, Y. Kim, Y. Yang, T. Lee, *Adv. Funct. Mater.* **2020**, *30*, 2005292.

[21] A. Monkman, *ACS Appl. Mater. Interfaces* **2021**, *14*, 20463.

[22] C.-W. Han, K.-M. Kim, S.-J. Bae, H.-S. Choi, J.-M. Lee, T.-S. Kim, Y. H. Tak, S.-Y. Cha, B.-C. Ahn, *SID Symp. Dig. Tech. Pap.* **2012**, *43*, 279.

[23] H. Lee, Y. Kwon, C. Lee, *J. Soc. Inf. Disp.* **2012**, *20*, 640.

[24] S. Stolz, S. Meyer, A. Hayer, R. Linge, M. Engel, L.-I. Rodríguez, M. Hamburger, H.-R. Tseng, A. Jatsch, R. Anémian, *SID Symp. Dig. Tech. Pap.* **2021**, *52*, 264.

[25] S. Wang, Y. C. Wu, S. Jiao, T. Shi, N. Ai, Y. Zhang, S. Iguchi, P. Y. Lu, H. Zhou, *SID Int. Symp.* **2019**, *50*, 1157.

[26] T. Kang, H. G. Kim, H. R. Mun, J. Lee, S. Kim, J. Ha, *Dig. Tech. Pap. to SID Int. Symp.* **2021**, *52*, 267.

This article is protected by copyright. All rights reserved.

Accepted Article

15214095, ja, Downloaded from https://onlinelibrary.wiley.com/doi/10.1002/adma.202207454 by Seoul National University, Wiley Online Library on [28/11/2022]. See the Terms and Conditions (https://onlinelibrary.wiley.com/terms-and-conditions) on Wiley Online Library for rules of use; OA articles are governed by the applicable Creative Commons License

[27] K. Iida, H. Gorohmaru, K. Ishibashi, Y. Shoji, *Dig. Tech. Pap.SID Int. Symp.* **2020**, *51*, 399.

[28] J. G. Kang, Y. Koo, J. Ha, C. Lee, *Dig. Tech. Pap. - SID Int. Symp.* **2020**, *51*, 591.

[29] C. A. Annis, *SID Symp. Dig. Tech. Pap.* **2019**, *50*, 762.

[30] C. Li, *Inkjet Printing for AMOLED Technology & Market Report – 2019*, **2019**.

[31] C.-W. Han, M.-Y. Han, S.-R. Joung, J.-S. Park, Y.-K. Jung, J.-M. Lee, H.-S. Choi, G.-J. Cho, D.-H. Kim, M.-K. Yee, H.-G. Kim, H.-C. Choi, C.-H. Oh, I.-B. Kang, *SID Symp. Dig. Tech. Pap.* **2017**, *48*, 1.

[32] S. Wang, Z. Wang, L. Su, T. Dong, J. Zhuang, D. Fu, *Dig. Tech. Pap. - SID Int. Symp.* **2021**, *52*, 271.

[33] Z. Wu, L. Yan, Y. Li, H. Shih, X. Feng, T. Kim, Y. Peng, J. Yu, X. Dong, *Dig. Tech. Pap. - SID Int. Symp.* **2021**, *52*, 308.

[34] F. Hermerschmidt, S. A. Choulis, E. J. W. List-Kratochvil, *Adv. Mater. Technol.* **2019**, *4*, 1800474.

[35] S. Meyer, S. Stolz, M. Hamburger, H.-R. Tseng, M. Engel, A. Hayer, R. Linge, S. Tierney, G. Bernatz, R. Anémian, *SID Symp. Dig. Tech. Pap.* **2020**, *51*, 391.

[36] M. Singh, H. M. Haverinen, P. Dhagat, G. E. Jabbour, *Adv. Mater.* **2010**, *22*, 673.

[37] Y.-J. Pu, T. Chiba, K. Ideta, S. Takahashi, N. Aizawa, T. Hikichi, J. Kido, *Adv. Mater.* **2015**, *27*, 1327.

[38] N. Aizawa, Y.-J. Pu, M. Watanabe, T. Chiba, K. Ideta, N. Toyota, M. Igarashi, Y. Suzuri, H. Sasabe, J. Kido, *Nat. Commun.* **2014**, *5*, 5756.

[39] S. D. Hoath, S. Jung, W. K. Hsiao, I. M. Hutchings, *Org. Electron.* **2012**, *13*, 3259.

This article is protected by copyright. All rights reserved.

Accepted Article

15214095, ja, Downloaded from https://onlinelibrary.wiley.com/doi/10.1002/adma.202207454 by Seoul National University, Wiley Online Library on [28/11/2022]. See the Terms and Conditions (https://onlinelibrary.wiley.com/terms-and-conditions) on Wiley Online Library for rules of use; OA articles are governed by the applicable Creative Commons License

Accepted Article

[40] Z. Du, X. Yu, Y. Han, *Chinese Chem. Lett.* **2018**, *29*, 399.

[41] S. Ohisa, Y. J. Pu, N. L. Yamada, G. Matsuba, J. Kido, *ACS Appl. Mater. Interfaces* **2015**, *7*, 20779.

[42] S. Ohisa, G. Matsuba, N. L. Yamada, Y.-J. Pu, H. Sasabe, J. Kido, *Adv. Mater. Interfaces* **2014**, *1*, 1400097.

[43] S. H. Jeong, J. Park, T. H. Han, F. Zhang, K. Zhu, J. S. Kim, M. H. Park, M. O. Reese, S. Yoo, T. W. Lee, *Joule* **2020**, *4*, 1206.

[44] J. C. Deaton, F. N. Castellano, *Archetypal Iridium(III) Compounds for Optoelectronic and Photonic Applications*, John Wiley & Sons, Ltd, **2017**.

[45] M. A. Baldo, M. E. Thompson, S. R. Forrest, *Nature* **2000**, *403*, 750.

[46] A. K. Pal, S. Krotkus, M. Fontani, C. F. R. Mackenzie, D. B. Cordes, A. M. Z. Slawin, I. D. W. Samuel, E. Zysman-Colman, *Adv. Mater.* **2018**, *30*, 1804231.

[47] M. Y. Wong, E. Zysman-Colman, M. Y. Wong, E. Zysman-Colman, *Adv. Mater.* **2017**, *29*, 1605444.

[48] S. J. Woo, J. S. Kim, T. W. Lee, *Nat. Photonics 2021 159* **2021**, *15*, 630.

[49] F. So, D. Kondakov, *Adv. Mater.* **2010**, *22*, 3762.

[50] "JOLED starts mass producing inkjet-printed OLED displays under the OLEDIO brand," can be found under https://www.oled-info.com/joled-starts-mass-producing-inkjet-printed-oled-displays-under-oledio-brand, **2021**.

[51] H. G. Kim, S. M. Lee, D. Shin, J. Ha, C. Lee, *SID Symp. Dig. Tech. Pap.* **2020**, *51*, 395.

This article is protected by copyright. All rights reserved.

15214095, ja, Downloaded from https://onlinelibrary.wiley.com/doi/10.1002/adma.202207454 by Seoul National University, Wiley Online Library on [28/11/2022]. See the Terms and Conditions (https://onlinelibrary.wiley.com/terms-and-conditions) on Wiley Online Library for rules of use; OA articles are governed by the applicable Creative Commons License

[52] "Kyulux says it is on track to commercialize green Hyperfluorescence materials in 2023, red and blue in 2024," can be found under https://www.oled-info.com/kyulux-says-it-track-commercialize-green-hyperfluorescence-materials-2023-red%0A, **2022**.

[53] D. Fukushima, S. Tanaka, H. Kakimoto, T. Yamada, *Dig. Tech. Pap. - SID Int. Symp.* **2021**, *52*, 234.

[54] J.-H. Lee, C.-H. Chen, P.-H. Lee, H.-Y. Lin, M. Leung, T.-L. Chiu, C.-F. Lin, *J. Mater. Chem. C* **2019**, *7*, 5874.

[55] S. Meyer, S. Stolz, M. Hamburger, H. R. Tseng, M. Engel, A. Hayer, R. Linge, S. Tierney, G. Bernatz, R. Anémian, *Dig. Tech. Pap. - SID Int. Symp.* **2020**, *51*, 391.

[56] S. Cho, N. Y. Kwon, C. W. Kim, H. Lee, J. M. Ha, H. J. Kim, H. Y. Woo, S. Park, M. J. Cho, D. H. Choi, *Polym. Chem.* **2022**, *13*, 1824.

[57] J. Hwang, C. W. Koh, J. M. Ha, H. Y. Woo, S. Park, M. J. Cho, D. H. Choi, *ACS Appl. Mater. Interfaces* **2021**, *13*, 61454.

[58] J. Zhao, M. Lian, Y. Yu, X. Yan, X. Xu, X. Yang, G. Zhou, Z. Wu, *Macromol. Rapid Commun.* **2015**, *36*, 71.

[59] F. Samaeifar, H. Aziz, *ACS Appl. Mater. Interfaces* **2022**, *14*, 8199.

[60] T. H. Han, W. Song, T. W. Lee, *ACS Appl. Mater. Interfaces* **2015**, *7*, 3117.

[61] T.-H. Han, Y.-H. Kim, M. H. Kim, W. Song, T.-W. Lee, *ACS Appl. Mater. Interfaces* **2016**, *8*, 6152.

[62] S. A. Choulis, V.-E. Choong, A. Patwardhan, M. K. Mathai, F. So, *Adv. Funct. Mater.* **2006**, *16*, 1075.

This article is protected by copyright. All rights reserved.

Accepted Article

15214095, ja, Downloaded from https://onlinelibrary.wiley.com/doi/10.1002/adma.202207454 by Seoul National University, Wiley Online Library on [28/11/2022]. See the Terms and Conditions (https://onlinelibrary.wiley.com/terms-and-conditions) on Wiley Online Library for rules of use; OA articles are governed by the applicable Creative Commons License

[63] T.-H. Han, Y. Lee, M.-R. Choi, S.-H. Woo, S.-H. Bae, B. H. Hong, J.-H. Ahn, T.-W. Lee, *Nat. Photonics* **2012**, *6*, 105.

[64] S. Kwon, T. Han, T. Y. Ko, N. Li, Y. Kim, D. J. Kim, S. Bae, Y. Yang, B. H. Hong, K. S. Kim, S. Ryu, T. Lee, *Nat. Commun.* **2018**, *9*, DOI 10.1038/s41467-018-04385-4.

[65] T.-H. Han, S.-J. Kwon, N. Li, H.-K. Seo, W. Xu, K. S. Kim, T.-W. Lee, *Angew. Chemie Int. Ed.* **2016**, *55*, 6197.

[66] T.-H. Han, H. Kim, S.-J. Kwon, T.-W. Lee, *Mater. Sci. Eng. R Reports* **2017**, *118*, 1.

[67] J. Lee, T. H. Han, M. H. Park, D. Y. Jung, J. Seo, H. K. Seo, H. Cho, E. Kim, J. Chung, S. Y. Choi, T. S. Kim, T. W. Lee, S. Yoo, *Nat. Commun.* **2016**, *7*, 11791.

[68] K.-G. Lim, T.-H. Han, T.-W. Lee, *Energy Environ. Sci.* **2021**, *14*, 2009.

[69] K. S. Yook, S. O. Jeon, S. Y. Min, J. Y. Lee, H. J. Yang, T. Noh, S. K. Kang, T. W. Lee, *Adv. Funct. Mater.* **2010**, *20*, 1797.

[70] T.-H. Han, K. Y. Jang, Y. Dong, R. H. Friend, E. H. Sargent, T.-W. Lee, *Nat. Rev. Mater.* **2022**, DOI 10.1038/s41578-022-00459-4.

[71] S. Ho, S. Liu, Y. Chen, F. So, *J. Photonics Energy* **2015**, *5*, 057611.

[72] B. Derby, *Annu. Rev. Mater. Res.* **2010**, *40*, 395.

[73] B. Derby, N. Reis, *MRS Bull.* **2003**, *28*, 815.

[74] X. Cao, Y. Ye, X. Liu, T. Guo, Q. Tang, *SID Int. Symp.* **2021**, *52*, 395.

[75] R. D. Deegan, O. Bakajin, T. F. Dupont, G. Huber, S. R. Nagel, T. A. Witten, *Nature* **1997**, *389*, 827.

This article is protected by copyright. All rights reserved.

Accepted Article

15214095, ja, Downloaded from https://onlinelibrary.wiley.com/doi/10.1002/adma.202207454 by Seoul National University, Wiley Online Library on [28/11/2022]. See the Terms and Conditions (https://onlinelibrary.wiley.com/terms-and-conditions) on Wiley Online Library for rules of use; OA articles are governed by the applicable Creative Commons License

[76] D. Fukushima, S. Tanaka, H. Kakimoto, T. Yamada, *Dig. Tech. Pap. - SID Int. Symp.* **2021**, *52*, 315.

[77] Y. Pan, H. Liu, S. Wang, X. Han, X. Li, *J. Mater. Chem. C* **2021**, *9*, 12712.

[78] X. Zhao, S. Wang, J. You, Y. Zhang, X. Li, *J. Mater. Chem. C* **2015**, *3*, 11377.

[79] J. Kwak, Y. Y. Lyu, S. Noh, H. Lee, M. Park, B. Choi, K. Char, C. Lee, *Thin Solid Films* **2012**, *520*, 7157.

[80] C. Fan, Y. Chen, Z. Liu, Z. Jiang, C. Zhong, D. Ma, J. Qin, C. Yang, *J. Mater. Chem. C* **2013**, *1*, 463.

[81] I. Na, K. J. Kim, G. T. Kim, Y. Seo, Y. Kim, Y. K. Kim, M. K. Joo, *Appl. Phys. Lett.* **2020**, *117*, DOI 10.1063/5.0016096.

[82] I. Cho, S. H. Kim, J. H. Kim, S. Park, S. Y. Park, *J. Mater. Chem.* **2012**, *22*, 123.

[83] R. M. Soneira, *Inf. Disp. (1975).* **2013**, *29*, 12.

[84] M. Hack, M. S. Weaver, J. J. Brown, K. Parikh, K. Bui, V. Sinha, *Dig. Tech. Pap. - SID Int. Symp.* **2021**, *52*, 301.

[85] M. Eritt, C. May, K. Leo, M. Toerker, C. Radehaus, *Thin Solid Films* **2010**, *518*, 3042.

[86] D. M. Taylor, *Semicond. Sci. Technol.* **2015**, *30*, 054002.

[87] S. Wang, B. Zhang, Y. Wang, J. Ding, Z. Xie, L. Wang, *Chem. Commun.* **2017**, *53*, 5128.

[88] Y. E. Kim, A. Ko, H. J. Jang, S. J. Yoon, S. H. Roh, J. Y. Lee, J. Y. Lee, D. Kim, J. K. Kim, K. S. Yook, *Dye. Pigment.* **2021**, *187*, 109122.

This article is protected by copyright. All rights reserved.

Accepted Article

15214095, ja, Downloaded from https://onlinelibrary.wiley.com/doi/10.1002/adma.202207454 by Seoul National University, Wiley Online Library on [28/11/2022]. See the Terms and Conditions (https://onlinelibrary.wiley.com/terms-and-conditions) on Wiley Online Library for rules of use; OA articles are governed by the applicable Creative Commons License

[89] D. Liu, W. Tian, Y. Feng, X. Zhang, X. Ban, W. Jiang, Y. Sun, *ACS Appl. Mater. Interfaces* **2019**, *11*, 16737.

[90] B. Wei, H. Chen, W. Hua, M. Chen, X. Ding, C. Li, *Appl. Surf. Sci.* **2022**, *572*, 151419.

[91] Y. Jiang, L. Jiang, F. S. Yan Yeung, P. Xu, S. Chen, H. S. Kwok, G. Li, *ACS Appl. Mater. Interfaces* **2019**, *11*, 11119.

[92] B. S. Mashford, T.-L. Nguyen, G. J. Wilson, P. Mulvaney, *J. Mater. Chem.* **2010**, *20*, 167.

[93] H. J. Bolink, H. Brine, E. Coronado, M. Sessolo, *ACS Appl. Mater. Interfaces* **2010**, *2*, 2694.

[94] J. Zhang, X. Zhang, H. Feng, Z. Yu, J. Zhang, S. Liu, L. Zhang, W. Xie, *J. Mater. Chem. C* **2019**, *7*, 1991.

[95] X. Yu, T. J. Marks, A. Facchetti, *Nat. Mater. 2016 154* **2016**, *15*, 383.

[96] A. Gadisa, T. Hairfield, L. Alibabaei, C. L. Donley, E. T. Samulski, R. Lopez, *ACS Appl. Mater. Interfaces* **2013**, *5*, 8440.

[97] M. C. Gwinner, Y. Vaynzof, K. K. Banger, P. K. H. Ho, R. H. Friend, H. Sirringhaus, *Adv. Funct. Mater.* **2010**, *20*, 3457.

[98] Y. K. Lee, S. K. Kwon, T. Jin, M. Alsawafta, A. Almoabadi, S. Badilescu, R. Kasuga, M. Tachibana, N. Ohtani, *Jpn. J. Appl. Phys.* **2022**, *61*, 041001.

[99] C. Song, Z. Hu, Y. Luo, Y. Cun, L. Wang, L. Ying, F. Huang, J. Peng, J. Wang, Y. Cao, *Adv. Electron. Mater.* **2018**, *4*, 1700380.

[100] H. M. Kim, J. Kim, S. Y. Cho, J. Jang, *ACS Appl. Mater. Interfaces* **2017**, *9*, 38678.

[101] A. Perumal, H. Faber, N. Yaacobi-Gross, P. Pattanasattayavong, C. Burgess, S. Jha, M. A. McLachlan, P. N. Stavrinou, T. D. Anthopoulos, D. D. C. Bradley, *Adv. Mater.* **2015**, *27*, 93.

This article is protected by copyright. All rights reserved.

Accepted Article

15214095, ja, Downloaded from https://onlinelibrary.wiley.com/doi/10.1002/adma.202207454 by Seoul National University, Wiley Online Library on [28/11/2022]. See the Terms and Conditions (https://onlinelibrary.wiley.com/terms-and-conditions) on Wiley Online Library for rules of use; OA articles are governed by the applicable Creative Commons License

[102] Y.-Y. Ma, X.-C. Hua, T.-S. Zhai, Y.-H. Li, X. Lu, S. Duhm, M.-K. Fung, *Org. Electron.* **2019**, *68*, 236.

[103] W. Zhu, Y. Chen, L. Huang, K. Ding, J. Li, B. Wei, *J. Alloys Compd.* **2022**, *900*, 163481.

[104] Z. Hu, Q. Wang, Z. Zhong, Y. Chen, J. Peng, J. Wang, Y. Cao, *Synth. Met.* **2018**, *236*, 31.

[105] M. T. Greiner, Z. H. Lu, *NPG Asia Mater.* **2013**, *5*, e55.

[106] K. Kanai, K. Koizumi, S. Ouchi, Y. Tsukamoto, K. Sakanoue, Y. Ouchi, K. Seki, *Org. Electron.* **2010**, *11*, 188.

[107] M. T. Greiner, M. G. Helander, W.-M. Tang, Z.-B. Wang, J. Qiu, Z.-H. Lu, *Nat. Mater.* **2012**, *11*, 76.

[108] S. Ohisa, S. Kagami, Y.-J. Pu, T. Chiba, J. Kido, *ACS Appl. Mater. Interfaces* **2016**, *8*, 20946.

[109] Y. Zhang, W. Li, K. Xu, P. Kang, L. Liu, L. Wang, B. Wei, X. Zhang, *Opt. Laser Technol.* **2019**, *113*, 239.

[110] S. Höfle, M. Bruns, S. Strässle, C. Feldmann, U. Lemmer, A. Colsmann, *Adv. Mater.* **2013**, *25*, 4113.

[111] S. Höfle, H. Do, E. Mankel, M. Pfaff, Z. Zhang, D. Bahro, T. Mayer, W. Jaegermann, D. Gerthsen, C. Feldmann, U. Lemmer, A. Colsmann, *Org. Electron.* **2013**, *14*, 1820.

[112] C. Thu, P. Ehrenreich, K. K. Wong, E. Zimmermann, J. Dorman, W. Wang, A. Fakharuddin, M. Putnik, C. Drivas, A. Koutsoubelitis, M. Vasilopoulou, L. C. Palilis, S. Kennou, J. Kalb, T. Pfadler, L. Schmidt-Mende, *Sci. Rep.* **2018**, *8*, 1.

[113] L. Qian, Y. Zheng, K. R. Choudhury, D. Bera, F. So, J. Xue, P. H. Holloway, *Nano Today* **2010**, *5*, 384.

This article is protected by copyright. All rights reserved.

Accepted Article

15214095, ja, Downloaded from https://onlinelibrary.wiley.com/doi/10.1002/adma.202207454 by Seoul National University, Wiley Online Library on [28/11/2022]. See the Terms and Conditions (https://onlinelibrary.wiley.com/terms-and-conditions) on Wiley Online Library for rules of use; OA articles are governed by the applicable Creative Commons License

[114] J. H. Youn, S. J. Baek, H. P. Kim, D. H. Nam, Y. Lee, J. G. Lee, J. Jang, *J. Mater. Chem. C* **2013**, *1*, 3250.

[115] C. Wechwithayakhlung, D. M. Packwood, D. J. Harding, P. Pattanasattayavong, *J. Phys. Chem. Solids* **2021**, *154*, 110085.

[116] L. J. Xu, J. Y. Wang, X. F. Zhu, X. C. Zeng, Z. N. Chen, *Adv. Funct. Mater.* **2015**, *25*, 3033.

[117] J. Gao, J. B. Xu, M. Zhu, N. Ke, D. Ma, *J. Phys. D. Appl. Phys.* **2007**, *40*, 5666.

[118] C. Schünemann, D. Wynands, L. Wilde, M. P. Hein, S. Pfützner, C. Elschner, K. J. Eichhorn, K. Leo, M. Riede, *Phys. Rev. B - Condens. Matter Mater. Phys.* **2012**, *85*, 245314.

[119] C. V. Kumar, G. Sfyri, D. Raptis, E. Stathatos, P. Lianos, *RSC Adv.* **2015**, *5*, 3786.

[120] E. Nouri, J. V. S. Krishna, C. V. Kumar, V. Dracopoulos, L. Giribabu, M. R. Mohammadi, P. Lianos, *Electrochim. Acta* **2016**, *222*, 875.

[121] S. A. Van Slyke, C. H. Chen, C. W. Tang, *Appl. Phys. Lett.* **1996**, *69*, 2160.

[122] G. Sfyri, C. V. Kumar, Y. L. Wang, Z. X. Xu, C. A. Krontiras, P. Lianos, *Appl. Surf. Sci.* **2016**, *360*, 767.

[123] R. Bechara, J. Petersen, V. Gernigon, P. Lévêque, T. Heiser, V. Toniazzo, D. Ruch, M. Michel, *Sol. Energy Mater. Sol. Cells* **2012**, *98*, 482.

[124] Y. L. Deng, Y. M. Xie, L. Zhang, Z. K. Wang, L. S. Liao, *J. Mater. Chem. C* **2015**, *3*, 6218.

[125] T. W. Ng, M. F. Lo, M. K. Fung, W. J. Zhang, C. S. Lee, *Adv. Mater.* **2014**, *26*, 5569.

[126] T. Matsushima, G. H. Jin, Y. Kanai, T. Yokota, S. Kitada, T. Kishi, H. Murata, *Org. Electron.* **2011**, *12*, 520.

This article is protected by copyright. All rights reserved.

Accepted Article

15214095, ja, Downloaded from https://onlinelibrary.wiley.com/doi/10.1002/adma.202207454 by Seoul National University, Wiley Online Library on [28/11/2022]. See the Terms and Conditions (https://onlinelibrary.wiley.com/terms-and-conditions) on Wiley Online Library for rules of use; OA articles are governed by the applicable Creative Commons License

[127] R. Davis, P. P, *Mater. Sci. Semicond. Process.* **2021**, *125*, 105637.

[128] A. Lorente, P. Pingel, A. Miasojedovas, H. Krüger, S. Janietz, *ACS Appl. Mater. Interfaces* **2017**, *9*, 24043.

[129] S. Wang, Z. Yan, J. Ding, L. Wang, *Adv. Mater. Technol.* **2019**, *4*, 1900137.

[130] M. Takada, S. Furuta, T. Kobayashi, T. Nagase, T. Shinagawa, M. Izaki, H. Naito, *J. Appl. Phys.* **2016**, *120*, 185501.

[131] J. Kim, B. Yoon, J. Kim, Y. Choi, Y. W. Kwon, S. K. Park, K. S. Jeong, *RSC Adv.* **2017**, *7*, 38166.

[132] D. Bederak, D. N. Dirin, N. Sukharevska, J. Momand, M. V. Kovalenko, M. A. Loi, *Chem. Mater.* **2021**, *33*, 320.

[133] H. Shen, W. Cao, N. T. Shewmon, C. Yang, L. S. Li, J. Xue, *Nano Lett.* **2015**, *15*, 1211.

[134] P. Kathirgamanathan, M. Kumaraverl, N. Bramananthan, S. Ravichandran, *J. Mater. Chem. C* **2018**, *6*, 11622.

[135] K. Gugula, L. Stegemann, P. J. Cywiński, C. A. Strassert, M. Bredol, *RSC Adv.* **2016**, *6*, 10086.

[136] J. S. Wang, B. Ullrich, A. Das, C. M. Wai, G. J. Brown, C. K. Dass, J. R. Hendrickson, *RSC Adv.* **2016**, *6*, 48651.

[137] P. Kumar, N. Agrawal, V. K. Pandey, A. K. Gautam, S. K. Sharma, S. D. Chaudhary, *Solid. State. Electron.* **2021**, *183*, 108031.

[138] G. Greczynski, M. Fahlman, W. R. Salaneck, *J. Chem. Phys.* **2000**, *113*, 2407.

[139] E. I. Haskal, A. Curioni, P. F. Seidler, W. Andreoni, *Appl. Phys. Lett.* **1997**, *71*, 1151.

This article is protected by copyright. All rights reserved.

Accepted Article

15214095, ja, Downloaded from https://onlinelibrary.wiley.com/doi/10.1002/adma.202207454 by Seoul National University, Wiley Online Library on [28/11/2022]. See the Terms and Conditions (https://onlinelibrary.wiley.com/terms-and-conditions) on Wiley Online Library for rules of use; OA articles are governed by the applicable Creative Commons License

[140] S. Van Reenen, S. Kouijzer, R. A. J. Janssen, M. M. Wienk, M. Kemerink, *Adv. Mater. Interfaces* **2014**, *1*, 1400189.

[141] T. Chiba, Y. J. Pu, H. Sasabe, J. Kido, Y. Yang, *J. Mater. Chem.* **2012**, *22*, 22769.

[142] Y. Lim, Y.-S. Park, Y. Kang, D. Y. Jang, J. H. Kim, J.-J. Kim, A. Sellinger, D. Y. Yoon, *J. Am. Chem. Soc.* **2011**, *133*, 1375.

[143] J. Rivnay, S. Inal, B. A. Collins, M. Sessolo, E. Stavrinidou, X. Strakosas, C. Tassone, D. M. Delongchamp, G. G. Malliaras, *Nat. Commun.* **2016**, *7*, 1.

[144] Y. Sun, S. Yang, P. Du, F. Yan, J. Qu, Z. Zhu, J. Zuo, C. Zhang, *Opt. Express* **2017**, *25*, 1723.

[145] S.-H. Jeong, H. Kim, M.-H. Park, Y. Lee, N. Li, H.-K. Seo, T.-H. Han, S. Ahn, J.-M. Heo, K. S. Kim, T.-W. Lee, *Nano Energy* **2019**, *60*, 324.

[146] K. G. Lim, S. Ahn, Y. H. Kim, Y. Qi, T. W. Lee, *Energy Environ. Sci.* **2016**, *9*, 932.

[147] M.-R. Choi, T.-H. Han, K.-G. Lim, S.-H. Woo, D. H. Huh, T.-W. Lee, *Angew. Chemie* **2011**, *123*, 6398.

[148] J. Wang, H. Liu, S. Wu, Y. Jia, H. Yu, X. Li, S. Wang, *Chem. Eng. J.* **2020**, *391*, 123479.

[149] Y. Xiang, G. Xie, Q. Li, L. Xue, Q. Xu, J. Zhu, Y. Tang, S. Gong, X. Yin, C. Yang, *ACS Appl. Mater. Interfaces* **2019**, *11*, 29105.

[150] J.-H. Jou, W.-B. Wang, M.-F. Hsu, J.-J. Shyue, C.-H. Chiu, I.-M. Lai, S.-Z. Chen, P.-H. Wu, C.-C. Chen, C.-P. Liu, S.-M. Shen, *ACS Nano* **2010**, *4*, 4054.

[151] S. Ahn, T.-H. Han, K. Maleski, J. Song, Y.-H. Kim, M.-H. Park, H. Zhou, S. Yoo, Y. Gogotsi, T.-W. Lee, S. Ahn, T. Han, Y. Kim, M. Park, H. Zhou, T. Lee, K. Maleski, Y. A. Gogotsi, J. Song, S. Yoo, *Adv. Mater* **2020**, *32*, DOI 10.1002/adma.202000919.

This article is protected by copyright. All rights reserved.

Accepted Article

15214095, ja, Downloaded from https://onlinelibrary.wiley.com/doi/10.1002/adma.202207454 by Seoul National University, Wiley Online Library on [28/11/2022]. See the Terms and Conditions (https://onlinelibrary.wiley.com/terms-and-conditions) on Wiley Online Library for rules of use; OA articles are governed by the applicable Creative Commons License

[152] S. Ahn, S.-H. Jeong, T.-H. Han, T.-W. Lee, *Adv. Opt. Mater.* **2017**, *5*, 1600512.

[153] T. H. Han, M. H. Park, S. J. Kwon, S. H. Bae, H. K. Seo, H. Cho, J. H. Ahn, T. W. Lee, *NPG Asia Mater. 2016 89* **2016**, *8*, e303.

[154] T.-H. Han, S.-J. Kwon, N. Li, H.-K. Seo, W. Xu, K. S. Kim, T.-W. Lee, *Angew. Chemie Int. Ed.* **2016**, *55*, 6197.

[155] K.-G. Lim, T.-H. Han, T.-W. Lee, *Energy Environ. Sci.* **2021**, *14*, 2009.

[156] B. Zhang, W. Li, J. Yang, Y. Fu, Z. Xie, S. Zhang, L. Wang, *J. Phys. Chem. C* **2009**, *113*, 7898.

[157] P. Dąbczyński, M. M. Marzec, Ł. Pięta, K. Fijałkowski, J. Raczkowska, A. Bernasik, A. Budkowski, J. Rysz, *ACS Omega* **2018**, *3*, 3631.

[158] B. Li, D. Song, Z. Xu, B. Qiao, W. Zheng, J. Yang, W. Jing, S. Zhao, *Org. Electron.* **2020**, *83*, 105721.

[159] H. Yan, P. Lee, N. R. Armstrong, A. Graham, G. A. Evmenenko, P. Dutta, T. J. Marks, *J. Am. Chem. Soc.* **2005**, *127*, 3172.

[160] Y. Liu, X. Wei, Z. Li, J. Liu, R. Wang, X. Hu, P. Wang, Y. Yamada-Takamura, T. Qi, Y. Wang, *ACS Appl. Energy Mater.* **2018**, *1*, 543.

[161] K. R. Choudhury, J. Lee, N. Chopra, A. Gupta, X. Jiang, F. Amy, F. So, *Adv. Funct. Mater.* **2009**, *19*, 491.

[162] D. G. Yoon, Y. J. Kang, R. Bail, B. D. Chin, *J. Inf. Disp.* **2021**, *22*, 91.

[163] D. K. Dubey, S. S. Swayamprabha, R. A. Kumar Yadav, D. Tavgeniene, D. Volyniuk, S. Grigalevicius, J. H. Jou, *Org. Electron.* **2019**, *73*, 94.

This article is protected by copyright. All rights reserved.

Accepted Article

15214095, ja, Downloaded from https://onlinelibrary.wiley.com/doi/10.1002/adma.202207454 by Seoul National University, Wiley Online Library on [28/11/2022]. See the Terms and Conditions (https://onlinelibrary.wiley.com/terms-and-conditions) on Wiley Online Library for rules of use; OA articles are governed by the applicable Creative Commons License

[164] C. D. Müller, A. Falcou, N. Reckefuss, M. Rojahn, V. Wiederhirn, P. Rudati, H. Frohne, O. Nuyken, H. Becker, K. Meerholz, *Nature* **2003**, *421*, 829.

[165] R.-Q. Png, P.-J. Chia, J.-C. Tang, B. Liu, S. Sivaramakrishnan, M. Zhou, S.-H. Khong, H. S. O. Chan, J. H. Burroughes, L.-L. Chua, R. H. Friend, P. K. H. Ho, *Nat. Mater.* **2010**, *9*, 152.

[166] Y.-H. Niu, M. S. Liu, J.-W. Ka, J. Bardeker, M. T. Zin, R. Schofield, Y. Chi, A. K.-Y. Jen, *Adv. Mater.* **2007**, *19*, 300.

[167] N. Aizawa, Y.-J. Pu, T. Chiba, S. Kawata, H. Sasabe, J. Kido, *Adv. Mater.* **2014**, *26*, 7543.

[168] F. Huang, H. Wu, Y. Cao, *Chem. Soc. Rev.* **2010**, *39*, 2500.

[169] B. Zhang, C. Qin, X. Niu, Z. Xie, Y. Cheng, L. Wang, X. Li, *Appl. Phys. Lett.* **2010**, *97*, 043506.

[170] Y. Zhou, C. Fuentes-Hernandez, J. Shim, J. Meyer, A. J. Giordano, H. Li, P. Winget, T. Papadopoulos, H. Cheun, J. Kim, M. Fenoll, A. Dindar, W. Haske, E. Najafabadi, T. M. Khan, H. Sojoudi, S. Barlow, S. Graham, J. L. Brédas, S. R. Marder, A. Kahn, B. Kippelen, *Science (80-.).* **2012**, *336*, 327.

[171] C. V. Hoven, R. Yang, A. Garcia, V. Crockett, A. J. Heeger, G. C. Bazan, T. Q. Nguyen, *Proc. Natl. Acad. Sci. U. S. A.* **2008**, *105*, 12730.

[172] I. D. Parker, Y. Cao, C. Y. Yang, *J. Appl. Phys.* **1999**, *85*, 2441.

[173] T. W. Lee, M. G. Kim, S. H. Park, S. Y. Kim, O. Kwon, T. Noh, J. J. Park, T. L. Choi, J. H. Park, B. D. Chin, *Adv. Funct. Mater.* **2009**, *19*, 1863.

[174] L. S. Hung, C. W. Tang, M. G. Mason, *Appl. Phys. Lett.* **1997**, *70*, 152.

[175] P. Piromreun, H. S. Oh, Y. Shen, G. G. Malliaras, J. C. Scott, P. J. Brock, *Appl. Phys. Lett.* **2000**, *77*, 2403.

This article is protected by copyright. All rights reserved.

Accepted Article

15214095, ja, Downloaded from https://onlinelibrary.wiley.com/doi/10.1002/adma.202207454 by Seoul National University, Wiley Online Library on [28/11/2022]. See the Terms and Conditions (https://onlinelibrary.wiley.com/terms-and-conditions) on Wiley Online Library for rules of use; OA articles are governed by the applicable Creative Commons License

[176] H. Wu, F. Huang, J. Peng, Y. Cao, *Org. Electron.* **2005**, *6*, 118.

[177] D. An, J. Zou, H. Wu, J. Peng, W. Yang, Y. Cao, *Org. Electron.* **2009**, *10*, 299.

[178] B. H. Wallikewitz, D. Kabra, S. Gélinas, R. H. Friend, *Phys. Rev. B* **2012**, *85*, 045209.

[179] M. A. Baldo, D. F. O'Brien, M. E. Thompson, S. R. Forrest, *Phys. Rev. B* **1999**, *60*, 14422.

[180] H. Yersin, in *Transit. Met. Rare Earth Compd. Top. Curr. Chem.*, **2012**, pp. 1–26.

[181] J. Widengren, U. Mets, R. Rigler, *J. Phys. Chem.* **1995**, *99*, 13368.

[182] A. F. Rausch, M. E. Thompson, H. Yersin, *Chem. Phys. Lett.* **2009**, *468*, 46.

[183] H. Yersin, A. F. Rausch, R. Czerwieniec, T. Hofbeck, T. Fischer, *Coord. Chem. Rev.* **2011**, *255*, 2622.

[184] M. K. Etherington, J. Gibson, H. F. Higginbotham, T. J. Penfold, A. P. Monkman, *Nat. Commun.* **2016**, *7*, 13680.

[185] D. Thakur, D. K. Dubey, R. A. Kumar Yadav, S. Banik, J. Jayakumar, C.-H. Cheng, J.-H. Jou, S. Ghosh, *Org. Electron.* **2021**, *93*, 106127.

[186] J. W. Ma, Z. Liang, C. Jin, X. Y. Jiang, Z. L. Zhang, *Solid State Commun.* **2009**, *149*, 214.

[187] P. Wei, S. Zhao, Z. Xu, D. Song, B. Qiao, P. Wang, J. Yang, *Synth. Met.* **2019**, *252*, 15.

[188] X. Ban, W. Jiang, K. Sun, X. Xie, L. Peng, H. Dong, Y. Sun, B. Huang, L. Duan, Y. Qiu, *ACS Appl. Mater. Interfaces* **2015**, *7*, 7303.

[189] J. Y. Lee, J. Kim, H. Kim, M. C. Suh, *SID Int. Symp.* **2020**, *51*, 172.

[190] Y. Gu, X. Zhou, Y. Li, K. Wu, F. Wang, M. Huang, F. Guo, Y. Wang, S. Gong, D. Ma, C. Yang, *Org. Electron.* **2015**, *25*, 193.

This article is protected by copyright. All rights reserved.

Accepted Article

15214095, ja, Downloaded from https://onlinelibrary.wiley.com/doi/10.1002/adma.202207454 by Seoul National University, Wiley Online Library on [28/11/2022]. See the Terms and Conditions (https://onlinelibrary.wiley.com/terms-and-conditions) on Wiley Online Library for rules of use; OA articles are governed by the applicable Creative Commons License

[191] S. Tokito, T. Iijima, Y. Suzuri, H. Kita, T. Tsuzuki, F. Sato, *Appl. Phys. Lett.* **2003**, *83*, 569.

[192] J. H. Kim, D. Y. Yoon, J. W. Kim, J.-J. Kim, *Synth. Met.* **2007**, *157*, 743.

[193] H. Uoyama, K. Goushi, K. Shizu, H. Nomura, C. Adachi, *Nature* **2012**, *492*, 234.

[194] Y. Suzuki, Q. Zhang, C. Adachi, *J. Mater. Chem. C* **2015**, *3*, 1700.

[195] M. Godumala, J. Hwang, H. Kang, J.-E. Jeong, A. K. Harit, M. J. Cho, H. Y. Woo, S. Park, D. H. Choi, *ACS Appl. Mater. Interfaces* **2020**, *12*, 35300.

[196] C. Adachi, T. Tsutsui, S. Saito, *Appl. Phys. Lett.* **1989**, *55*, 1489.

[197] J. Li, D. Liu, Y. Li, C.-S. Lee, H.-L. Kwong, S. Lee, *Chem. Mater.* **2005**, *17*, 1208.

[198] J. Salbeck, N. Yu, J. Bauer, F. Weissörtel, H. Bestgen, *Synth. Met.* **1997**, *91*, 209.

[199] F. Lindla, M. Boesing, P. Van Gemmern, D. Bertram, D. Keiper, M. Heuken, H. Kalisch, R. H. Jansen, *Appl. Phys. Lett.* **2011**, *98*, 173304.

[200] S.-C. Dong, L. Xu, C. W. Tang, *Org. Electron.* **2017**, *42*, 379.

[201] J. Ràfols-Ribé, A. Vila-Costa, C. Rodríguez-Tinoco, A. F. Lopeandiá, J. Rodríguez-Viejo, M. Gonzalez-Silveira, *Phys. Chem. Chem. Phys.* **2018**, *20*, 29989.

[202] G. Vamvounis, H. Aziz, N.-X. Hu, Z. D. Popovic, *Synth. Met.* **2004**, *143*, 69.

[203] Y. Qi, J. Zhao, X. Wang, J. Yu, Z. Chi, *Org. Electron.* **2016**, *36*, 185.

[204] C. Adachi, T. Tsutsui, S. Saito, *Appl. Phys. Lett.* **1990**, *56*, 799.

[205] M.-F. Wu, S.-J. Yeh, C.-T. Chen, H. Murayama, T. Tsuboi, W.-S. Li, I. Chao, S.-W. Liu, J.-K. Wang, *Adv. Funct. Mater.* **2007**, *17*, 1887.

[206] S. J. Su, H. Sasabe, T. Takeda, J. Kido, *Chem. Mater.* **2008**, *20*, 1691.

This article is protected by copyright. All rights reserved.

Accepted Article

15214095, ja, Downloaded from https://onlinelibrary.wiley.com/doi/10.1002/adma.202207454 by Seoul National University, Wiley Online Library on [28/11/2022]. See the Terms and Conditions (https://onlinelibrary.wiley.com/terms-and-conditions) on Wiley Online Library for rules of use; OA articles are governed by the applicable Creative Commons License

[207] S. O. Jeon, K. S. Yook, C. W. Joo, J. Y. Lee, *Adv. Funct. Mater.* **2009**, *19*, 3644.

[208] S. O. Jeon, K. S. Yook, C. W. Joo, J. Y. Lee, *Appl. Phys. Lett.* **2009**, *94*, 013301.

[209] K. S. Yook, S. E. Jang, S. O. Jeon, J. Y. Lee, *Adv. Mater.* **2010**, *22*, 4479.

[210] H. S. Son, C. W. Seo, J. Y. Lee, *J. Mater. Chem.* **2011**, *21*, 5638.

[211] X. Ren, J. Li, R. J. Holmes, P. I. Djurovich, S. R. Forrest, M. E. Thompson, *Chem. Mater.* **2004**, *16*, 4743.

[212] J.-J. Lin, W.-S. Liao, H.-J. Huang, F.-I. Wu, C.-H. Cheng, *Adv. Funct. Mater.* **2008**, *18*, 485.

[213] R. Kumaresan, A. Maheshwaran, H.-Y. Park, K. Sung, J. Choi, W. Cho, M. Song, S. Il Ahn, S.-H. Jin, *J. Mater. Chem. C* **2020**, *8*, 12959.

[214] M. J. Percino, M. Cerón, P. Venkatesan, E. Pérez-Gutiérrez, P. Santos, P. Ceballos, A. E. Castillo, P. Gordillo-Guerra, K. Anandhan, O. Barbosa-García, W. Bernal, S. Thamotharan, *RSC Adv.* **2019**, *9*, 28704.

[215] S. Grimme, C. Diedrich, M. Korth, *Angew. Chemie Int. Ed.* **2006**, *45*, 625.

[216] Q. Li, Z. Li, *Acc. Chem. Res.* **2020**, *53*, 962.

[217] K. Tuong Ly, R.-W. Chen-Cheng, H.-W. Lin, Y.-J. Shiau, S.-H. Liu, P.-T. Chou, C.-S. Tsao, Y.-C. Huang, Y. Chi, *Nat. Photonics* **2017**, *11*, 63.

[218] J. Li, T. Zhang, Y. Liang, R. Yang, *Adv. Funct. Mater.* **2013**, *23*, 619.

[219] B. Liang, L. Wang, Y. Xu, H. Shi, Y. Cao, *Adv. Funct. Mater.* **2007**, *17*, 3580.

[220] J. Ding, B. Zhang, J. Lü, Z. Xie, L. Wang, X. Jing, F. Wang, *Adv. Mater.* **2009**, *21*, 4983.

This article is protected by copyright. All rights reserved.

Accepted Article

15214095, ja, Downloaded from https://onlinelibrary.wiley.com/doi/10.1002/adma.202207454 by Seoul National University, Wiley Online Library on [28/11/2022]. See the Terms and Conditions (https://onlinelibrary.wiley.com/terms-and-conditions) on Wiley Online Library for rules of use; OA articles are governed by the applicable Creative Commons License

[221] D. Xia, B. Wang, B. Chen, S. Wang, B. Zhang, J. Ding, L. Wang, X. Jing, F. Wang, *Angew. Chemie* **2014**, *126*, 1066.

[222] B. Zhang, G. Tan, C.-S. Lam, B. Yao, C.-L. Ho, L. Liu, Z. Xie, W.-Y. Wong, J. Ding, L. Wang, *Adv. Mater.* **2012**, *24*, 1873.

[223] Z. Ma, W. Dong, J. Hou, Q. Duan, S. Shao, L. Wang, *J. Mater. Chem. C* **2019**, *7*, 11845.

[224] W. Maison, J. V. Frangioni, N. Pannier, *Org. Lett.* **2004**, *6*, 4567.

[225] S.-C. Lo, N. A. H. Male, J. P. J. Markham, S. W. Magennis, P. L. Burn, O. V. Salata, I. D. W. Samuel, *Adv. Mater.* **2002**, *14*, 975.

[226] J. Ding, B. Wang, Z. Yue, B. Yao, Z. Xie, Y. Cheng, L. Wang, X. Jing, F. Wang, *Angew. Chemie Int. Ed.* **2009**, *48*, 6664.

[227] G. Gustafsson, Y. Cao, G. M. Treacy, F. Klavetter, N. Colaneri, A. J. Heeger, *Nature* **1992**, *357*, 477.

[228] M. Redecker, D. D. C. Bradley, M. Inbasekaran, W. W. Wu, E. P. Woo, *Adv. Mater.* **1999**, *11*, 241.

[229] M. Redecker, D. D. C. Bradley, M. Inbasekaran, E. P. Woo, *Appl. Phys. Lett.* **1998**, *73*, 1565.

[230] A. J. Campbell, D. D. C. Bradley, H. Antoniadis, *Appl. Phys. Lett.* **2001**, *79*, 2133.

[231] H. J. Bolink, E. Coronado, D. Repetto, M. Sessolo, E. M. Barea, J. Bisquert, G. Garcia-Belmonte, J. Prochazka, L. Kavan, *Adv. Funct. Mater.* **2008**, *18*, 145.

[232] K. Morii, M. Ishida, T. Takashima, T. Shimoda, Q. Wang, M. K. Nazeeruddin, M. Grätzel, *Appl. Phys. Lett.* **2006**, *89*, 183510.

[233] D. Kabra, M. H. Song, B. Wenger, R. H. Friend, H. J. Snaith, *Adv. Mater.* **2008**, *20*, 3447.

This article is protected by copyright. All rights reserved.

Accepted Article

15214095, ja, Downloaded from https://onlinelibrary.wiley.com/doi/10.1002/adma.202207454 by Seoul National University, Wiley Online Library on [28/11/2022]. See the Terms and Conditions (https://onlinelibrary.wiley.com/terms-and-conditions) on Wiley Online Library for rules of use; OA articles are governed by the applicable Creative Commons License

[234] H. Becker, H. Spreitzer, W. Kreuder, E. Kluge, H. Schenk, I. Parker, Y. Cao, *Adv. Mater.* **2000**, *12*, 42.

[235] S. R. Tseng, H. F. Meng, K. C. Lee, S. F. Horng, *Appl. Phys. Lett.* **2008**, *93*, 153308.

[236] S. Burns, J. MacLeod, T. Trang Do, P. Sonar, S. D. Yambem, *Sci. Rep.* **2017**, *7*, 40805.

[237] J. Liu, T.-F. Guo, Y. Yang, *J. Appl. Phys.* **2002**, *91*, 1595.

[238] W. Li, Q. Wang, J. Cui, H. Chou, S. E. Shaheen, G. E. Jabbour, J. Anderson, P. Lee, B. Kippelen, N. Peyghambarian, N. R. Armstrong, T. J. Marks, *Adv. Mater.* **1999**, *11*, 730.

[239] Y.-J. Cheng, M. S. Liu, Y. Zhang, Y. Niu, F. Huang, J.-W. Ka, H.-L. Yip, Y. Tian, A. K. Y. Jen, *Chem. Mater.* **2008**, *20*, 413.

[240] A. Bacher, C. H. Erdelen, W. Paulus, H. Ringsdorf, H. W. Schmidt, P. Schuhmacher, *Macromolecules* **1999**, *32*, 4551.

[241] M. Hengge, P. Hänsch, D. Ehjeij, F. S. Benneckendorf, J. Freudenberg, U. H. F. Bunz, K. Müllen, E. J. W. List-Kratochvil, F. Hermerschmidt, *J. Polym. Sci.* **2022**, *60*, 1878.

[242] B. R. Lee, E. D. Jung, J. S. Park, Y. S. Nam, S. H. Min, B.-S. Kim, K.-M. Lee, J.-R. Jeong, R. H. Friend, J.-S. Kim, S. O. Kim, M. H. Song, *Nat. Commun.* **2014**, *5*, 4840.

[243] S. Nowy, B. C. Krummacher, J. Frischeisen, N. A. Reinke, W. Brütting, *J. Appl. Phys.* **2008**, *104*, 123109.

[244] D. Y. Kondakov, *Philos. Trans. R. Soc. A Math. Phys. Eng. Sci.* **2015**, *373*, 20140321.

[245] C.-L. Lee, K. B. Lee, J.-J. Kim, *Appl. Phys. Lett.* **2000**, *77*, 2280.

[246] Q. Zhao, S.-J. Liu, W. Huang, *Macromol. Rapid Commun.* **2010**, *31*, 794.

This article is protected by copyright. All rights reserved.

Accepted Article

15214095, ja, Downloaded from https://onlinelibrary.wiley.com/doi/10.1002/adma.202207454 by Seoul National University, Wiley Online Library on [28/11/2022]. See the Terms and Conditions (https://onlinelibrary.wiley.com/terms-and-conditions) on Wiley Online Library for rules of use; OA articles are governed by the applicable Creative Commons License

[247] F.-C. Chen, G. He, Y. Yang, *Appl. Phys. Lett.* **2003**, *82*, 1006.

[248] X. Yang, D. C. Müller, D. Neher, K. Meerholz, *Adv. Mater.* **2006**, *18*, 948.

[249] T.-F. Guo, S.-C. Chang, Y. Yang, R. C. Kwong, M. E. Thompson, *Org. Electron.* **2000**, *1*, 15.

[250] B.-Y. Yu, C.-H. Kuo, W.-B. Wang, G.-J. Yen, S. Iida, S.-Z. Chen, W.-C. Lin, S.-H. Lee, W.-L. Kao, C.-Y. Liu, H.-Y. Chang, Y.-W. You, C.-J. Chang, C.-P. Liu, J.-H. Jou, J.-J. Shyue, *Analyst* **2011**, *136*, 716.

[251] S. Tokito, M. Suzuki, F. Sato, M. Kamachi, K. Shirane, *Org. Electron.* **2003**, *4*, 105.

[252] M. Suzuki, S. Tokito, F. Sato, T. Igarashi, K. Kondo, T. Koyama, T. Yamaguchi, *Appl. Phys. Lett.* **2005**, *86*, 103507.

[253] A. Endo, M. Ogasawara, A. Takahashi, D. Yokoyama, Y. Kato, C. Adachi, *Adv. Mater.* **2009**, *21*, 4802.

[254] A. E. Nikolaenko, M. Cass, F. Bourcet, D. Mohamad, M. Roberts, *Adv. Mater.* **2015**, *27*, 7236.

[255] H. J. Kim, C. Lee, M. Godumala, S. Choi, S. Y. Park, M. J. Cho, S. Park, D. H. Choi, *Polym. Chem.* **2018**, *9*, 1318.

[256] Y. Long, X. Chen, H. Wu, Z. Zhou, S. Sriram Babu, M. Wu, J. Zhao, M. P. Aldred, S. Liu, X. Chen, Z. Chi, J. Xu, Y. Zhang, *Angew. Chemie Int. Ed.* **2021**, *60*, 7220.

[257] J. Luo, G. Xie, S. Gong, T. Chen, C. Yang, *Chem. Commun.* **2016**, *52*, 2292.

[258] G. Xie, J. Luo, M. Huang, T. Chen, K. Wu, S. Gong, C. Yang, *Adv. Mater.* **2017**, *29*, 1604223.

[259] Z. Ren, R. S. Nobuyasu, F. B. Dias, A. P. Monkman, S. Yan, M. R. Bryce, *Macromolecules* **2016**, *49*, 5452.

This article is protected by copyright. All rights reserved.

Accepted Article

15214095, ja, Downloaded from https://onlinelibrary.wiley.com/doi/10.1002/adma.202207454 by Seoul National University, Wiley Online Library on [28/11/2022]. See the Terms and Conditions (https://onlinelibrary.wiley.com/terms-and-conditions) on Wiley Online Library for rules of use; OA articles are governed by the applicable Creative Commons License

[260] C. Rothe, A. Monkman, *J. Chem. Phys.* **2005**, *123*, 244904.

[261] Y. H. Park, H. J. Jang, J. Y. Lee, *Polym. Chem.* **2019**, *10*, 4872.

[262] A. Cravcenco, C. Ye, J. Gräfenstein, K. Börjesson, *J. Phys. Chem. A* **2020**, *124*, 7219.

[263] T. Basel, D. Sun, B. Gautam, Z. Valy Vardeny, *J. Lumin.* **2014**, *155*, 89.

[264] S. Bai, P. Zhang, D. N. Beratan, *J. Phys. Chem. C* **2020**, *124*, 18956.

[265] S. Bai, P. Zhang, P. Antoniou, S. S. Skourtis, D. N. Beratan, *Faraday Discuss.* **2019**, *216*, 301.

[266] X. Gong, J. C. Ostrowski, D. Moses, G. C. Bazan, A. J. Heeger, *Adv. Funct. Mater.* **2003**, *13*, 439.

[267] J.-H. Lee, C.-I. Wu, S.-W. Liu, C.-A. Huang, Y. Chang, *Appl. Phys. Lett.* **2005**, *86*, 103506.

[268] Q. Fu, J. Chen, C. Shi, D. Ma, *ACS Appl. Mater. Interfaces* **2012**, *4*, 6579.

[269] C.-H. Hsiao, Y.-H. Chen, T.-C. Lin, C.-C. Hsiao, J.-H. Lee, *Appl. Phys. Lett.* **2006**, *89*, 163511.

[270] N. Chopra, J. S. Swensen, E. Polikarpov, L. Cosimbescu, F. So, A. B. Padmaperuma, *Appl. Phys. Lett.* **2010**, *97*, 033304.

[271] N. C. Giebink, S. R. Forrest, *Phys. Rev. B* **2008**, *77*, 235215.

[272] M. W. Ha, M. H. Park, J. Y. Hwang, J. Kim, D. H. Kim, T. W. Lee, Y. H. Kim, *Dye. Pigment.* **2021**, *185*, 108880.

[273] S. Wang, B. Zhang, X. Wang, J. Ding, Z. Xie, L. Wang, *Adv. Opt. Mater.* **2015**, *3*, 1349.

[274] Y.-S. Park, S. Lee, K.-H. Kim, S.-Y. Kim, J.-H. Lee, J.-J. Kim, *Adv. Funct. Mater.* **2013**, *23*, 4914.

[275] C.-K. Moon, J.-S. Huh, J.-M. Kim, J.-J. Kim, *Chem. Mater.* **2018**, *30*, 5648.

[276] N. Matsumoto, M. Nishiyama, C. Adachi, *J. Phys. Chem. C* **2008**, *112*, 7735.

This article is protected by copyright. All rights reserved.

Accepted Article

15214095, ja, Downloaded from https://onlinelibrary.wiley.com/doi/10.1002/adma.202207454 by Seoul National University, Wiley Online Library on [28/11/2022]. See the Terms and Conditions (https://onlinelibrary.wiley.com/terms-and-conditions) on Wiley Online Library for rules of use; OA articles are governed by the applicable Creative Commons License

[277] E. Angioni, M. Chapran, K. Ivaniuk, N. Kostiv, V. Cherpak, P. Stakhira, A. Lazauskas, S. Tamulevičius, D. Volyniuk, N. J. Findlay, T. Tuttle, J. V. Grazulevicius, P. J. Skabara, *J. Mater. Chem. C* **2016**, *4*, 3851.

[278] J.-H. Lee, H. Shin, J.-M. Kim, K.-H. Kim, J.-J. Kim, *ACS Appl. Mater. Interfaces* **2017**, *9*, 3277.

[279] M. Li, W. Li, L. Chen, Z. Kong, B. Chu, B. Li, Z. Hu, Z. Zhang, *Appl. Phys. Lett.* **2006**, *88*, 091108.

[280] G. Cheng, Y. Zhang, Y. Zhao, S. Liu, Z. Xie, H. Xia, M. Hanif, Y. Ma, *Appl. Phys. Lett.* **2005**, *87*, 013506.

[281] X. K. Liu, Z. Chen, C. J. Zheng, M. Chen, W. Liu, X. H. Zhang, C. S. Lee, *Adv. Mater.* **2015**, *27*, 2025.

[282] Y.-S. Park, W.-I. Jeong, J.-J. Kim, *J. Appl. Phys.* **2011**, *110*, 124519.

[283] W. Song, J. Y. Lee, *Appl. Phys. Lett.* **2015**, *106*, 123306.

[284] J.-H. Lee, S.-H. Cheng, S.-J. Yoo, H. Shin, J.-H. Chang, C.-I. Wu, K.-T. Wong, J.-J. Kim, *Adv. Funct. Mater.* **2015**, *25*, 361.

[285] L. Niu, Y. Zhang, L. Chen, Q. Zhang, Y. Guan, *Org. Electron.* **2020**, *87*, 105971.

[286] D. Graves, V. Jankus, F. B. Dias, A. Monkman, *Adv. Funct. Mater.* **2014**, *24*, 2343.

[287] K. Goushi, K. Yoshida, K. Sato, C. Adachi, *Nat. Photonics* **2012**, *6*, 253.

[288] L. Zeng, T. Y. H. Lee, P. B. Merkel, S. H. Chen, *J. Mater. Chem.* **2009**, *19*, 8772.

[289] M. Cai, T. Xiao, E. Hellerich, Y. Chen, R. Shinar, J. Shinar, *Adv. Mater.* **2011**, *23*, 3590.

[290] D. Zhang, M. Cai, Y. Zhang, Z. Bin, D. Zhang, L. Duan, *ACS Appl. Mater. Interfaces* **2016**, *8*, 3825.

This article is protected by copyright. All rights reserved.

Accepted Article

15214095, ja, Downloaded from https://onlinelibrary.wiley.com/doi/10.1002/adma.202207454 by Seoul National University, Wiley Online Library on [28/11/2022]. See the Terms and Conditions (https://onlinelibrary.wiley.com/terms-and-conditions) on Wiley Online Library for rules of use; OA articles are governed by the applicable Creative Commons License

[291] Y. Seino, H. Sasabe, Y. J. Pu, J. Kido, *Adv. Mater.* **2014**, *26*, 1612.

[292] S. Wang, X. Wang, B. Yao, B. Zhang, J. Ding, Z. Xie, L. Wang, *Sci. Rep.* **2015**, *5*, 12487.

[293] B. Yao, X. Lin, B. Zhang, H. Wang, X. Liu, Z. Xie, *J. Mater. Chem. C* **2018**, *6*, 4409.

[294] B. Zhao, T. Zhang, B. Chu, W. Li, Z. Su, H. Wu, X. Yan, F. Jin, Y. Gao, C. Liu, *Sci. Rep.* **2015**, *5*, 10697.

[295] M. Pope, H. P. Kallmann, P. Magnante, *J. Chem. Phys.* **1963**, *38*, 2042.

[296] M. A. Baldo, S. Lamansky, P. E. Burrows, M. E. Thompson, S. R. Forrest, *Appl. Phys. Lett.* **1999**, *75*, 4.

[297] C. Adachi, M. A. Baldo, M. E. Thompson, S. R. Forrest, *J. Appl. Phys.* **2001**, *90*, 5048.

[298] K. Kawano, K. Nagayoshi, T. Yamaki, C. Adachi, *Org. Electron.* **2014**, *15*, 1695.

[299] Y. J. Cho, K. S. Yook, J. Y. Lee, *Adv. Mater.* **2014**, *26*, 6642.

[300] W. Li, J. Zhao, L. Li, X. Du, C. Fan, C. Zheng, S. Tao, *Org. Electron.* **2018**, *58*, 276.

[301] P. S. Ngo, M.-K. Hung, K.-W. Tsai, S. Sharma, S.-A. Chen, *ACS Appl. Mater. Interfaces* **2019**, *11*, 45939.

[302] C. C. Peng, S. Y. Yang, H. C. Li, G. H. Xie, L. S. Cui, S. N. Zou, C. Poriel, Z. Q. Jiang, L. S. Liao, *Adv. Mater.* **2020**, *32*, 2003885.

[303] D. W. Lee, J. Hwang, H. J. Kim, H. Lee, J. M. Ha, H. Y. Woo, S. Park, M. J. Cho, D. H. Choi, *ACS Appl. Mater. Interfaces* **2021**, *13*, 49076.

[304] S. K. Jeon, H.-J. Park, J. Y. Lee, *ACS Appl. Mater. Interfaces* **2018**, *10*, 5700.

This article is protected by copyright. All rights reserved.

Accepted Article

15214095, ja, Downloaded from https://onlinelibrary.wiley.com/doi/10.1002/adma.202207454 by Seoul National University, Wiley Online Library on [28/11/2022]. See the Terms and Conditions (https://onlinelibrary.wiley.com/terms-and-conditions) on Wiley Online Library for rules of use; OA articles are governed by the applicable Creative Commons License

[305] F. Wang, J. Hu, X. Cao, T. Yang, Y. Tao, L. Mei, X. Zhang, W. Huang, *J. Mater. Chem. C* **2015**, *3*, 5533.

[306] H.-F. Chen, S.-J. Yang, Z.-H. Tsai, W.-Y. Hung, T.-C. Wang, K.-T. Wong, *J. Mater. Chem.* **2009**, *19*, 8112.

[307] K. Togashi, S. Nomura, N. Yokoyama, T. Yasuda, C. Adachi, *J. Mater. Chem.* **2012**, *22*, 20689.

[308] R. Komatsu, H. Sasabe, S. Inomata, Y.-J. Pu, J. Kido, *Synth. Met.* **2015**, *202*, 165.

[309] C. H. Jeong, M. Godumala, J. Yoon, S. Choi, Y. W. Kim, D. H. Choi, M. J. Cho, D. H. Choi, *ACS Appl. Mater. Interfaces* **2019**, *11*, 17602.

[310] K.-W. Tsai, M.-K. Hung, Y.-H. Mao, S.-A. Chen, K.-W. Tsai, M.-K. Hung, Y.-H. S. Mao, -A Chen, *Adv. Funct. Mater.* **2019**, *29*, 1901025.

[311] Z. He, C. Wang, J. Zhao, X. Du, H. Yang, P. Zhong, C. Zheng, H. Lin, S. Tao, X. Zhang, *J. Mater. Chem. C* **2019**, *7*, 11806.

[312] D. H. Ahn, J. H. Jeong, J. Song, J. Y. Lee, J. H. Kwon, *ACS Appl. Mater. Interfaces* **2018**, *10*, 10246.

[313] D. Chen, X. Cai, X.-L. Li, Z. He, C. Cai, D. Chen, S.-J. Su, *J. Mater. Chem. C* **2017**, *5*, 5223.

[314] L. Zhang, K. W. Cheah, *Sci. Rep.* **2018**, *8*, 8832.

[315] H. Nakanotani, T. Higuchi, T. Furukawa, K. Masui, K. Morimoto, M. Numata, H. Tanaka, Y. Sagara, T. Yasuda, C. Adachi, *Nat. Commun.* **2014**, *5*, 4016.

[316] N. R. Wallwork, M. Mamada, A. Shukla, S. K. M. McGregor, C. Adachi, E. B. Namdas, S. C. Lo, *J. Mater. Chem. C* **2022**, *10*, 4767.

[317] J. Hu, Y. Wang, Q. Li, S. Shao, L. Wang, X. Jing, F. Wang, *Chem. Sci.* **2021**, *12*, 13083.

This article is protected by copyright. All rights reserved.

Accepted Article

15214095, ja, Downloaded from https://onlinelibrary.wiley.com/doi/10.1002/adma.202207454 by Seoul National University, Wiley Online Library on [28/11/2022]. See the Terms and Conditions (https://onlinelibrary.wiley.com/terms-and-conditions) on Wiley Online Library for rules of use; OA articles are governed by the applicable Creative Commons License

[318] Y.-F. Chang, C.-H. Yu, S.-C. Yang, I.-H. Hong, S.-C. Jiang, H.-F. Meng, H.-L. Huang, H.-W. Zan, S.-F. Horng, *Org. Electron.* **2017**, *42*, 75.

[319] D. Y. Kondakov, T. D. Pawlik, W. F. Nichols, W. C. Lenhart, *J. Soc. Inf. Disp.* **2008**, *16*, 37.

[320] S. Scholz, D. Kondakov, B. Lüssem, K. Leo, *Chem. Rev.* **2015**, *115*, 8449.

[321] K. Kishore Kesavan, J. Jayakumar, M. Lee, C. Hexin, S. Sudheendran Swayamprabha, D. Kumar Dubey, F.-C. Tung, C.-W. Wang, J.-H. Jou, *Chem. Eng. J.* **2022**, *435*, 134879.

[322] N. C. Giebink, B. W. D'Andrade, M. S. Weaver, P. B. MacKenzie, J. J. Brown, M. E. Thompson, S. R. Forrest, *J. Appl. Phys.* **2008**, *103*, 044509.

[323] M. R. Nagar, A. Choudhury, D. Tavgeniene, R. Beresneviciute, D. Blazevicius, V. Jankauskas, K. Kumar, S. Banik, S. Ghosh, S. Grigalevicius, J.-H. Jou, *J. Mater. Chem. C* **2022**, *10*, 3593.

[324] T. N. Le, E. Y. Park, V. Thangaraji, M. C. Suh, *Org. Electron.* **2021**, *99*, 106346.

[325] S.-W. Liu, J.-K. Wang, *https://doi.org/10.1117/12.682857* **2006**, *6333*, 359.

[326] S. Stolz, M. Petzoldt, N. Kotadiya, T. Rödlmeier, R. Eckstein, J. Freudenberg, U. H. F. Bunz, U. Lemmer, E. Mankel, M. Hamburger, G. Hernandez-Sosa, *J. Mater. Chem. C* **2016**, *4*, 11150.

[327] I. R. De Moraes, S. Scholz, M. Hermenau, M. L. Tietze, T. Schwab, S. Hofmann, M. C. Gather, K. Leo, *Org. Electron.* **2015**, *26*, 158.

[328] J. R. Sheats, H. Antoniadis, M. Hueschen, W. Leonard, J. Miller, R. Moon, D. Roitman, A. Stocking, *Science (80-.).* **1996**, *273*, 884.

[329] B. C. D. Salert, H. Krueger, S. A. Bagnich, T. Unger, F. Jaiser, M. Al-Sa'di, D. Neher, A. Hayer, T. Eberle, *J. Polym. Sci. Part A Polym. Chem.* **2013**, *51*, 601.

This article is protected by copyright. All rights reserved.

Accepted Article

15214095, ja, Downloaded from https://onlinelibrary.wiley.com/doi/10.1002/adma.202207454 by Seoul National University, Wiley Online Library on [28/11/2022]. See the Terms and Conditions (https://onlinelibrary.wiley.com/terms-and-conditions) on Wiley Online Library for rules of use; OA articles are governed by the applicable Creative Commons License

[330] "LG Display to start pilot production of ink-jet OLEDs in 2017," can be found under https://www.oled-info.com/lg-display-start-pilot-p, **2017**.

[331] Z. Gao, L. Yu, Z. Li, W. Shi, C. Li, L. Yuan, X. Sun, D. Fu, *Dig. Tech. Pap. - SID Int. Symp.* **2021**, *52*, 312.

[332] X. Ren, Y. Zou, A. Fennimore, H. Hlaing, H. Skulason, *SID Symp. Dig. Tech. Pap.* **2018**, *49*, 280.

[333] H. J. Kim, E. Y. Lee, M. Y. Kim, J. S. Kim, B. D. Chin, *ECS J. Solid State Sci. Technol.* **2021**, *10*, 106005.

[334] H. Yildirim Erbil, *Adv. Colloid Interface Sci.* **2015**, *222*, 275.

[335] M. Cinquino, C. T. Prontera, A. Zizzari, A. Giuri, M. Pugliese, R. Giannuzzi, A. G. Monteduro, M. Carugati, A. Banfi, S. Carallo, A. Rizzo, A. Andretta, G. Dugnani, G. Gigli, V. Maiorano, *J. Sci. Adv. Mater. Devices* **2022**, *7*, 100394.

[336] C. M. Hansen, *Prog. Org. Coatings* **2004**, *51*, 77.

[337] B. He, S. Yang, Z. Qin, B. Wen, C. Zhang, *Sci. Reports 2017 71* **2017**, *7*, 1.

[338] C. N. Hoth, P. Schilinsky, S. A. Choulis, C. J. Brabec, *Nano Lett.* **2008**, *8*, 2806.

[339] J. Carter, A. Wehrum, M. C. Dowling, M. Cacheiro-Martinez, N. de B. Baynes, *Proc. SPIE* **2003**, *4800*, 34.

[340] H. Hu, R. G. Larson, *J. Phys. Chem. B* **2006**, *110*, 7090.

[341] D. Y. Kim, Y. J. Han, J. Choi, C. Sakong, B. K. Ju, K. H. Cho, *Org. Electron.* **2020**, *84*, 105814.

[342] S. Kommeren, M. J. J. Coenen, T. M. Eggenhuisen, T. W. L. Slaats, H. Gorter, P. Groen, *Org. Electron.* **2018**, *61*, 282.

This article is protected by copyright. All rights reserved.

Accepted Article

15214095, ja, Downloaded from https://onlinelibrary.wiley.com/doi/10.1002/adma.202207454 by Seoul National University, Wiley Online Library on [28/11/2022]. See the Terms and Conditions (https://onlinelibrary.wiley.com/terms-and-conditions) on Wiley Online Library for rules of use; OA articles are governed by the applicable Creative Commons License

[343] H. Y. Park, B. J. Kang, D. Lee, J. H. Oh, *Thin Solid Films* **2013**, *546*, 162.

[344] D. Tian, Y. Song, L. Jiang, *Chem. Soc. Rev.* **2013**, *42*, 5184.

[345] W. Hou, Q. Dai, Y. Song, Y. Cui, C. Hu, H.-T. Shih, *SID Symp. Dig. Tech. Pap.* **2018**, *49*, 743.

[346] Z. Du, H. Zhou, X. Yu, Y. Han, *Colloids Surfaces A Physicochem. Eng. Asp.* **2020**, *602*, 125111.

[347] S. S. Kim, H. S. Kim, J. G. Lee, C. W. Seo, *SID Symp. Dig. Tech. Pap.* **2018**, *49*, 839.

[348] T. Chiba, Y.-J. Pu, J. Kido, T. Chiba, Y.-J. Pu, J. Kido, *Adv. Mater.* **2015**, *27*, 4681.

[349] S. Höfle, A. Schienle, C. Bernhard, M. Bruns, U. Lemmer, A. Colsmann, *Adv. Mater.* **2014**, *26*, 5155.

[350] M. R. Maciejczyk, S. Zhang, G. J. Hedley, N. Robertson, I. D. W. Samuel, M. Pietraszkiewicz, *Adv. Funct. Mater.* **2019**, *29*, 1807572.

[351] S. Sato, S. Ohisa, Y. Hayashi, R. Sato, D. Yokoyama, T. Kato, M. Suzuki, T. Chiba, Y. Pu, J. Kido, *Adv. Mater.* **2018**, *30*, 1705915.

[352] Q. Liu, S. Chavhan, H. Zhang, H. Sun, A. J. Brock, S. Manzhos, Y. Chen, K. Feron, S. E. Bottle, J. C. McMurtrie, J. Jou, H. Chen, M. R. Nagar, W. Hu, Y. Noh, Y. Zhen, P. Sonar, *Adv. Electron. Mater.* **2021**, *7*, 2000804.

[353] X. Wu, D. G. Chen, D. Liu, S. H. Liu, S. W. Shen, C. I. Wu, G. Xie, J. Zhou, Z. X. Huang, C. Y. Huang, S. J. Su, W. Zhu, P. T. Chou, *J. Am. Chem. Soc.* **2020**, *142*, 7469.

[354] T. Sudyoadsuk, P. Chasing, C. Chaiwai, T. Chawanpunyawat, T. Kaewpuang, T. Manyum, S. Namuangruk, V. Promarak, *J. Mater. Chem. C* **2020**, *8*, 10464.

[355] R. Kumaresan, H. Y. Park, A. Maheshwaran, H. Park, Y. Do, M. Song, J. Yoon, S. Il Ahn, S. H. Jin, *Adv. Opt. Mater.* **2022**, *10*, 2101686.

This article is protected by copyright. All rights reserved.

Accepted Article

15214095, ja, Downloaded from https://onlinelibrary.wiley.com/doi/10.1002/adma.202207454 by Seoul National University, Wiley Online Library on [28/11/2022]. See the Terms and Conditions (https://onlinelibrary.wiley.com/terms-and-conditions) on Wiley Online Library for rules of use; OA articles are governed by the applicable Creative Commons License

[356] T. Giridhar, T. H. Han, W. Cho, C. Saravanan, T. W. Lee, S. H. Jin, *Chem. - A Eur. J.* **2014**, *20*, 8260.

[357] G. Kreiza, D. Berenis, D. Banevičius, S. Juršėnas, T. Javorskis, E. Orentas, K. Kazlauskas, *Chem. Eng. J.* **2021**, *412*, 128574.

[358] S. Cho, N. Y. Kwon, C. W. Kim, H. Lee, J. M. Ha, H. J. Kim, H. Y. Woo, S. Park, M. J. Cho, D. H. Choi, *Polym. Chem.* **2022**, *13*, 1824.

[359] D. Jiang, H. Sasabe, H. Arai, K. Nakao, K. Kumada, J. Kido, *Adv. Opt. Mater.* **2022**, *10*, 2102774.

[360] J. Chen, Y. Xiao, K. Wang, D. Sun, X. Fan, X. Zhang, M. Zhang, Y. Shi, J. Yu, F. Geng, C. Lee, X. Zhang, *Angew. Chemie Int. Ed.* **2021**, *60*, 2478.

[361] T. Chiba, Y.-J. Pu, T. Ide, S. Ohisa, H. Fukuda, T. Hikichi, D. Takashima, T. Takahashi, S. Kawata, J. Kido, *ACS Appl. Mater. Interfaces* **2017**, *9*, 18113.

This article is protected by copyright. All rights reserved.

Accepted Article

15214095, ja, Downloaded from https://onlinelibrary.wiley.com/doi/10.1002/adma.202207454 by Seoul National University, Wiley Online Library on [28/11/2022]. See the Terms and Conditions (https://onlinelibrary.wiley.com/terms-and-conditions) on Wiley Online Library for rules of use; OA articles are governed by the applicable Creative Commons License

Accepted Article

Author biography

Joo Yoon Woo is currently a Ph.D. student under the supervision of Prof. Tae-Hee Han in Division of Materials Science and Engineering, Hanyang University, Republic of Korea. She received her B.S. in Division of Materials Science and Engineering, Hanyang University, Republic of Korea (2021). Her research interests include organic/inorganic hybrid perovskites and solution-processed organic light-emitting diodes.

Su-Hun Jeong received his B.S. (February 2012) and Ph.D (August 2017) in the department of Materials Science and Engineering from the Pohang University of Science and Engineering (POSTECH), Republic of Korea. He worked as a postdoctoral researcher in the department of Materials Science and Engineering at the Seoul National University, Republic of Korea (August 2017 to December 2018). He is currently working as a professional researcher in LG Chem, Republic of Korea (January 2019 to present). His research interests include printed optoelectronic devices.

This article is protected by copyright. All rights reserved.

15214095, ja, Downloaded from https://onlinelibrary.wiley.com/doi/10.1002/adma.202207454 by Seoul National University, Wiley Online Library on [28/11/2022]. See the Terms and Conditions (https://onlinelibrary.wiley.com/terms-and-conditions) on Wiley Online Library for rules of use; OA articles are governed by the applicable Creative Commons License

Accepted Article

Tae-Woo Lee is a professor in the Department of MSE at Seoul National University, South Korea. He received his Ph.D. in Chemical Engineering from KAIST, South Korea in 2002. He joined Bell Laboratories, USA, as a postdoctoral researcher and worked at Samsung Advanced Institute of Technology as a research staff (2003–2008). He was an associate professor in MSE at Pohang University of Science and Technology (POSTECH), South Korea, until August 2016. His research focuses on printed or soft electronics that use organic and organic-inorganic hybrid materials for flexible/stretchable displays, solid-state lighting, solar energy conversion devices, and bioinspired neuromorphic devices.

Tae-Hee Han is an associate professor in Division of Materials Science and Engineering, Hanyang University, Republic of Korea. He received his B.S. (February 2010) and Ph.D. (Feburuary 2015) in Materials Science and Engineering from Pohang University of Science and Technology (POSTECH), Republic of Korea. He was a postdoctoral research associate in Prof. Yang Yang`s group in University of California Los Angeles (UCLA) (2017-2019). His research focuses on organic and organic/inorganic hybrid materials for optoelectronic applications, such as photovoltaic cells, and light-emitting diodes.

This article is protected by copyright. All rights reserved.

15214095, ja, Downloaded from https://onlinelibrary.wiley.com/doi/10.1002/adma.202207454 by Seoul National University, Wiley Online Library on [28/11/2022]. See the Terms and Conditions (https://onlinelibrary.wiley.com/terms-and-conditions) on Wiley Online Library for rules of use; OA articles are governed by the applicable Creative Commons License

Accepted Article

The review outlines industrial demands for commercial solution-processed organic light-emitting diode (SOLED) displays and current status of SOLEDs in industries and academia. For their practical use in displays, technical challenges and directions of research and development in SOLEDs to achieve high efficiency, long lifetime, and good processability are reviewed in this article.

J. Y. Woo, M.-H. Park, S.-H. Jeong, Y.-H. Kim, B. Kim, T.-W. Lee*, T.-H. Han*

Advances in Solution-processed OLEDs and their Prospects for Use in Displays

ToC figure

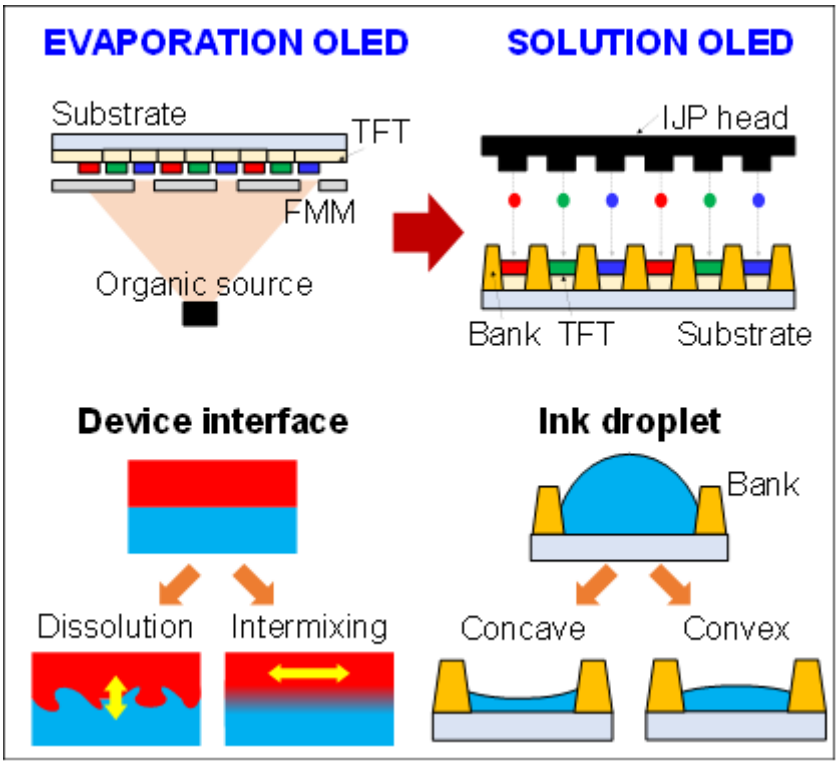

This article is protected by copyright. All rights reserved.

15214095, ja, Downloaded from https://onlinelibrary.wiley.com/doi/10.1002/adma.202207454 by Seoul National University, Wiley Online Library on [28/11/2022]. See the Terms and Conditions (https://onlinelibrary.wiley.com/terms-and-conditions) on Wiley Online Library for rules of use; OA articles are governed by the applicable Creative Commons License